

**IMPROVING PROCESS AND COOLING/LUBRICATION CONDITIONS
THROUGH MODELING AND EXPERIMENTAL INVESTIGATION OF
DEFORMATION, THERMAL, AND TRIBOLOGY MECHANISMS IN
HYBRID MANUFACTURING PROCESSES**

by

Amin Bagherzadeh

Submitted to the Graduate School of Engineering and Natural Sciences in partial fulfillment
of the requirements for the degree of Doctor of Philosophy

Sabancı University

July 2023

Amin Bagherzadeh 2023 ©

All Rights Reserved

ABSTRACT

IMPROVING PROCESS AND COOLING/LUBRICATION CONDITIONS THROUGH MODELING AND EXPERIMENTAL INVESTIGATION OF DEFORMATION, THERMAL, AND TRIBOLOGY MECHANISMS IN HYBRID MANUFACTURING PROCESSES

Amin Bagherzadeh

MANUFACTURING ENGINEERING PH.D. DISSERTATION, July 2023

Dissertation Supervisor: Prof. Dr. ERHAN BUDAK

Traditional cutting fluids are known to pose environmental and health concerns, and dry machining is not efficient for difficult-to-cut materials. Therefore, it is important to identify green cutting solutions for such materials, including titanium and nickel alloys. Alternative green solutions, such as vegetable oil using minimum quantity lubrication, cryogenics, and hybrid methods, can be explored and developed. The performance of these methods was evaluated by measuring tool wear, temperature, cutting forces and surface integrity. The primary objective of this study is to demonstrate the feasibility and determine the performance of these alternative methods on hard-to-cut materials. Subsequently, the aim is to apply the best-performing solutions to enhance the hybrid additive/subtractive processes. While the combination of additive and machining processes can lead to sustainable and cleaner production, there is a lack of literature on material deformation and friction behavior in hybrid additive/subtractive manufacturing, which hinders the ability to effectively model and optimize the process. To address this gap, the study investigates the material deformation behavior using parameters such as shear stress, shear angle, and friction. A dual-zone thermomechanical model approach is proposed to modify the commonly used Johnson-Cook model for hybrid manufacturing under both dry and different cooling/lubrication conditions. This approach significantly reduces the experimental effort required for material model and friction identification, as only a few orthogonal cutting tests are needed. In addition, the JC parameters are adjusted for selective laser melting (SLM), directed energy deposition (DED), and wrought materials in various cooling/lubrication conditions to cater to the requirements of hybrid manufacturing modeling.

Keywords:

Hybrid Additive Manufacturing, Direct Energy Deposition, Laser Powder Bed Fusion, Machining, Constitutive Model, Nickel Alloy 718, Hybrid Carbon Dioxide, Hybrid Liquid Nitrogen

ÖZET

HİBRİT ÜRETİM SÜREÇLERİNDE DEFORMASYON, TERMAL VE TRİBOLOJİ MEKANİZMALARIN MODELLEME VE DENEYSEL ARAŞTIRMA YOLUYLA İYİLEŞTİRİLMESİ VE SOĞUTMA/YAĞLAMA KOŞULLARININ GELİŞTİRİLMESİ

Amin Bagherzadeh

ÜRETİM MÜHENDİSLİĞİ DOKTORA TEZİ, Temmuz 2023

Tez Danışmanı: Prof. Dr. ERHAN BUDAK

Geleneksel kesme sıvıları çevresel ve sağlık sorunlarına neden olabileceği bilinmektedir ve kuru işleme, zor kesilebilen malzemeler için verimli değildir. Bu nedenle, titanyum ve nikel alaşımları dahil olmak üzere böyle malzemeler için yeşil kesme çözümlerini belirlemek önemlidir. Sebze yağı kullanarak minimum miktar yağlama, kriyogenik ve hibrit yöntemler gibi alternatif yeşil çözümler araştırılabilir ve geliştirilebilir. Bu yöntemlerin performansı, takım aşınması, sıcaklık, kesme kuvvetleri ve yüzey bütünlüğü ölçülerek değerlendirilmiştir. Bu çalışmanın temel amacı, zor kesilebilen malzemeler üzerinde bu alternatif yöntemlerin uygulanabilirliğini ve performansını göstermektir. Ardından, en iyi performans gösteren çözümlerin hibrit eklemeli/çıkarmalı süreçleri geliştirmek için uygulanması amaçlanmaktadır. Eklemeli ve işleme süreçlerinin kombinasyonu sürdürülebilir ve daha temiz üretime yol açabilse de, hibrit eklemeli/çıkarmalı imalatta malzeme deformasyonu ve sürtünme davranışı konusunda literatür eksikliği vardır, bu da süreci etkin bir şekilde modellemeyi ve optimize etmeyi engeller. Bu boşluğu doldurmak için, çalışma kesme stresi, kesme açısı ve sürtünme gibi parametreleri kullanarak malzeme deformasyon davranışını araştırmaktadır. Kurumlu ve farklı soğutma/yağlama koşullarında kurutma ve yağlama parametreleri dikkate alınarak, hibrit imalat modellemesi için yaygın olarak kullanılan Johnson-Cook modelini değiştirmek için çift bölgeli termomekanik bir model yaklaşımı önerilmektedir. Bu yaklaşım, malzeme modeli ve sürtünme tanımlaması için gereken deneysel çabayı önemli ölçüde azaltır, çünkü sadece birkaç dik kesme testi gereklidir. Ayrıca, JC parametreleri, seçici lazer eritme (SLM), yönlendirilmiş enerji birikimi (DED) ve dövme malzemeler için çeşitli soğutma/yağlama koşullarında hibrit imalat modellemesi gereksinimlerine uyacak şekilde ayarlanmıştır.

Anahtar kelimeler:

Hibrit Eklemeli İmalat, Doğrudan Enerji Birikimi, Lazer Toz Yatağı Birleştirme, İşleme, Yapısal Model, Nikel Alaşımı 718, Hibrit Karbondioksit, Hibrit Sıvı Azot

Table of contents

1. INTRODUCTION	11
2. LITERATURE REVIEW	14
3. EXPERIMENTAL EVALUATION OF ECO-FRIENDLY HYBRID COOLING METHODS IN SLOT MILLING OF TITANIUM ALLOY	25
3.1. Experimental Setup.....	25
3.2. Results and Discussion	29
3.2.1. Tool Wear	29
3.2.2. Temperature	35
3.2.4. Surface Roughness	40
3.3. Conclusions.....	43
4. HIGH-SPEED MACHINING OF ADDITIVELY MANUFACTURED INCONEL 718 USING HYBRID CRYOGENIC COOLING METHODS	46
4.1. Experimental Setup.....	46
4.2. Results and Discussion	50
4.2.1. Tool life	50
4.2.2. Cutting Forces	53
4.2.3. Temperature	55
4.2.4. Surface finish	57
4.2.5. Phase analyses	60
4.2.6. Energy Efficiency and Cost of Additive-Subtractive Production	64
4.3. Conclusions.....	66
5. MACHINING BEHAVIOR OF INCONEL 718 IN HYBRID ADDITIVE AND SUBTRACTIVE MANUFACTURING	68
5.1. Investigation of additively manufactured metal cutting behavior through thermomechanical approach.....	68
5.2. Materials and methods	71
5.2.1. Sample preparation	71
5.2.2. Machining tests	73
5.3. Results and discussion	74
5.3.1. Evaluation of edge forces and friction coefficient	74
5.3.2. Evaluation of shear stress	77
5.3.3. Evaluation of shear angle	80
5.3.4. Evaluation of cutting constants and the identification of a sliding friction coefficient model	82
5.4. Conclusion	85
6. FUTURE WORK	86
References	88
APPENDIX	101

LIST OF FIGURES

Fig. 3-1: Experimental set-up	28
Fig. 3-2: Flank wear under all lubricating/cooling methods for cutting speed of a) 60 m/min, b) 120 m/min.....	32
Fig. 3-3: Final (at the end of cutting length of 917.5 mm) tool wear of inserts for all lubricating/cooling methods.....	34
Fig. 3-4: The trend of workpiece temperature measured by thermocouple for all lubricating/cooling methods at the cutting speed of 60 m/min.....	37
Fig. 3-5: a) F_x at the cutting speed of 60 m/min, b) F_y at the cutting speed of 60 m/min, c) F_x at the cutting speed of 120 mm/min, and d) F_y at the cutting speed of 120 m/min under all lubricating/cooling methods.....	40
Fig. 3-6: a) R_a at the cutting speed of 60 m/min, b) R_z at the cutting speed of 60 m/min, c) R_a at the cutting speed of 120 mm/min, and d) R_z at the cutting speed of 120 m/min under all lubricating/cooling methods.....	42
Fig.4-1: The morphology and size of Inconel 718 powders. a) SLM powder b) DED powder	46
Fig.4-2: a) Working principle of DED process b) hybrid additive/subtractive hybrid machine using DED c) Working principle of SLM process d) SLM machine.....	48
Fig. 4-3: a) Experimental setup of the machining tests b) Schematics of the methods c) position of thermocouples fitted into the workpiece.....	49
Fig. 4-4: Flank wear under all lubricating/cooling methods for a) As-built SLM, b) Heat-treated SLM.	51
Fig. 4-5: Flank wear under all lubricating/cooling methods for a) DED, b) Heat-treated DED	52
Fig. 4-6: a) F_x during machining of as-built SLM, b) F_y during machining of as-built SLM, c) F_x during machining of heat-treated SLM, and d) F_y during machining of heat-treated SLM under all lubricating/cooling methods.	54
Fig. 4-7: a) F_x during machining of as-built DED, b) F_y during machining of as-built DED, c) F_x during machining of heat-treated DED, and d) F_y during machining of heat-treated DED under all lubricating/cooling methods.	55
Fig. 4-8: Measured temperatures during milling under different lubricating/cooling methods.	57
Fig. 4-9: a) R_a during machining of as-built SLM samples, b) R_z during machining of as-built SLM samples, c) R_a during machining of heat-treated SLM samples, and d) R_z during machining of heat-treated SLM samples under all lubricating/cooling methods.	58
Fig. 4-10: a) R_a during machining of as-built DED samples, b) R_z during machining of as-built DED samples, c) R_a during machining of heat-treated DED samples, and d) R_z during machining of heat-treated DED samples under all lubricating/cooling methods.	59
Fig. 4-11: SEM image of the generated surface in the machining of as-built SLM under different machining strategies.....	60
Fig. 4-12: The normalized XRD patterns of (a) machined as-built SLM, (b) machined HT-SLM, (c) machined as-built DED, and (d) machined HT-DED under different cooling/lubrication conditions.	63

Fig. 5-1: Schematic of orthogonal cutting and the cutting force diagram	68
Fig. 5-2: The morphology and size of Inconel 718 powders. a) SLM powder b) DED powder	72
Fig. 5-3: a) Working principles of DED process, b) Working principles of SLM process, c) The illustration of SLM manufactured Inconel microstructure, d) The illustration of DED manufactured Inconel microstructure.	73
Fig. 5-4: Friction coefficient of nickel alloy 718 in hybrid manufacturing compared to machining of the wrought samples. a) at the feed rate of 0.02, b) at the feed rate of 0.04, c) at the feed rate of 0.06, d) at the feed rate of 0.08 (mm/rev).	77
Fig. 5-5: Comparison of the friction coefficient between dry and wet orthogonal cutting of SLM Inconel 718. a) at the feed rate of 0.02, b) at the feed rate of 0.04, c) at the feed rate of 0.06, d) at the feed rate of 0.08 (mm/rev).	77
Fig. 5-6: Shear stress of nickel alloy 718 in hybrid manufacturing compared to orthogonal cutting of the wrought samples for cutting speeds of a) 30 m/min b) 60 m/min c) 90m/min.	79
Fig. 5-7: Comparison of the shear stresses between dry and wet orthogonal cutting of SLM Inconel 718 for cutting speeds of a) 30 m/min b) 60 m/min c) 90m/min.	79
Fig. S0-1: The specific scenarios of heat treatment method	101
Fig. S0-2: The surface of manufactured AM parts a) as-built SLM, b) HT-SLM, c) as-built DED, d) HT-DED.	102
Fig. S0-3. Hardness value of as-built and heat-treated additively manufactured parts.	102
Fig. S0-4: SEM image of the generated surface in the machining of as-built SLM under Wet (a-d), MQL (e-h), CO ₂ (i-l), LN ₂ (m-p), CO ₂ MQL (q-t), LN ₂ MQL (u-x).	103
Fig. S0-5: SEM image of the generated surface in the machining of HT-SLM under Wet (a-d), MQL (e-h), CO ₂ (i-l), LN ₂ (m-p), CO ₂ MQL (q-t), LN ₂ MQL (u-x).	104
Fig. S0-6: SEM image of the generated surface in the machining of as-built DED under Wet (a-d), MQL (e-h), CO ₂ (i-l), LN ₂ (m-p), CO ₂ MQL (q-t), LN ₂ MQL (u-x).	105
Fig. S0-7: SEM image of the generated surface in the machining of HT-DED under Wet (a-d), MQL (e-h), CO ₂ (i-l), LN ₂ (m-p), CO ₂ MQL (q-t), LN ₂ MQL (u-x).	106

LIST OF SYMBOLS

F_t	Measured tangential force
F_f	Measured feed force
F_{tc}	Shear force in the tangential direction
F_{fc}	Shear force in the feed direction
F_{te}	Edge force in the tangential direction
F_{fe}	Edge force in the feed direction
r_c	Chip ratio
ϕ_c	Shear angle
α_r	Rake angle
τ_s	Shearing stress
F_s	Shearing force
A_s	Shear plane area
β_a	Friction angle
μ_a	Friction coefficient
A	Yield stress at the reference temperature and strain rate
B	Coefficient of strain hardening
n	The exponent of strain hardening
C	Coefficient of strain rate hardening
m	Thermal softening exponent
ε	True strain
$\dot{\varepsilon}^*$	Dimensionless strain rate
b	Width of cut
h	Depth of cut
V	Cutting speed
γ	Shear strain
$\dot{\gamma}$	Shear strain rate

$\dot{\gamma}_0$	Reference shear strain rate
T	Absolute temperature
T_m	Melting temperatures
T_r	Reference temperatures

1. INTRODUCTION

The positive effects of cutting fluids on the machinability performance are well known in machining industry. However, it is also known that their use causes environmental and health problems. Moreover, manufacturers are faced with strict environmental regulations in order to employ dry machining, which is not efficient especially in machining of difficult-to-cut materials such as titanium alloys. Therefore, machining industry developed alternative green machining solutions such as minimum quantity of lubrication, vegetable based cutting fluids, cryogenics and hybrid cooling (combination of cryogenics and minimum quantity of lubrication). Up to now, no work has been documented in the literature on comparison of cryogenics and hybrid cooling with minimum quantity of lubrication. Furthermore, as no information regarding the effects of hybrid cooling on workpiece temperatures during milling of titanium alloy is available, this research aims to demonstrate the feasibility of implementing cryogenics and hybrid cooling method in slot milling of titanium alloy. Thus, the aim of this experimental study was to determine the machining performance of titanium alloy under various green lubricating/cooling methods. In order to do so, minimum quantity of lubrication, cryogenic cooling by spraying liquid nitrogen, cryogenic cooling by spraying carbon dioxide, simultaneous spraying of carbon dioxide and minimum quantity of lubrication, and simultaneous spraying of liquid nitrogen and minimum quantity of lubrication were applied during slot milling process under different cutting speeds. The performance of these methods was evaluated by measuring tool wear, temperature, cutting forces and surface roughness. The results showed that the efficiency of cryogenic cooling was based on the cutting speed where better results were obtained at higher speeds. It was also concluded that the simultaneous spray of cryogenic fluid and minimum quantity of lubrication improved the machinability of titanium alloy as compared to only spray of cryogenics because of both lubricating and cooling effects. In terms of environmental impact of machining operations, hybrid cryogenic methods offer an efficient solution to improve the process sustainability towards cleaner production since the coolant volume is reduced substantially compared to conventional cooling methods decreasing pollutants, and lung and skin diseases experienced by the workers in production facilities.

Although additive Manufacturing technologies offer fabrication of highly complex parts while reducing energy and material consumption, the manufactured parts using this technology generally have poor surface quality. Since low machinability of hard-to-cut additively manufactured materials, a synergistic approach using advantages of additive

manufacturing and machining processes is needed. This study investigates high-speed machining of additively manufactured for Inconel 718 nickel alloys using hybrid cryogenic cooling methods for machinability. For the first time, a comprehensive study has been presented to compare the synergistic effect of hybrid cooling and lubrication strategies in high-speed milling of additively manufactured parts produced by laser powder bed fusion (L-PBF) and directed energy deposition (DED).

Although highly complex parts can be produced using additive manufacturing processes, the resulting surfaces usually have poor quality. Therefore, post-processing is necessary to improve the surface quality after additive manufacturing processes using machining operations. Moreover, a synergistic approach of integrating additive and machining processes offers many benefits over additive manufacturing and machining alone, such as precision manufacturing, finishing complex internal features, repairing and finishing damage parts. Up to now, no work has been documented in the literature on the fundamental understanding of material deformation and friction during hybrid additive and subtractive manufacturing process. For the first time, the fundamentals of material deformation behavior in dry and wet hybrid manufacturing conditions are studied using shear stress, shear angle, and friction coefficient. Although the Johnson-Cook (JC) model has been widely used model to determine material constants, the Johnson-Cook constitutive law may not properly represent the material behavior in hybrid additive and subtractive manufacturing process. Here, a dual-zone thermomechanical model is applied in hybrid metal additive and subtractive manufacturing process. Using this model, a few orthogonal cutting experiments are needed to directly identify the parameters of the material model and the friction coefficient. Then, the Johnson-Cook constitutive equation and analytical models for prediction of the sliding friction have been determined for Inconel 718 under additive and machining conditions manufactured by laser powder bed fusion and direct energy deposition processes. Moreover, all the results are compared with the cutting of wrought material. The huge differences in the friction and material model between the hybrid manufacturing and the machining of wrought nickel alloy 718 showed the significant requirement of the material calibration for hybrid manufacturing. The results presented in this study can contribute to understanding and modeling of the hybrid manufacturing processes.

This thesis addresses challenges in the machining industry and additive manufacturing field, with a focus on environmental sustainability, surface quality improvement, and understanding material behavior in hybrid processes. It consists of three key chapters that contribute to

advancements in science and technology. Chapter 3 examines eco-friendly hybrid cooling methods in slot milling of titanium alloy. The study evaluates alternative solutions to traditional cutting fluids, such as cryogenic cooling and simultaneous spray of cryogenic fluid and minimum quantity of lubrication. The findings demonstrate the benefits of these methods in mitigating environmental and health problems associated with cutting fluids, contributing to cleaner production practices. In Chapter 4, high-speed machining of additively manufactured Inconel 718 using hybrid cryogenic cooling methods is investigated. The study compares various cooling and lubrication strategies, focusing on improving machinability and surface quality in parts produced by laser powder bed fusion (L-PBF) and directed energy deposition (DED). This research offers practical guidance for enhancing the machining of additively manufactured parts. Chapter 5 explores the machining behavior of Inconel 718 in hybrid additive and subtractive manufacturing. The study delves into material deformation and friction in these processes, utilizing a dual-zone thermomechanical model to gain a deeper understanding. By determining material parameters and friction coefficients, the research enhances the modeling and optimization of hybrid manufacturing processes. Overall, this thesis provides practical solutions for the machining industry, improves surface quality in additive manufacturing, and advances the understanding of hybrid manufacturing processes. It has the potential to influence industry practices, promote sustainability, and guide future developments in machining and additive manufacturing.

2. LITERATURE REVIEW

Titanium (Ti) and its alloys are extensively employed in the medical and aerospace industries owing to their superior properties such as high strength, light weight, high corrosion and wear resistance. However, Ti alloys are well known as difficult-to-cut materials as their machinability is poor compared to many other engineering materials such as aluminium and steel. Poor machinability of Ti alloys is due to the low thermal conductivity of these materials, which causes high cutting temperature during machining process, and thus excessive diffusive wear is observed as a result of this high temperature (Park et al., 2015). Therefore, machinability of Ti6Al4V is improved by flooding cutting fluids to the working zone has been studied by researchers (Yong et al., 2011). However, it is known that the cutting fluids generally include mineral oil and additives such as chlorinated paraffin, fatty material, free sulphur, phosphorus compound and sulphurized oil (Gajrani et al., 2019), which negatively affects the environment and workers' health (Faga et al., 2017; Pereira et al., 2017). These additives react with workpiece material and cutting tool, forming metal chlorides, phosphates and sulphides which are harmful to human health (Gajrani et al., 2019). In manufacturing facilities with many machine tools, produced high volume of hot chips causes cutting fluids to evaporate contaminating the air. Owing to the increasing environmental consciousness and strict regulations (Dureja et al., 2015), it is mandatory to take into consideration new green cooling/lubricating methods. One of the alternatives to mineral based cutting fluids is to use small amount of biodegradable oil with a reduced flow rate, which is called minimum quantity lubrication (MQL) an extensively employed method in machining industries for about 2 decades. Although MQL has good lubrication properties, its cooling properties are poor (Pereira et al., 2017). Therefore, machining industry has developed a cryogenic cooling which injects a liquefied gas in the cutting region to provide better cooling (Jawahir et al., 2016). When cryogenic cooling is implemented, no contaminants are left on the workpieces and chips, thus resulting in the reduction of the chip disposal costs and diminishing breath and skin diseases for the operators. Moreover, it can help reducing the cleaning stages before the final sterilization at the manufacturing of surgical prostheses. During the cleaning stage, the finished parts are washed by consuming a significant amount of electrical energy, water and chemical reagents thus increasing the operation time (Bordin et al., 2017). Cryogenic cooling or MQL have been implemented during the machining of difficult-to-cut materials to enhance tool life and surface quality by reducing the working zone temperature (Aramcharoen, 2016). The majority of the studies about cryogenic cooling are focused on the turning process employing various workpiece materials such as Ti6Al4V

(Rotella et al., 2014), AISI 304 stainless steel (Pereira et al., 2016), magnesium (Dinesh et al., 2017, 2015), Inconel 718 (Iturbe et al., 2016), nimonic (Chetan et al., 2016). However, the studies about cryogenic cooling in milling of Ti alloys are very limited. Owing to the intermittent nature of milling operation, the experience obtained from turning cannot be directly applied to milling. Controversial results about the effect of cryogenic cooling on the performance of milling process have been presented in the literature. Nalbant and Yildiz (2011) reported that cryogenic cooling by spraying liquid nitrogen (LN₂) had no positive effect on the performance in milling of AISI 304 material in comparison to dry milling. Yong et al (2011) used dry, wet, MQL and nitrogen gas jet during milling of Ti6Al4V alloy and the effectiveness of these cooling/lubricating techniques were evaluated with respect to the surface roughness and cutting force. In general, the lowest cutting force and surface roughness were obtained with wet machining and nitrogen gas jet. Cryogenic cooling caused 33% reduction in the average arithmetic surface roughness (Ra) and 40% reduction in mean peak-to-valley height (Rz) in comparison to dry machining at very early stages of milling (machining length of 0-50 mm). When machining length was increased to 250 mm during milling of Inconel 718, significantly higher surface roughness values were measured as compared to dry condition (Shokrani et al., 2012). Tyler and Schmitz (2014) found that cryogenic cooling with carbon dioxide (CO₂) resulted in shorter tool life as compared to MQL due to the catastrophic failure caused by thermal fatigue cycling during milling of Hastelloy X alloy. Pereira et al. (2015) determined the tool life in milling of Inconel 718 by employing five different cooling/lubricating techniques (cryogenic CO₂, MQL, combining cryogenic CO₂ and MQL, dry and wet). The longest tool life was obtained under wet machining and followed by combining cryogenic with CO₂ and MQL conditions. However, the advantage of using cryogenic cooling in milling was also reported in the literature. Very low temperature of liquefied gases not only enhances the machinability but also allows to use higher cutting speeds improving productivity in milling of Inconel 718 (Shokrani et al., 2012). Cryogenic cooling with LN₂ gave positive results by increasing cutting speed from 10 m/min to 120 m/min as compared to an application of oil based coolant during milling of Udimet 720 (a nickel-based alloy) material (Truesdale and Shin, 2009). The performance of dry, flooding, nitrogen-oil-mist, compressed cold nitrogen gas at 0 and -10°C, and compressed cold nitrogen gas and oil mist were compared in milling of Ti6Al4V alloy by evaluating the tool life. Experimental results showed that the highest tool life was achieved with compressed cold nitrogen gas and oil mist (Su et al., 2006). In milling of Ti6Al4V, the order of better machinability had derived as CO₂, flood cooling and MQL in terms of chip

analysis, cutting force, cutting temperature, residual stress, surface roughness and tool wear (Jamil et al., 2020). In milling of hardened AISI H13 tool steel, cryogenic cooling with LN₂ decreased the cutting temperature, flank wear, cutting forces and surface roughness in comparison to dry and wet machining. However, Ravi and Kumar concluded that the cooling effect of LN₂ decreased when the cutting speed increased (Ravi and Pradeep Kumar, 2011). Cryogenic cooling with LN₂ in the milling of hardened AISI D3 tool steel reduced the cutting temperature by 43-48% and 26-35% as compared to dry and wet machining due to higher penetration and cooling effects. These researchers also found that cryogenic cooling with LN₂ decreased the mean cutting force by 40-50% and 22-39% in comparison to dry and wet machining, respectively, and it reduced flank wear by 23-32% and 15-25% in comparison to dry and wet machining, respectively. A better chip breakability by lowering chip temperature was observed by applying cryogenic cooling with LN₂, which improved the surface finish (Ravi and Kumar, 2012). It was reported that cryogenic cooling with LN₂ resulted in the reduction of tool wear and temperature, less friction at the secondary deformation zone and lower energy consumption as compared to dry and conventional oil-based coolant conditions during milling of Inconel 718 alloy because of better lubrication effect (Aramcharoen and Chuan, 2014). (Joseph M Flynn et al., 2016) compared the performance of cryogenic cooling with flooding and dry condition in milling of Ti6Al4V alloy. It was concluded that extremely low temperatures in cryogenic cooling reduced the chemical reactivity between tool and workpiece materials and decelerated thermally induced tool wear. Cryogenic cooling increased the tool life up to three-fold in comparison with flooding and reduced surface roughness by 30 and 40%, respectively, as compared to dry and flooding conditions (Shokrani et al., 2016a). Lower surface defects were observed in the samples milled with cryogenic LN₂ cooling as compared to dry and flood conditions. Their investigation showed that cryogenic cooling improved surface integrity and final part quality, but they mentioned further investigation was needed to identify the effect of cryogenics on tool wear and tool life in end milling of hard materials (Shokrani et al., 2016b). Surface integrity was also influenced by the cryogenic cooling. In milling of aluminium-lithium alloy, residual stresses under cryogenic cooling with LN₂ were found to be less than those under dry machining (Zhang et al., 2015). Lee et al., (2015) conducted milling of titanium alloy (Ti6Al4V) under three machining environments: dry, cryogenic and the combination of the cryogenic cooling and preheating of the workpiece. It was concluded that the combination of the cryogenic cooling and preheating of the workpiece improved the tool, thus this approach can also be considered as a clean manufacturing method. Augspurger et al., (2019) presented an analytical model to

quantify the influence of CO₂ cooling in the milling of Ti6Al4V. They found that model and measurement gave good accordance. The cryogenics showed the marginal effects during machining of different materials and also when applied different cutting conditions. Here, a question comes up why in some cases cryogenic coolants have less impact on machinability. On the one hand, the cooling and lubrication characteristics of each supply can be the main reasons for their effectiveness on machinability. On the other hand, high cutting speeds are better to analyze the cooling/lubrication effects, since similarly cryogenic LN₂ showed less impact on high speed milling in literature. In order to investigate effects of cooling/lubrication for cryogenics, it is needed to take into consideration both cryogenic LN₂ and CO₂, as well as hybrid LN₂ and hybrid CO₂ in a single experiment for normal and high speed milling. Furthermore, using MQL can compare mainly lubrication method with the mainly cooling and lubri-cooling methods.

MQL method provides lubrication between the cutting tool and the workpiece while cryogenic method provides only cooling. Therefore, combination of cryogenic and MQL (hybrid method) were also employed to enhance both lubrication and cooling performance during milling. Park et al., (2015) employed various cooling/lubricating methods namely, flooding, MQL with nano particle (hexagonal boron nitride), external cryogenic, internal cryogenic and the combination of both MQL with nano particle and internal cryogenic during milling of Ti6Al4V alloy. It was found that the combination of MQL with nano particle and internal cryogenic cooling outperformed the conventional flooding in terms of tool life and cutting force. The combination of cooling and lubricating enhanced the tool life by up to 32% as compared to conventional flooding method. In another study (Park et al., 2017) conducted the experiments under dry, wet, MQL with and without exfoliated graphite nano-platelets and cryogenic cooling with LN₂ in the milling of Ti6Al4V alloy. Results demonstrated that both MQL and cryogenic cooling enhanced the performance with respect to dry and wet milling. However, cryogenic cooling resulted in the thermal gradient on the tools and the increment in the hardness of workpiece material during milling, which caused excessive wear and micro-fracture and the increase in the cutting forces. The lowest cutting force was measured with the simultaneous spray of cryogenic fluid and MQL oil. MQL with exfoliated graphite nano-platelets gave the lowest tool wear value. More recently, (Bagherzadeh and Budak, 2018) proposed CMQL as a new and an alternative method of cryogenic supply to enhance machinability, productivity and final part quality in machining of hard-to-cut materials. They investigated different cooling and lubricating strategies, and then they proposed a new

combined method of cooling/lubrication as well as a modified cryogenic supply to improve effectiveness of the cutting process. It was concluded that in the high speed machining of Ti6Al4V and Inconel 718, single cooling or lubricating method is not effective as much as the hybrid method and the effectiveness of hybrid methods depend on the cutting material. They reported that the cooling and lubricating of the cutting process should be balanced using different strategies and CMQL enhanced the tool life and surface finish, and reduced the cutting temperature and process forces (Bagherzadeh, 2018). It was declared that hybrid method combining CO₂ and MQL was more advantageous in comparison to flood cooling and MQL in milling of Ti6Al4V (Gross et al., 2019; Hanenkamp et al., 2018). Bergs et al. (2019) designed a single channel system to implement CO₂ and MQL simultaneously in milling of Ti6Al4V. The longest tool life was obtained with a single channel system as compared to two channel system and flood lubrication.

Based on the literature review, it can be seen that limited studies were conducted on the milling of Ti6Al4V with hybrid cooling. Furthermore, there is no information on the effectiveness of hybrid cooling on the temperature during milling of Ti6Al4V. The current study aimed to fill the gap in this field. The original contribution of this study is to compare the performances of several lubricating/cooling strategies during milling of Ti6Al4V. Up to now, no study on the comparison of MQL, CO₂, LN₂ and hybrid cooling (MQL and cryogenics) during milling of Ti6Al4V was reported. Therefore, in the current study, the effects of various green lubricating/cooling methods on tool wear, temperature, cutting forces and surface roughness are studied in milling of Ti6Al4V alloy at different cutting speeds. MQL, cooling by spraying LN₂ and CO₂, simultaneous spraying of CO₂ and MQL, and simultaneous spraying of LN₂ and MQL were applied during milling. Thus, the performances of cryogenic cooling and hybrid method were determined and compared with MQL in milling of Ti6Al4V alloy. Finally, the performance of hybrid CO₂+MQL and LN₂+MQL methods was compared and the reasons for the differences were explained in detail. It is very important to conduct the experiments taking into consideration all possible lubricating/cooling strategies to achieve the best choice. The novelty of current study is to compare all possible eco-friendly coolant alternatives to identify the best one for Ti6Al4V by taking tool wear, temperature, cutting force and surface roughness into account. In addition, this study was related to a notable intention to reach a higher eco-efficiency of milling process by proposing the improvement of cooling/lubrication and production speed in the Ti6Al4V cutting, which is one of the hard to cut materials and the most used energy during the cutting.

Metal additive manufacturing (MAM) technology offers several advantages in comparison to the conventional manufacturing processes, such as easy prototyping, reduction in manufacturing lead time and waste material, and more importantly, the capability of manufacturing components with complex geometries (Oliveira et al., 2020b, 2020a; Sing et al., 2021; Sing and Yeong, 2020; Tan et al., 2020a). Laser powder bed fusion (L-PBF) and Direct energy deposition (DED) as a popular subset of MAM are already being increasingly used in functional part production in various industries from automotive to aerospace (Avila et al., 2020; Bandyopadhyay et al., 2019b; Do and Li, 2016; Isik et al., 2020a; Loh et al., 2014; Yap et al., 2016).

Laser-powder bed fusion (L-PBF) or Selective Laser Melting (SLM) process, also known as or direct metal laser melting (DMLM), is one of the most common metal-based additive manufacturing processes (Papadakis et al., 2014; Song et al., 2019; Tan et al., 2017). SLM uses a focused laser beam to selectively melt the subsequent layer in a powder bed, creating the AM part layer-by-layer (Lam et al., 2015; Torres-Carrillo et al., 2020; Yi et al., 2020). In the process, the size of the parts that can be produced depends on the chamber size of SLM machines (Komarasamy et al., 2019a; Song et al., 2019). Usually, the fabricated parts using SLM have poor mechanical properties and high geometrical accuracy; nevertheless, actual build time could take longer depending on the size and the complexity of the part (Zhu et al., 2019). In the DED processes, also known as laser metal deposition (LMD), laser engineered net shaping (LENS), laser cladding, ultra-high frequency pulsed wire arc melting or pulsed-gas metal arc welding (P-GMAW), a laser beam or ultra-high frequency pulse/gas-pulse melts the powder/wire feedstock and is deposited layer-by-layer to form the AM part (Ke et al., 2022; Peng et al., 2019; Rodrigues et al., 2021; Singh et al., 2020; Wolff et al., 2019). Although DED can manufacture parts much quickly, DED-manufactured parts have rougher surface and less geometrical accuracy than SLM-manufactured parts. DED process can also be used for part restoration and surface cladding (Godec et al., 2021a). Despite all the benefits that metal additive manufacturing processes such as SLM or DED can offer, additively manufactured parts still have various limiting factors such as poor dimensional accuracy, unsatisfactory surface quality, poor uniformity, and residual stresses while noting that also processing with traditional fabrication methods combining heat treatments would give rise to formation of residual stress. Therefore, additively manufactured parts almost always require consequent post-process finishing and/or post-heat treatment to achieve the desired properties (Al-Rubaie et al., 2020; Joseph M. Flynn et al., 2016).

The investigation of heat-treatment effects on machining processes, microstructure and properties of the fabricated parts is of fundamental significance to have a better understanding in order to develop optimized production methods. Inconel 718 is a Ni-based superalloy strengthened primarily by γ'' -Ni₃Nb and γ' -Ni₃(Ti, Al). It has been widely used in high-temperature applications because of its excellent mechanical and chemical properties under extreme mechanical and temperature conditions (Cheng et al., 2016; Isik et al., 2019). Due to the nature of additively manufactured parts, heat treatment is usually applied to enhance the microstructure and the mechanical properties of Inconel 718; the usual heat treatment applied to Inconel 718 to enhance their properties are 1) homogenization, 2) solid solution, and 3) precipitation hardening, resulting in different effects on the microstructure and mechanical properties of Inconel 718 (Fayed et al., 2021; Tucho and Hansen, 2019). The application of the homogenization and solid solution treatments are realized at the temperatures ranging between 980-200 °C to dissolve unfavorable phases, for example Laves phases, δ phase precipitates and to release age-hardening elements into the γ matrix (Fayed et al., 2021). The realization of the precipitation hardening treatment is done in two consecutive steps for precipitating the strengthening phases (γ' and γ'' phases). The first step is applied at a temperature range between 704-899 °C whereas the second step is realized at a temperature ranging between 593-704 °C (Tucho and Hansen, 2019). There has been already conducted studies regarding the application of heat treatments on Inconel. For example, the application of two or three steps post-heat treatment methods has been investigated (Yu et al., 2020). In this study, after homogenization, solution and then ageing treatment of AM Inconel 718, it was found that micro-segregation completely eliminated, laves phase mostly disappeared, and abundant γ''/γ' phases precipitated in bimodal recrystallized grains. Additively manufactured samples show the finest fatigue striations and the maximum resistance to crack growth in comparison to other samples namely as-fabricated, heat-treated using direct aging, heat-treated employing solution treatment plus aging (Yu et al., 2020).

Recently, the machining of additively manufactured components has been studied as a mandatory step of additive manufacturing processes (Brown et al., 2018a; Lopes et al., 2020; Oyelola et al., 2018). The microstructures and mechanical properties of Inconel 718 alloy built with different production methods are unusually dissimilar (Al-Rubaie et al., 2020) resulting in different machinability though there are exceptions in some cases, such demonstrated by Lopes et al. (Lopes et al., 2020), machining performance is more sensitive to machining parameters such as cutting speed and feed rate rather than influence of the

mechanical property of the as-built part. By judging these, therefore, the machining strategies suitable for the conventionally manufactured parts is not certain to success when applied to the additively manufactured parts. Nonetheless, it has been found that synergistic additive and subtractive strategy is critical for improving energy and material efficiency (Peng et al., 2018). Investigations on the machining of AM Inconel 718 in the literature are rare. Although the hybrid additive/subtractive systems can offer increased energy and material efficiency, the resulting low machinability of Inconel 718 causes long processing times. Therefore, alternative high-speed-machining strategies of AM Inconel 718 are crucial for optimization of the hybrid additive/subtractive process, thereby enhancing efficiency, productivity as well as sustainability.

In our recent work, a novel sustainable machining strategy, employing frozen oil particles (CMQL) has been introduced to improve the high-speed machining of hard-to-cut materials such as Inconel 718 (Bagherzadeh, 2018b; Bagherzadeh and Budak, 2018b). It was reported that in the high speed machining of hard-to-cut materials, the supply of frozen oil particles balanced the lubricating and cooling of the machining process and CMQL showed the most favorable cooling effect considering surface quality, tool wear, cutting forces and environmental impact. More recently, Bagherzadeh et al. (Bagherzadeh et al., 2021a) reported that the hybrid cryogenic and minimum quantity lubrication method (CMQL) enable reliable high-speed machining compared to other cooling methods such as MQL, liquid nitrogen and carbon dioxide leading to enhanced productivity, product quality and cleaner production.

The mechanical properties of the SLM and DED fabricated parts demonstrates differences. This outcome naturally causes experiencing different material behaviors during machining procedure when the same material processed with SLM and DED methods, and are compared. In addition, the variations in cutting force due to material's anisotropy is an important aspect in tool wear and surface quality as suggested by previous scholars (Pérez-Ruiz et al., 2022, 2021a). What is more, using a combination of cooling and lubrication or solely one of those liquids generates different machining response/performance. Hence, to elucidate the impact of additive manufacturing method on a material's machining performance or cooling/lubrication strategies were determined to become main target of the current study. To the best of our knowledge, there hasn't been any work related to hybrid cooling and cryogenics on the subsequent milling of additively manufactured (via SLM or DED) Inconel 718 in the literature. There is no comprehensive study on the comparison of various cooling/ lubrication methods during milling of additively manufactured Inconel 718.

Furthermore, the performances of different machining and cooling strategies on machinability of post-heat-treated additive parts have never been studied.

The present study aims to fill the gap in this field. Therefore, the present novel study analyzes the machinability, surface quality, tool life, cutting temperature, cutting forces, and Inconel 718 phases in high-speed milling of heat-treated and as-built SLM and DED parts in detail taking into consideration of comprehensive lubricating/cooling strategies to achieve the best efficient mechanism of additive/subtractive hybrid manufacturing.

Compared to traditional manufacturing methods, metal additive manufacturing (MAM) technology offers several benefits, such as rapid prototyping, the ability to produce components with intricate geometries, shorter lead times, and reduced waste materials. This results in lower costs and a reduced environmental impact of the manufacturing process. To produce functional parts for a variety of industries, laser powder bed fusion (L-PBF) and directed energy deposition (DED), as a popular subset of MAM, are used more frequently (Bandyopadhyay et al., 2019a; Isik et al., 2020b).

One of the most popular MAM techniques is the L-PBF or selective laser melting (SLM) process, also known as direct metal laser melting (Xie et al., 2021). DED process is sometimes referred to as wire arc additive manufacturing (WAAM), laser metal deposition, laser cladding, and laser engineered net shaping (Chen et al., 2022). Despite much higher production speed of DED compared to SLM, parts produced by DED have less geometrical accuracy and rougher surface. Although the MAM processes and AM products have different merits, AM products still have various limiting factors such as unsatisfactory surface quality, poor dimensional accuracy, non-uniformity, and high residual stresses (Bagherzadeh et al., 2022). To improve their qualities, additively manufactured parts therefore almost always need subsequent post-processing, machining and/or post-heat treatment (Brown et al., 2018b).

Hybrid metal manufacturing processes offer the advantage of achieving a more precise and high-quality finish while simultaneously reducing waste and material usage (Le et al., 2017; Qian et al., 2019). Additionally, these processes can help to reduce energy consumption, making them a more sustainable option compared to traditional manufacturing methods and only AM processes (Liu et al., 2021). Although technological developments in hybrid additive/subtractive manufacturing have resulted in significant progress over the last decades, modeling is still needed to predict and overcome the process limitations. The use of modeling and simulation in the hybrid additive/subtractive manufacturing process of Inconel 718 has

significant potential to improve sustainability by minimizing material waste and energy consumption, ensuring product quality and integrity, and facilitating the adoption of sustainable practices (Ford and Despeisse, 2016; Wippermann et al., 2020). Numerous models for machining have been proposed using analytical (Merchant, 1945) semi-analytical (Budak et al., 1996) and numerical methods (Yen et al., 2004). Analytical models provide fast results, but typically have low accuracy (Williams, 1991). Semi-analytical models, on the other hand, have much better accuracy but require test data for various cutting conditions and cutting tool geometry (Altintas, 2012). Most numerical methods used for metal cutting are based on Finite Element Methods (FEM) (Ceretti et al., 1997). Two important inputs for these models are the material deformation properties and the friction coefficient between the tool and the workpiece material. These two inputs can be considered to be independent of the cutting mechanics as they are related to the mechanical and physical properties of the materials (Wang et al., 2021). Identification of both properties is very critical for accurate modeling of the hybrid additive and subtractive processes.

The JC constitutive relation is a one-dimensional, straightforward model that takes strain, strain rate, and thermal softening effects on the flow stress employing the von Mises yield criterion (Zhang et al., 2022). Nevertheless, the classical methods of obtaining JC parameters, e.g. tensile tests cannot be used to obtain high strain rates required for the metal cutting. Results for the JC parameters determined by non-cutting tests like the Split Hopkinson Bar (SHPB) are usually inaccurate (Ozlu et al., 2009). While SHPB testing are typically limited to values in the range of 10^3 s⁻¹, the strain rates in metal cutting can reach the order of 10^5 s⁻¹. Furthermore, these tests are time consuming and require large space.

Additively manufactured Inconel exhibits variation in JC parameters depending on the specific combination of additive manufacturing parameters and scanning strategies used. The complexity of additive manufacturing processes and the resulting microstructure and properties of the material are impacted by thermal and mechanical interactions (Shakil et al., 2022; Tan et al., 2020b). Laser power, scanning speed, and scanning pattern modifications can affect the material's cooling rate, grain structure, and residual stresses, which ultimately impact deformation and failure behavior. Experimental testing to determine JC parameters is necessary to accurately model the material's behavior in simulations for each specific combination of AM parameters and scanning strategies. Therefore, due to the variation in JC parameters of additively manufactured Inconel, it is essential to develop a simple and reliable in-process experimental method for AM parts that can facilitate the determination of JC

parameters for each specific combination of additive manufacturing parameters and scanning strategies. This will enable accurate prediction of the mechanical behavior of additively manufactured Inconel and enhance the quality control of AM parts.

In a prior research (Budak and Ozlu, 2008a), we proposed using orthogonal tube cutting experiments to calibrate the material model coefficients. This strategy differs from the mechanistic technique in that substantially fewer calibration tests are required. Only a few cutting experiments are required for calibration since the suggested model take into account the effects of the cutting tool rake angle and the feed rate on the cutting process (Ozlu et al., 2009).

Ozlu et al. (Budak and Ozlu, 2008b; Ozlu et al., 2009) proposed an analytical cutting model, which considers the sticking and sliding contact regions on the rake face of the cutting tool and uses JC constitutive model for deformation zones. This model offers both the calibration of JC parameters required for metal cutting and prediction capabilities. The proposed empirical relation is relatively simple to calibrate for a given material, making it a valuable tool for researchers and manufacturers seeking to optimize and improve their manufacturing processes.

Up to now, there is no information on the fundamentals of material deformation behavior and there is no study on the friction model for the synergistic approach of additive manufacturing and machining processes. The current study aimed to fill the gap in this field. Therefore, the effects of AM on the cutting behavior are studied using orthogonal cutting of the SLM, DED, and wrought Inconel 718 as widely used material in different industries. The shear stress, shear angle, and friction coefficients in the machining of AM Inconel 718 material are evaluated using a modeling approach to describe material behavior. It suggests that the temperature has a significant impact on the machining process, implying that the temperature needs to be controlled and optimized to achieve the desired results(Weng et al., 2023). Using a coolant or lubricant can aid in controlling temperature, decreasing tool wear, prolonging tool life, and enhancing the surface finish and dimensional accuracy of the machined part. Nevertheless, it is crucial to carefully choose the suitable coolant or lubricant and machining parameters to attain the intended outcomes(Bagherzadeh et al., 2021b). Therefore, the effect of wet cooling is also assessed. Moreover, the models of calibration and prediction of material constants have been provided. The material constants as well as the identification

model of sliding friction during hybrid additive/subtractive manufacturing have been presented.

3. EXPERIMENTAL EVALUATION OF ECO-FRIENDLY HYBRID COOLING METHODS IN SLOT MILLING OF TITANIUM ALLOY

3.1. Experimental Setup

The milling tests were performed on Mazak Nexus 510C-II milling machine with a maximum spindle speed of 12000 rpm and motor power of 18.5 kW. Ti6Al4V titanium alloy (with a chemical composition of Al = 5.84 wt%, V = 3.88 wt%, Fe = 0.114 wt%, C = 0.013 wt%, N = 0.024 wt%, Ti = Balance) was selected as the workpiece material in the experiments where the workpiece was mounted on the dynamometer (Kistler 9257BA type dynamometer and charge amplifier of Kistler 5233A type) which was clamped on the table. Rectangular blocks of Ti6Al4V were prepared with the dimensions of 132.5 × 183.5 × 12.5 mm. Coarse grain uncoated carbide inserts (Sandvik R390-11 T3 08M-KM H13A) were employed in this study and were clamped on the tool holder (Sandvik R390-012A16-11L) with a single cutting edge at the overhang length of 44 mm (Fig. 1). Uncoated inserts were used to eliminate the effect of coating delamination. Uncoated carbide tools are used commonly in milling of titanium in industry such as in machining of turbine engine disks, blisks, shafts, impellers etc. The coated tools with AlTiN or TiAlN coatings have strong affinity with work material, i.e. Ti. Also, in the literature, it was stated that the coating did not contribute to the tool life in cryogenic milling of Ti6Al4V (Sadik and Isakson, 2017). The insert had a nose radius of 0.8 mm, lead angle of 90° and positive rake angle. The diameter of tool was 12 mm.

Since MQL could remove only a very small amount of heat, temperature related tool wear was high during milling with MQL. Heat transfer coefficient is estimated as 99.1 W/m² °C for compressed air cooling (-20 °C) and 70 W/m² °C for MQL by using finite element simulation (Jiang et al., 2016). In another study, heat transfer coefficient of MQL is found as 204 W/m² °C and this coefficient is 5230 W/m² °C in flood coolant (Kurgin et al., 2012). Therefore, as an alternative to MQL, cooling (employing either CO₂ or LN₂) and hybrid method (simultaneous spraying of CO₂ or LN₂ and MQL) were used in this study to control the temperature effectively during milling. Five different lubricating/cooling methods namely, MQL, only CO₂ spraying, only LN₂ spraying, Cryo-MQL hybrid lubri-cooling method (simultaneous spraying of CO₂ and MQL (CO₂+MQL) and simultaneous spraying of

LN₂ and MQL (LN₂+MQL)) were applied during milling of Ti6Al4V. The distance of nozzle from the tool was adjusted as 15 mm for all lubricating/cooling methods. In MQL system, vegetable oil with freezing point of -39 °C, boiling point of 200 °C and viscosity of 35 mm²/s (UNILUBE 2032 lubricant) was employed and it was sprayed to the working zone at the nozzle angle of 45°, pressure of 6 bar and flow rate of 90 ml/h. The cutting fluids were positioned behind the tool because the cutting edge transfers the cutting fluids to the cutting zone. Furthermore, the cutting edge will be cool down or lubricated when is out of cut. When the nozzles are positioned in front of the tool, there is no chance the cutting fluid enters to the cutting zone when is cutting. Therefore, only the workpiece and the cutting tool's body will be targeted by cutting fluid at this position. In CO₂ spraying experiments, CO₂ cylinders including both gaseous and liquid CO₂ were employed. The pressure in the cylinders was 57 bar. When pressurized liquid CO₂ depressurizes, its temperature drops and produces the mixture of CO₂ snow and CO₂ gas, where the temperature of the CO₂ snow is theoretically -79.05 °C. CO₂ diagram phases shows that CO₂ is a very compressible gas which has important pipe solidification problems. Then, it should be considered that during the transferring CO₂ from tube to the nozzle, do not resist the flow of CO₂ by bending the channels or using the unsuitable nozzles and adaptors. All connection parts were made of insulated, short and smooth stainless steel to resist high pressure, pressure drop and pipe solidification problem in the channel. CO₂ was delivered through a thin nozzle with a diameter of 0.5 mm at the flow rate of 10.8 kg/h. In each experiment, spraying of LN₂/CO₂ was activated before starting the cutting process to use the stable LN₂/CO₂ for the experiment. In cryogenic cooling by spraying liquid nitrogen (LN₂), LN₂ was sent through a nozzle with diameter of 4.7 mm at about 36 kg/h mass flow rate at 15 bar pressure and at the tool-chip interface. A bigger nozzle diameter used for LN₂ supply compared to the one used for CO₂. The usage of nozzles with different diameters has two reasons. If a nozzle used as small as CO₂ nozzle for LN₂ supply, it was not possible to deliver nitrogen in the liquid phase. The very low boiling temperature of LN₂ causes that when the pressure of supply is low, liquid nitrogen changes into the gaseous form in the nozzle with small diameter. In hybrid cooling (CO₂+MQL or LN₂+MQL), CO₂ or LN₂ and MQL were sprayed simultaneously to the working zone using the same conditions in spraying of only CO₂ or LN₂ and MQL.

Experimental conditions selected according to the literature and preliminary tests are summarized in Table 1 whereas the experimental set-up is shown in Fig. 1. As shown in Table 1, feed rate, axial depth of cut and radial depth of cut were kept constant during all

lubricating/cooling methods, while cutting speed was set to two different values since it was reported that the benefit of cryogenic cooling was a function of the cutting speed (Venugopal et al., 2007).

Table 3-1 : Experimental conditions

Lubricating/cooling methods	Cutting speed (m/min)	Feed rate (mm/rev)	Axial depth of cut (mm)	Radial depth of cut (mm)
MQL	60			
CO ₂	60			
LN ₂	60			
CO ₂ +MQL	60			
LN ₂ +MQL	60	0.1	1	12
MQL	120			
CO ₂	120			
LN ₂	120			
CO ₂ +MQL	120			
LN ₂ +MQL	120			

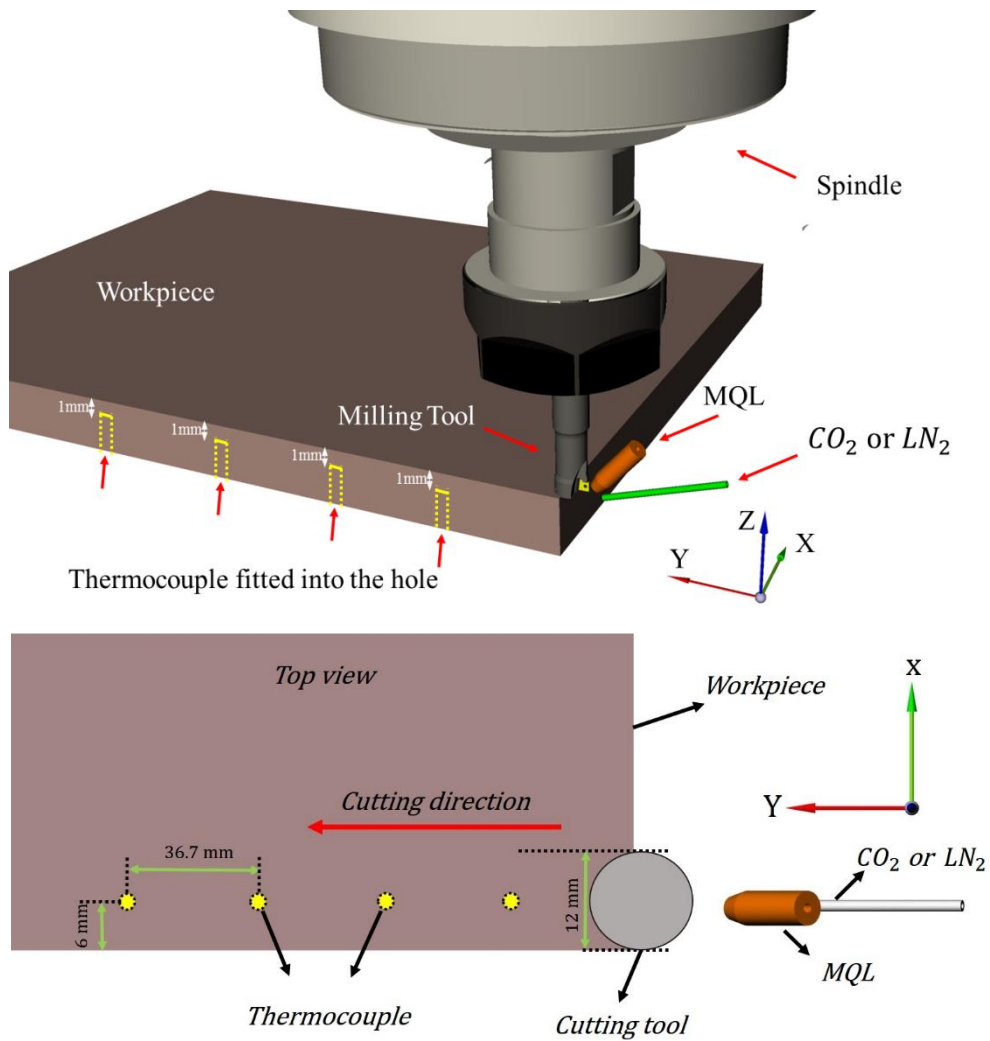


Fig 3-1

Fig. 3-1: Experimental set-up

Flank wear was measured on the flank face of the inserts at constant intervals by Nano Focus μ Surf non-contact 3D profilometer. The tests were interrupted at specified machining intervals in order to identify the progress of the wear. The cutting inserts were examined after

each predetermined feed length (183.5 mm) until they reached the 5th slot (total feed length of 917.5 mm).

To measure the temperature, workpiece materials were drilled with a diameter of 1 mm and four K-type thermocouples (Omega) with a diameter of 0.25 mm were fitted into the holes as illustrated in Fig. 1. The space between the workpiece and thermocouple was filled by a high thermally conductive high temperature cement (Omegabond 600, magnesium phosphate cement powder) in order to enhance the heat conduction. DT9805 data translation device using QuickDAQ software employed to evaluate temperature data. The workpiece temperature under each cooling strategy is measured when the cutting tool is cutting the materials, exactly becomes tangential to the thermocouples. Thus, the sampling of the temperature measurement should be enough to measure the highest temperature in a portion of time. In this experiment, sampling rate of 6000 Hz applied for 360000 scans per second where the samples interval was 0.000166667 second. The temperature value presented in this study was the average of four measurements obtained from four thermocouples fitted into the holes as shown in Fig. 1. This experiment for every cooling strategy was repeated two times.

The cutting forces were measured employing a Kistler dynamometer attached under the workpiece and the force signals were recorded as a real-time at a sampling rate of 2000 Hz by LabVIEW software. Average value of the force obtained in a steady cutting state was taken into consideration for machining forces. Milling forces are periodic in nature, and thus their average values are used. Similar calculation for force components was also implemented in the literature (Goindi et al, 2018; Bolar et al., 2018)

Measurement of surface roughness was conducted with the aid of Mahr PRN10 roughness instrument in the feed direction. In the measurements, cut-off length and sampling number were chosen as 0.8 mm and 5, respectively. Surface roughness was measured at four points on the surface along the machining path and the average value of these measurements was taken into consideration in the analysis.

3.2. Results and Discussion

3.2.1. Tool Wear

Fig. 2 presents the flank wear measurement for all lubricating/cooling environments at the cutting speed of 60 and 120 m/min. Fig. 2 illustrates the final tool wear of inserts for all lubricating/cooling methods. At the cutting speed of 60 m/min, the flank wear increased at a lower rate with the feed length under MQL and LN₂+MQL environments. However, the flank

wear increased rapidly under other environments, especially when applying CO₂. The higher flank wear rate in cryogenic cooling by spraying CO₂ or LN₂ was due to the lack of lubrication and the lack of thermal softening (Truesdale and Shin, 2009). Excessive cooling capability of cryogenics (CO₂ or LN₂) increased the hardness and strength of workpiece material resulting in higher flank wear. With the application of cryogenics (CO₂ or LN₂) and MQL together (hybrid method), the reduction in the tool wear was observed. It is well known that the application of cryogenics increased the hardness and strength of the workpiece (Nalbant and Yildiz, 2011), which negatively influenced the tool wear. Therefore, the lower tool wear of hybrid method as compared to only cryogenics was because of the better lubrication capability of MQL. At the cutting speed of 60 m/min, CO₂+MQL reduced the flank wear by 31.8% as compared to CO₂ and LN₂+MQL decreased the flank wear by 59.6% as compared to LN₂ when the wear after the feed length of 917.5 mm was taken into consideration.

When cutting speed was increased to 120 m/min, the highest flank wear was measured with MQL application. In general, the lower flank wear was achieved with LN₂ and LN₂+MQL environments under this high cutting speed. CO₂, LN₂, CO₂+MQL and LN₂+MQL diminished the flank wear by 35.4, 29.6, 38.9 and 53.6%, respectively in comparison to MQL method when the wear after the feed length of 917.5 mm was considered. The comparison of MQL, hybrid cooling and cryogenic cooling in machining with normal speeds shows that the influence of lubrication is much bigger than cooling effect. Nevertheless, usage of MQL does not have the same application as much as machining with normal speeds. In high-speed machining due to the higher generation of the temperature, oil evaporates or burns rapidly and thus, lubrication characteristic of oil decreases. As explained in chapter two, the lubricants freezing point is at -39 °C. As a result, in hybrid methods, combination of oil and cryogenic supply result in oil cooling and solidification of oil. This effect not only does not decrease the lubrication effect of the oil, but also improves the oil life to reach the working zone and consequently, improves the lubrication effect of the oil as is explained precisely by Bagherzadeh and Budak (2018). In hybrid method, the frozen oil is not directly burning or evaporating, since the portion of transferred temperature to the frozen oil reduces when oil changes from solid state to liquid form. This leads that oil does not reach the boiling point before entering to the working zone. Furthermore, the transition of temperature between oil and cryogenics increases the cryogenics' temperature and lead to control the cooling effect on the tool brittleness in hybrid methods. However, if the generated

cutting temperature is not high enough, the frozen oil provides worse lubrication as is discussed by Bagherzadeh and Budak (2018).

When progress of tool wear under LN₂ and CO₂ at the cutting speed of 60 m/min (Fig. 2a) and 120 m/min (Fig. 2b) were compared, LN₂ totally resulted in higher tool wear at the cutting speed of 60 m/min and lower tool wear at the cutting speed of 120 m/min in comparison to CO₂. Furthermore, temperature measurements of these methods (Table 2) supported that the cooling effect of LN₂ supply was more than CO₂ supply, but extra cooling effect of LN₂ under the lower cutting speed leading lower temperature generation affected the tool wear negatively. This result was due to the increase in the workpiece hardness with the implementation of LN₂. Moreover, since high cutting speed of 120 m/min generated higher temperature compared to 60 m/min, LN₂ showed better effect than CO₂. In addition to the temperature measurements, the higher cutting force with LN₂ compared to CO₂ supports this claim that the reason roots in the lower lubrication effect or/and higher cooling characteristics of LN₂. When environmental impacts of CO₂ and LN₂ are compared, it can be declared that CO₂ is more sustainable than LN₂. CO₂ has low gas expansion value giving lower environmental hazards as compared to LN₂. A healthier, safer, and more sustainable working environment can be achieved by the use of non-toxic CO₂ (Mulyana et al., 2017). From the light of this information, it can be concluded that the selection of more appropriate methods was a trade-off between technological (flank wear) and environmental impact.

Cooling by spraying CO₂ or LN₂ to the machining area had an advantage over MQL in term of tool wear under high cutting speed and this advantage was more intense with the application of hybrid method. It was declared that CO₂ (Jamil et al., 2020) and LN₂ (Chetan et al., 2019) cooling decreased the flank wear in comparison to MQL (Chetan et al., 2019; Jamil et al., 2020) owing to the high coefficient of heat transfer (Chetan et al., 2019). At low cutting speed (60 m/min), tool wear of both CO₂ and LN₂ were found to be higher in comparison to MQL condition. Excessive cooling by spraying CO₂ or LN₂ caused the increase in the brittleness of tool insert material and the increase in the hardness of workpiece material, which affected the tool wear negatively. This negative effect of cryogenic cooling on the tool wear owing to the reduction of lubrication at lower cutting speed was enhanced by applying the combination of MQL and cooling (CO₂+MQL or LN₂+MQL). High velocity and pressure of cryogenics caused better penetration of the lubricant to the tool-chip interface and this better penetration decreased friction thus tool wear reduced. However, with the increase in the cutting speed to 120 m/min, the temperature at the machining zone increased and cryogenic cooling helped the reduction in the temperature. This effect of cryogenic cooling

decreased the tool wear in milling of Ti6Al4V alloy at higher cutting speed. The combination of MQL and LN₂ condition gave the best machining performance in term of tool wear by supplying both cooling and lubrication at higher cutting speed. The lubrication effect of hybrid cooling caused the reduction in temperature and friction during machining owing to the formation of thin lubrication film, and this subsequently decreased the tool wear (Mulyana et al., 2017; Kalita et al., 2012). Though MQL was the most eco-friendly method (Pereira et al., 2016), with LN₂+MQL the tool wear decreased in comparison with MQL. In addition, with this cryogenic method, some advantages such as dry chip generation, minimization of cutting fluid costs and reduction of cutting fluid consumption were obtained (Pereira et al., 2016). Cryogenics evaporate without any waste when they are injected and oil in MQL systems is biodegradable thus, can be negligible. Therefore, taking into consideration of technical and ecological factors, it was concluded that implementation of LN₂+MQL resulted in the equilibrium between ecological and technological factors.

As can be seen in Fig. 2a, progress of tool wear for hybrid LN₂+MQL and hybrid CO₂+MQL at the cutting speed of 60 m/min were similar, but during the feed length of 917.5 mm, tool wear increased rapidly under hybrid CO₂+MQL; however, hybrid LN₂+MQL completely had lower tool wear than hybrid CO₂+MQL at the cutting speed of 120 m/min (Fig. 2b).

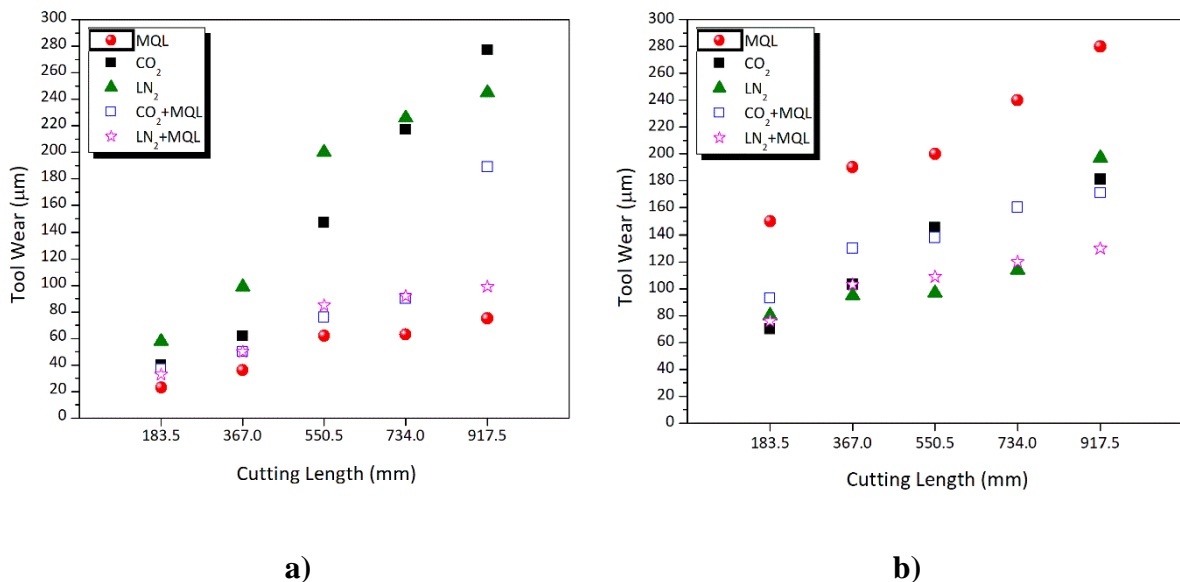
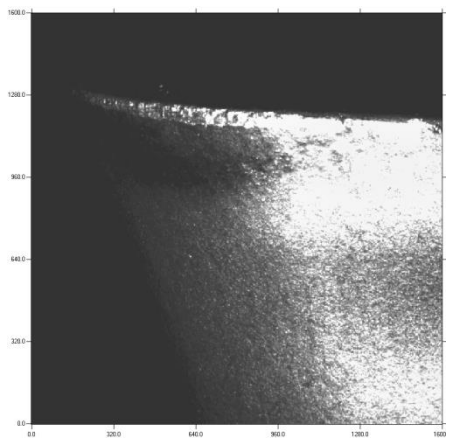
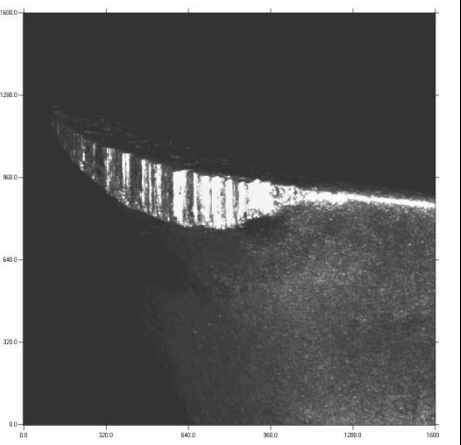
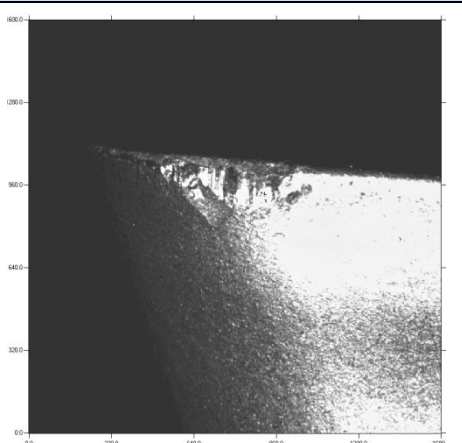
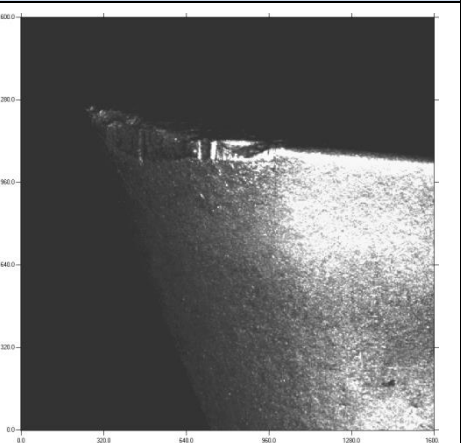
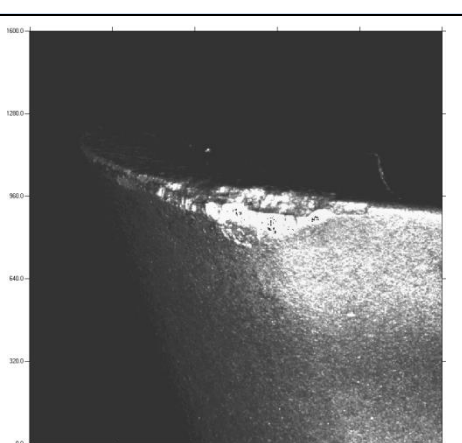
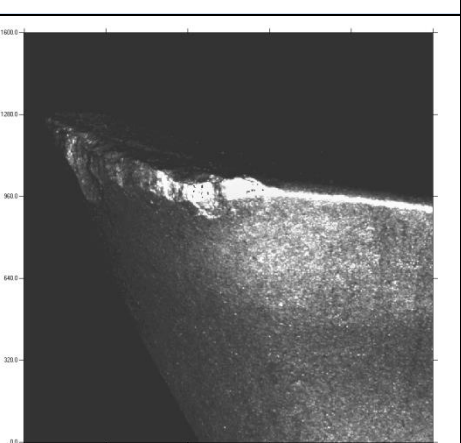


Fig. 3-2: Flank wear under all lubricating/cooling methods for cutting speed of a) 60 m/min, b) 120 m/min.

Lubricating/Cooling Methods	Cutting Speed (m/min)	
	60	120
MQL		
CO ₂		
LN ₂		

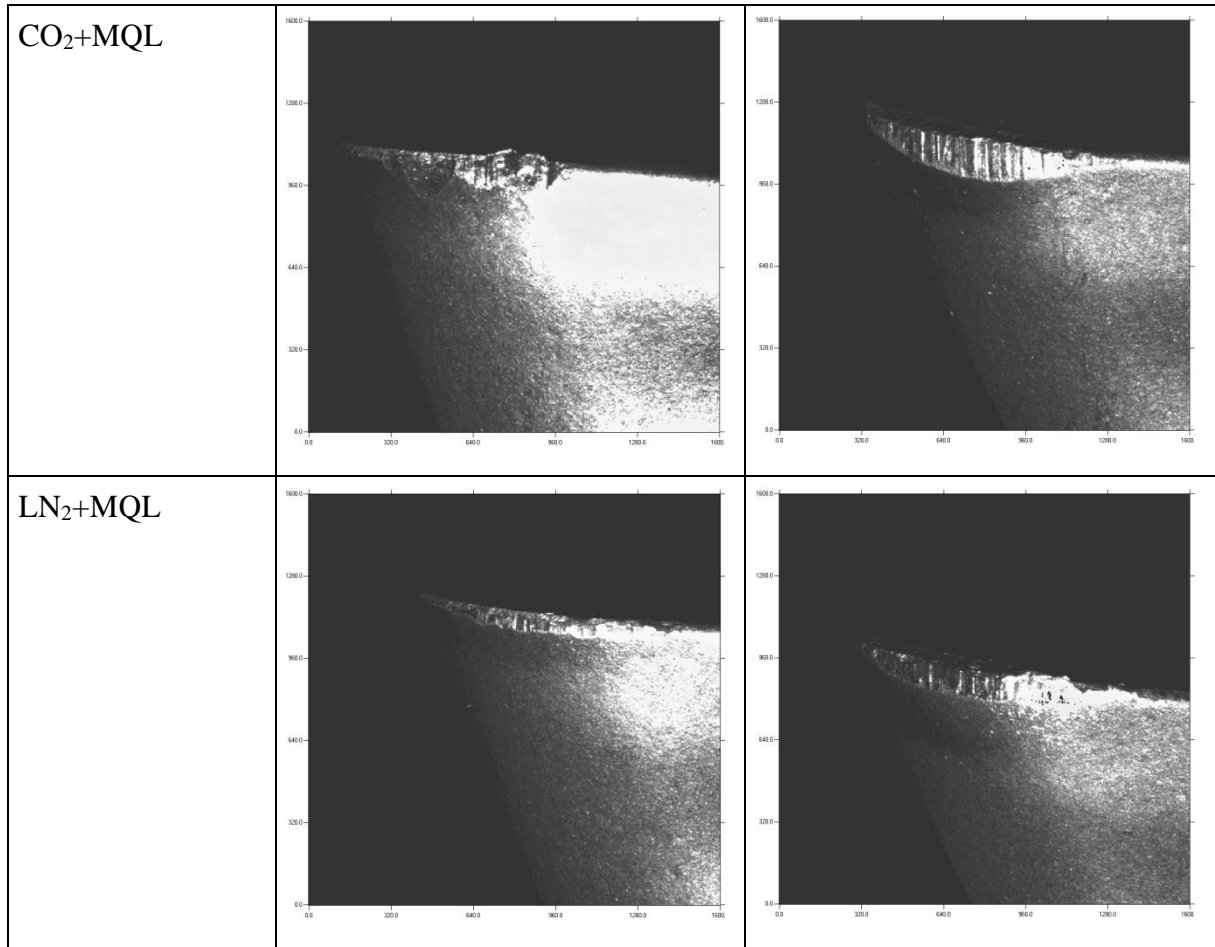


Fig. 3-3: Final (at the end of cutting length of 917.5 mm) tool wear of inserts for all lubricating/cooling methods.

The positive effect of cryogenic cooling on tool wear decreased with decreasing cutting speed. Sadik and Isakson (2017) declared that the performance of cryogenic cooling depended on the cutting conditions and inappropriate cutting conditions eliminated the advantage of cryogenic cooling. These researchers stated that the cryogenic cooling with CO₂ could give up to 6 times longer tool life than flooding method employing the right combination of cutting parameters. Therefore, it is important to find optimum range of cutting parameters to obtain full advantage of cryogenic cooling to enhance productivity (Sadik and Isakson, 2017). In their study, feed per tooth (0.1 and 0.2 mm/tooth), cutting speed (60, 80 and 100 m/min), cooling strategy (emulsion and CO₂) and coating (uncoated and PVD TiAlN coated) were varied with respect to a full factorial design of experiments. They found that the highest tool life was obtained at the cutting speed of 80 m/min and feed of 0.1 mm/tooth under CO₂ environment with coated tools. These researchers also declared that at the highest cutting speed of 100 m/min, the results for moderate (0.15 mm/tooth) and

high (0.2 mm/tooth) feed were nearly same for all combinations of cooling strategy and choice of uncoated or coated inserts.

Predominant wear for all lubricating/cooling environments was observed as flank wear (Fig. 3). The flank wear was found to be more uniform in MQL and LN₂+MQL environments than in the rest of the environments. It was seen that the flaking of tool formed on the flank surface under CO₂ and LN₂ conditions. When only CO₂ or LN₂ was used it had no lubricating property leading to an increment in the friction at the tool-chip interface. This friction resulted in the formation of flaking during milling with cryogenics. No flaking was observed with the simultaneous application of CO₂ or LN₂ and MQL because of the lubrication effect of MQL. Less adhesion was also seen under all lubricating/cooling environments due to the effective cooling of these methods. Mulyana et al. (2017) declared that a low cutting temperature under cryogenic with lubricant condition reduced the adhesion formation. Low temperatures generated because of CO₂ and LN₂ application to the working zone were found to be sufficient to dissipate the heat occurred during machining process, reducing the diffusion mechanism, hence diminishing the formation of adhesion (Sartori et al., 2017). In comparison to MQL, hybrid methods prolonged the tool life. In other words, with hybrid methods less cutting tools will be employed. Considering the benefits from cryogenic LN₂ or CO₂ additions to MQL, the cost of tool materials are significantly higher than the costs of CO₂ or LN₂ thus production costs are significantly reduced with hybrid methods.

3.2.2. Temperature

Fig. 4 shows the trend of workpiece temperature measured by thermocouple at the cutting speed of 60 m/min. The embedded position of thermocouple affects the value of temperature measurement and the position used in this study was given in Fig. 1. Only one temperature graph is demonstrated to show the trend of temperature, and the workpiece temperature of various lubricating/cooling methods with both cutting speeds are reported in detail in Table 2. As shown in Fig. 1, the distance between the holes drilled for the thermocouples is exactly 1 mm away from the unmachined surface. Since the depth of cut is 1 mm, during the cutting, cutting tool becomes tangential to the thermocouples in order and there is no material remains between the thermocouple and cutting surface. Since Ti6Al4V has poor heat conduction, if material remains between the thermocouple and the cutting surface, there will be too much differences between the real generated temperature and measured temperature. As is

displayed in Fig. 4, pre-cooling of the workpiece for each cooling method clearly is shown, when the thermocouples have 1 mm distance to the unmachined surface and the measured temperature before cutting shows the workpiece temperature (MQL=22°C, CO₂=8°C, CO₂+MQL=0°C, LN₂=-16°C, LN₂+MQL=-19°C). The temperature decreased when cryogenic cooling was applied in milling of Ti6Al4V. More temperature reduction with the use of LN₂ was found in comparison to the other cooling/lubricating methods employed in this study. This is owing to the different temperature, latent heat, sensible heat, thermal conductivity, heat capacity, pressure, flow and the different phases of the cooling/lubricating methods. The maximum workpiece temperature in MQL condition reached to 64 °C at the cutting speed of 60 m/min and 68 °C at the cutting speed of 120 m/min. The lower temperature measured for cooling by applying CO₂ or LN₂ was the evidence of the effective penetration of cryogenics into the machining zone. With the application of cryogenic cooling, both the workpiece temperature at the insert tip area and surrounding area reduced. When CO₂ or LN₂ are delivered to the tool-chip interface, they evaporated quickly by absorbing the heat, which reduced the temperature (Ravi and Kumar, 2011). It was also reported that LN₂ in gaseous form penetrated into the machining area more effectively than the conventional liquid coolant and reduced the temperature by decreasing the contact friction between chip tool interface (Jerold and Kumar, 2012). The simultaneous application of cryogenics and MQL outperformed only MQL application in term of workpiece temperature due to the higher cooling efficiency of cryogenics. The temperature of CO₂ with MQL was found to be lower in comparison to CO₂ alone due to the combined effects of low cooling temperature and high lubrication reducing frictional forces on the tool/chip and tool/workpiece interfaces (Mulyana et al., 2017). The temperature of the CO₂, LN₂ and MQL at the outlet of the nozzles respectively was measured as -72°C, -187°C and +19°C, respectively. Nevertheless, in atmosphere temperature of 24°C, when the thermocouples became tangential to the surface after cutting, the measured fluids' temperatures were -51°C, -163°C and +27°C, at speed of 60 m/min respectively. These measurements during cutting speeds of 120 m/min were -41°C, -61°C and +35°C, respectively.

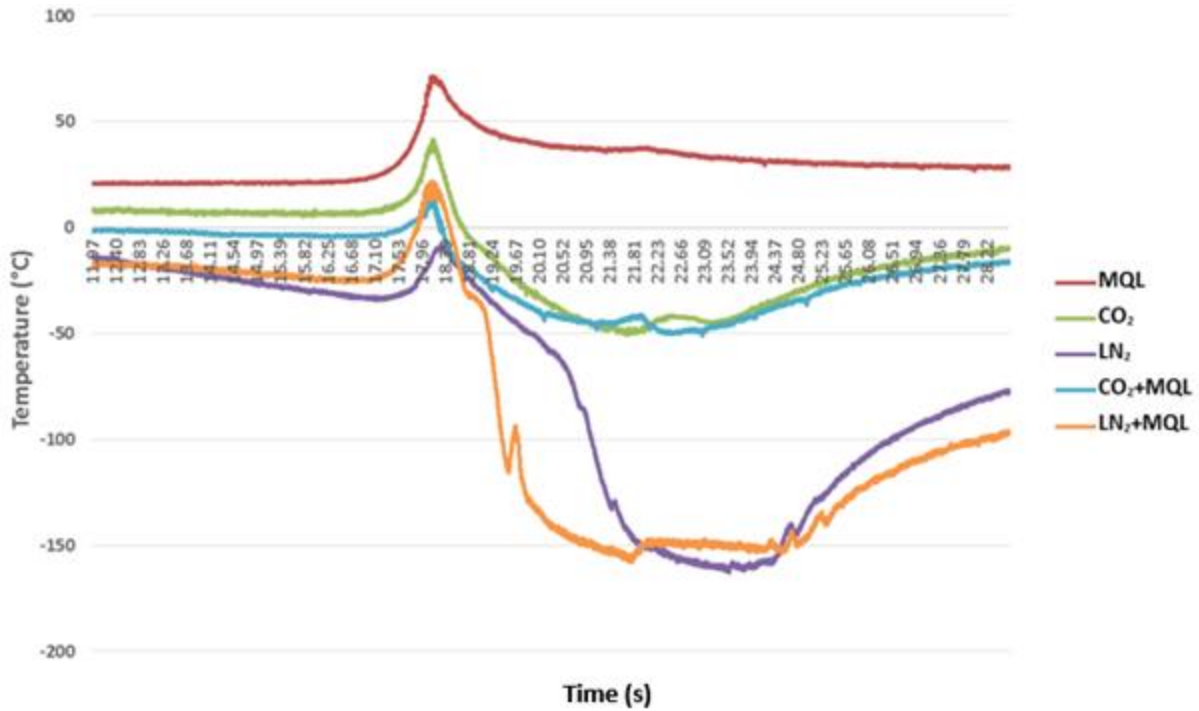


Fig. 3-4: The trend of workpiece temperature measured by thermocouple for all lubricating/cooling methods at the cutting speed of 60 m/min.

Table 2

Measured temperature during milling under different lubricating/cooling methods.

Lubricating/cooling methods	60 m/min		120 m/min	
	Maximum temperature (°C)	Minimum temperature (°C)	Maximum temperature (°C)	Minimum temperature (°C)
MQL	64	25	68	30
CO ₂	42	-51	48	-41
LN ₂	12	-163	28	-61
CO ₂ +MQL	18	-51	25	-22
LN ₂ +MQL	22	-158	47	-102

3.2.3. Cutting Forces

All cutting force components were measured during milling of five slots and Fig. 5 shows F_x and F_y forces as a function of feed length at the cutting speed of 60 and 120 m/min. F_z values

are very low as compared to F_x and F_y forces; therefore, in current study F_z values are not presented. Similar approach was also implemented in another study (Goindi, 2018). The lowest F_x was measured in MQL condition irrespective of cutting speed. This result was the evidence that the lubrication was more important than cooling in the reduction of cutting forces. The highest F_x for the cutting speed of 60 m/min was recorded in cryogenic cooling spraying LN_2 , while LN_2 +MQL gave the highest F_x at the cutting speed of 120 m/min. MQL gave the lowest F_y at the cutting speed of 60 m/min, whereas the lowest F_y was measured in CO_2 +MQL at the cutting speed of 120 m/min. Lower force values were measured with CO_2 in comparison with LN_2 . Applying of LN_2 resulted in the higher surface hardness (Jerold and Kumar, 2012; Bruschi et al., 2016) owing to its extreme low temperature as compared to CO_2 and this was the reason why cutting forces in LN_2 were higher when compared to the employing CO_2 (Jerold and Kumar, 2012). In general, F_x and F_y forces decreased with the increase in the cutting speed for all environments and this conclusion was in consistent with the study about cryogenic milling of hardened steel (Ravi and Kumar, 2011). This result for cryogenic cooling was due to the reduced volume of the cryogenic per unit time. Lee et al., (2015) investigated the effect of the machining environment on the cutting forces at two cutting speeds. They declared that since the supply of cryogenic fluid was constant, the volume of the applied cryogenic fluid per unit time was halved at the higher cutting speed, and hence the cutting forces decreased. However, it could be due to thermal softening at higher speed, too. The higher force was obtained with cryogenics, especially with LN_2 due to the lower temperature of the cryogenics.

In general, the cutting forces in cooling (CO_2 or LN_2) were measured to be higher than those in MQL condition. Similar results were found in the literature (Giasin et al., 2016). This result was owing to the hardening of workpiece material under extreme lower temperature of cryogenic cooling. Thus, higher milling forces were needed to cut the material during machining with cryogenics. Nalbant and Yildiz (2011) declared that cutting forces in cryogenic cooling by spraying LN_2 were higher as compared to dry milling of stainless steel and these researchers proved the increment in the hardness of workpiece material after cryogenic cooling.

When CO_2 or LN_2 applied with MQL, cutting force components diminished as compared to only using CO_2 or LN_2 . At the cutting speed of 60 m/min, CO_2 +MQL reduced F_x and F_y by 10.2 and 4.4% as compared to CO_2 and LN_2 +MQL decreased F_x and F_y by 15.4 and 16.0% as compared to LN_2 when the force after the feed length of 917.5 mm was taken into consideration. This result was due to the decrement of the friction provided by the lubrication

effect of MQL reaching the working zone effectively. When cryogenics applied with MQL, thin lubrication film formed, as a result reduction in the shear strength of material occurred during the machining process. Micro-droplets of oil were able to reach the cutting area under high pressure and velocity, and helped the reducing friction and providing effective lubrication (Mulyana et al., 2017). Higher pressure caused more mass flow rate which helped in diminishing the cutting force (Rahim et al., 2015). Furthermore, the excellent cooling effect of cryogenics could decrease the material adhesion on the cutting tool and the lower adhesion gave lower frictional force (Zhang et al., 2012). As a result, superior lubrication and cooling performances of hybrid method provided the lower force values as compared to the application of only cryogenics at lower cutting speed. The main parameters effective on the cutting force are the lubrication and cooling in these tests. The lubrication and cooling at higher cutting speed of 120 m/min is more significant than cutting speed of 60 m/min where tool wear has higher progress. The investigation of cutting forces (Fig. 5) shows when all cooling/lubrication methods are used with cutting speed of 120 m/min, the cutting forces are lower in comparison with 60 m/min. But, this relation was not valid when LN₂+MQL supplied. In Fig. 6-d can be seen that LN₂+MQL has also the highest surface roughness at cutting speed of 120 m/min. The comparison of the forces for LN₂ and LN₂+MQL shows that in some points F_x and F_y are lower for LN₂+MQL. Consequently, it concluded that LN₂+MQL has not an enough process lubrication as much as need for high speed machining. As a result, the high flow of LN₂ resists that MQL completely enters to the working zone, but it does not conclude that MQL supply does not affect the cooling characteristic of LN₂ as is described in Chapter 3.2. However, when the cutting speed is doubled the penetration capacity of lubricant into the chip-tool interface is also reduced. The higher the cutting speed, the more difficult is the penetration of lubricant into the chip-tool interface because the oil has to penetrate against the chip flow movement. Furthermore, as is reported in Table 2, machining with LN₂ and LN₂+MQL experience minimum temperature of -61°C and -102°C respectively at cutting speed of 120 m/min. The lower temperature results in reduction of thermal softening and generation of the higher forces.

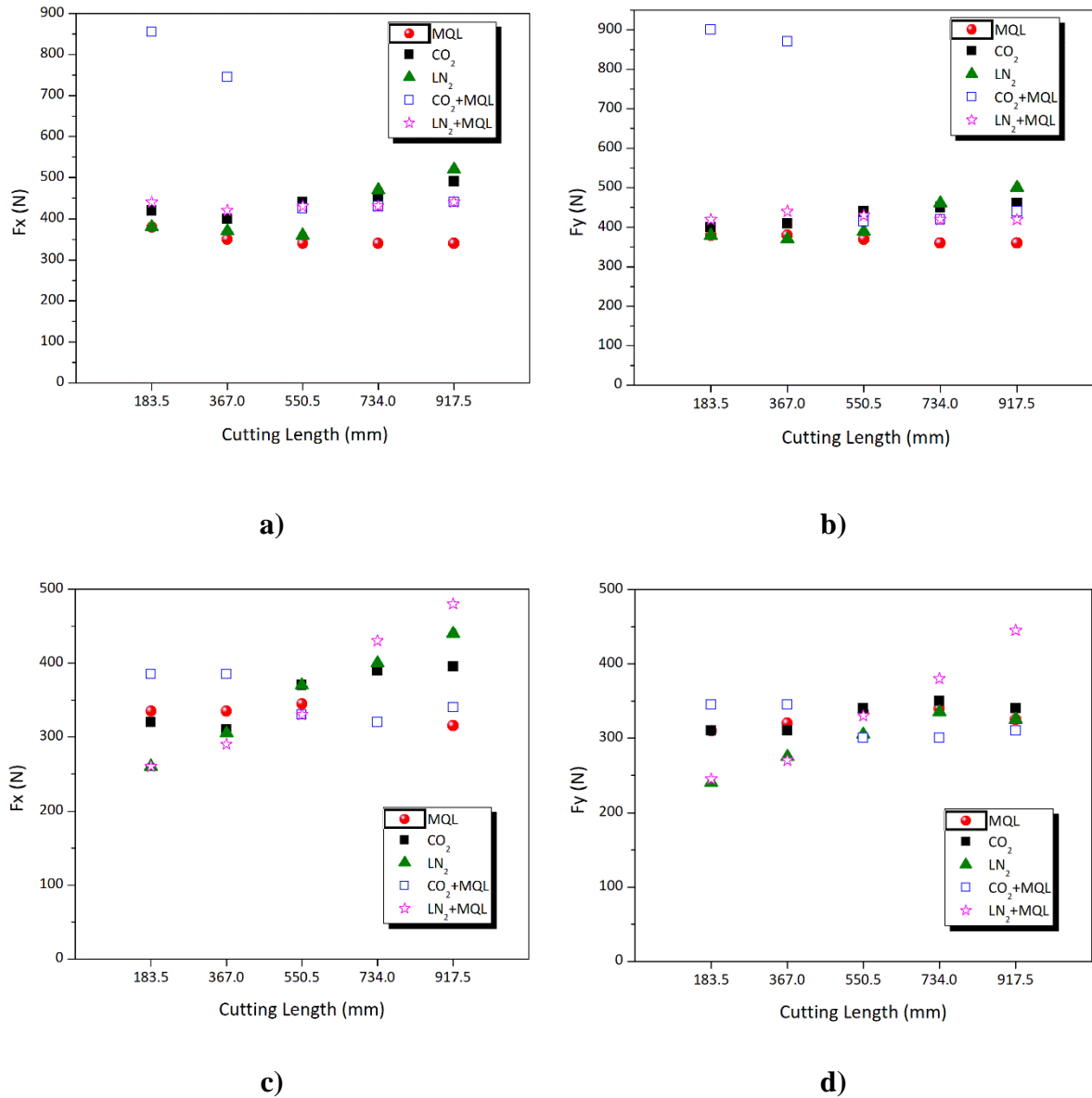


Fig. 3-5: a) F_x at the cutting speed of 60 m/min, b) F_y at the cutting speed of 60 m/min, c) F_x at the cutting speed of 120 mm/min, and d) F_y at the cutting speed of 120 m/min under all lubricating/cooling methods.

3.2.4. Surface Roughness

Fig. 6 shows the R_a and R_z values as a function of feed length for various lubricating/cooling methods in milling of Ti6Al4V alloy. In general, the increase of the cutting speed resulted in the increase of surface roughness. When cutting speed increased, the generated heat in addition to the low heat transfer coefficient of Ti6Al4V caused to an increment of the workpiece heat, and then the poor surface finish was obtained. The lowest R_a and R_z values were measured with LN_2 and the highest R_a and R_z values were obtained with CO_2+MQL during milling at the cutting speed of 60 m/min. LN_2 outperformed MQL owing to the

enhanced penetration of the chip-tool interface when utilizing cryogenics in their gaseous form. Under the improved penetration of cryogenics, the formation of BUE on the cutting tool reduced (Jerold and Kumar, 2012; Giasin et al., 2016), thus, lower surface roughness was obtained with LN₂. MQL and CO₂ methods gave to close Ra values. Values of Ra and Rz for the combination of CO₂ or LN₂ and MQL was found to be higher than that for only spraying of CO₂ or LN₂ at cutting speed of 60 m/min. This result showed that the simultaneous spraying of cryogenics and MQL negatively affected the surface quality when milling process was carried out at lower cutting speed. Tazehkandi et al. (2015) found similar result and it was concluded that MQL with LN₂ was effective to employ at higher cutting speeds. When cutting speed increased to 120 m/min, in general, the lowest Ra and Rz values were achieved with CO₂+MQL. This result was different from the cutting speed of 60 m/min. Lower surface roughness for hybrid LN₂+MQL at the cutting speed of 60 m/min and the higher surface roughness for hybrid LN₂+MQL at the cutting speed of 120 m/min in comparison to hybrid CO₂+MQL were achieved. Here, the reason for the different surface roughness normally can be attributed to two reasons. First, different temperature reduction of the cutting process leading to the different surface roughness and second, different lubrication characteristics of the supply resulting in different surface roughness can be claimed as the main reasons. As is displayed in Table 2, when MQL was added to CO₂, the maximum measured temperature of milling was decreased from 42°C to 18°C and from 48°C to 25°C for cutting speeds of 60 and 120 m/min, respectively. But, these measured temperatures were increased from 12°C to 22°C and from 28°C to 47°C by adding MQL to LN₂ for cutting speeds of 60 and 120 m/min, respectively. Thus, the effects of hybrid LN₂+MQL and hybrid CO₂+MQL seem to be different. LN₂ and CO₂ during the supply have different phases. Each phase depending on the temperature and pressure have different properties resulting different heat removal. Despite the fact that LN₂ has lower temperature than CO₂ and also, LN₂ has higher flow than CO₂ yielding to higher heat removal, the heat removal of hybrid LN₂+MQL was lower than hybrid CO₂+MQL regarding to the measured temperatures. In hybrid methods, the cooling effect of LN₂ nitrogen reduces in comparison to CO₂. When liquid nitrogen comes in contact with high pressure air molecules of MQL supply, LN₂ drastically missed the existing temperature because of the low boiling point of -196 °C, and since the pressure of CO₂ supply is higher than LN₂, hybrid CO₂+MQL penetrates the working zone more effectively than hybrid LN₂+MQL. The higher reduction in cooling effect of LN₂ than CO₂ in the hybrid methods caused that hybrid LN₂+MQL shows the inefficient cooling effect at high speed of 120 m/min and resulted in the higher surface roughness and cutting forces. However, at higher

cutting speed of 120 m/min with higher generation of temperature, hybrid CO₂+MQL not only does not show the negative effect, but also resulted in the lowest surface roughness and the lowest process forces. Moreover, the lower flow of CO₂ might have an effect on MQL-amount reaching the point of action and also higher workpiece temperatures might increase lubrication capability of frozen oil.

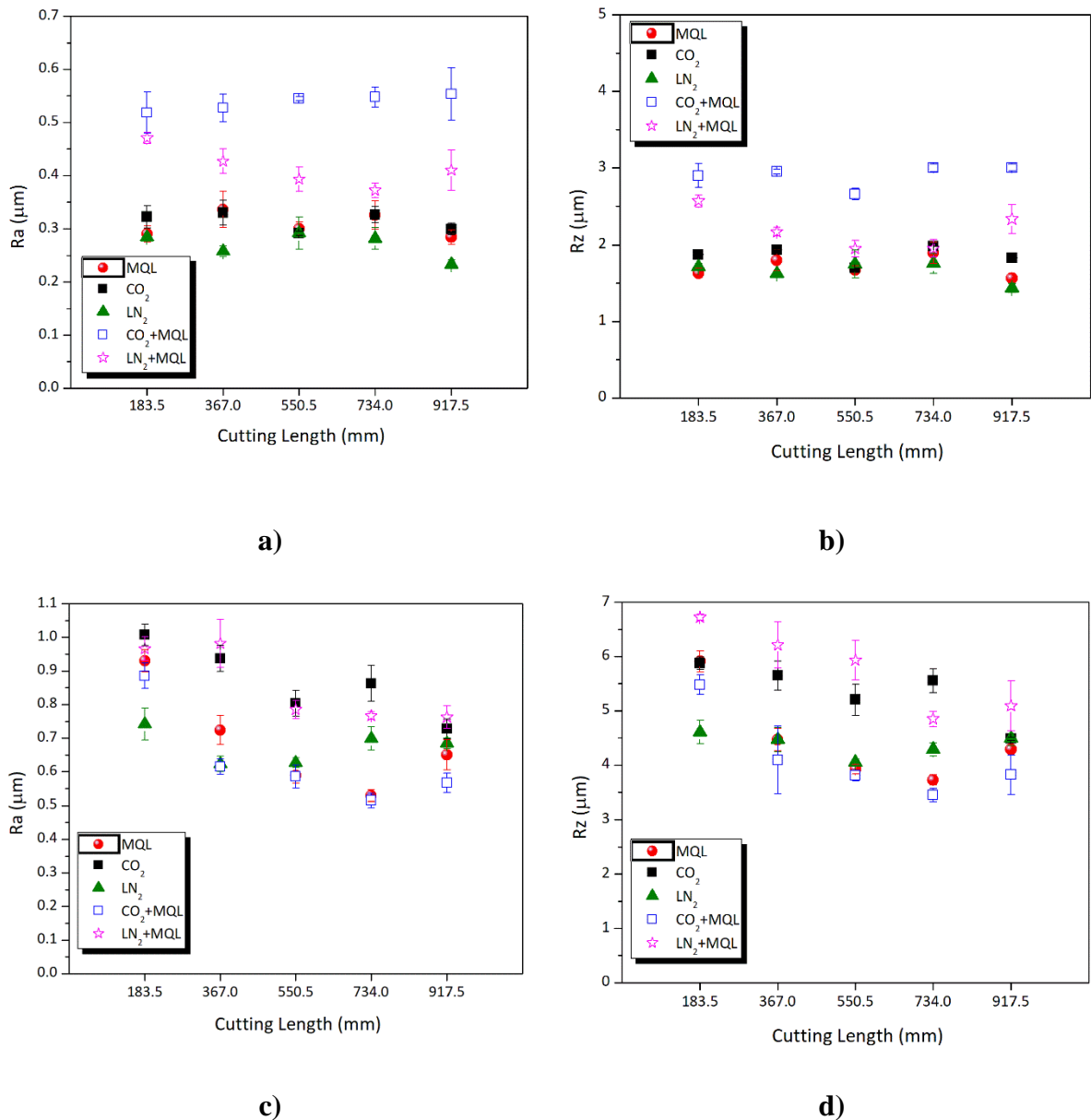


Fig. 3-6: a) Ra at the cutting speed of 60 m/min, b) Rz at the cutting speed of 60 m/min, c) Ra at the cutting speed of 120 mm/min, and d) Rz at the cutting speed of 120 m/min under all lubricating/cooling methods.

Use of cutting fluid amount in machining operations has been decreasing in recent years owing to the demands of environmental sustainability to reduce waste emissions. One of the recent trends in machining research is to investigate the feasibility of increasing machining parameters, such as feed rate and cutting speed by controlling the temperature in the machining region. The main motivation in these activities is to increase machining productivity; however, environmental concerns such as decreased cutting fluid consumption must be respected. By utilizing cryogenic or hybrid cooling methods, it is possible to reach this aim. With the MQL method, oil consumption, and thus lubricant cost could be decreased. Therefore, MQL and cryogenics could be applied to help environmental sustainability when machining difficult to cut materials such as Ti6Al4V.

Spraying of CO₂ or LN₂ with MQL was employed to drop the temperature of the machining area and to reduce the cost of lubricating/cooling methods. The tool wear analyses showed that MQL alone was not a suitable method for high speed machining due to the high wear rate. Nevertheless, Cryo-MQL hybrid methods made high speed milling possible leading to reduced tool wear and cutting forces, and improved surface finish. High speed Cryo-MQL hybrid milling resulted in lower machining time, lower cooling/lubrication spray, and energy consumption which led to the reduction of environmental effect and cost of production. MQL and hybrid method play an important role to reduce coolant amount. The hybrid method can enhance milling performance in terms of reduced tool wear, thus improved tool life. This causes reduced number of cutting tools per part resulting in savings in tool material and energy consumption during their production. Furthermore, since the hybrid method decreases cutting forces the energy consumption during the machining process also reduces promoting green manufacturing towards more sustainable environment. Finally, the total production cost per part can be decreased significantly by hybrid cryogenic machining through reduction of costs associated with energy, material and cutting tool.

3.3. Conclusions

In this work, the influences of various lubricating/cooling methods on the tool wear, temperature, cutting forces and surface roughness were studied during milling of Ti6Al4V alloy at different cutting speeds. Five different methods were used for lubricating/cooling techniques namely, MQL, only CO₂ spraying, only LN₂ spraying, simultaneous spraying of CO₂ and MQL (CO₂+MQL) and simultaneous spraying of LN₂ and MQL (LN₂+MQL). The major conclusions can be summarized as follows:

- The lowest flank wear was measured in MQL application at the cutting speed of 60 m/min, however LN₂+MQL method provided the lowest flank wear at the cutting speed of 120 m/min.
- Cryogenic cooling methods gave higher tool wear values as compared to MQL method at the cutting speed of 60 m/min. However, the highest tool wear value was obtained with MQL method at the cutting speed of 120 m/min. As a result, it was concluded that the benefit of cryogenic cooling in term of tool wear decreased with decreasing cutting speed and this proved that cryogenic cooling was effective at higher cutting speed. This is important for a higher eco-efficiency of the milling process by proposing the improvement of cooling/lubrication and production speed in the Ti6Al4V cutting requires more energy during the cutting.
- Hybrid cooling decreased the flank wear in comparison to the applying of only CO₂ or LN₂. At the cutting speed of 60 m/min, CO₂+MQL reduced the flank wear by 31.8% as compared to CO₂ and LN₂+MQL decreased the flank wear by 59.6% as compared to LN₂. When cutting speed was increased to 120 m/min, the highest flank wear was measured with MQL application. CO₂, LN₂, CO₂+MQL and LN₂+MQL reduced the flank wear by 35.4, 29.6, 38.9 and 53.6%, respectively in comparison to MQL method.
- The highest workpiece temperature was measured in MQL condition and it was found that cryogenics reduced the workpiece temperature during milling of Ti6Al4V alloy.
- In general, MQL condition gave the low cutting forces and they decreased with the increased cutting speed for all environments.
- In general, the cutting forces in cooling (CO₂ or LN₂) were found to be higher than those in MQL condition. As CO₂ or LN₂ sprayed with MQL simultaneously, cutting force components diminished in comparison to only applying CO₂ or LN₂. As a result, superior lubrication and cooling performances of hybrid method gave the lower force values as compared to the spraying of only cryogenics at lower cutting speed. Also, at the cutting speed of 120 m/min, CO₂+MQL showed the lowest cutting forces.
- The lowest Ra and Rz values were measured with LN₂ and the highest Ra and Rz values were obtained with CO₂+MQL during milling at the cutting speed of 60 m/min. When cutting speed was 120 m/min, in general, the lowest Ra and Rz values were achieved with CO₂+MQL.

- The simultaneous spray of cryogenic fluid and MQL oil enhanced the machinability of Ti6Al4V alloy as compared to only spray of cryogenics because of both lubrication and cooling capability.
- Under the cutting speed of 60 m/min, MQL was found to be the best option that resulted in the lowest flank wear and cutting forces. However, when the cutting speed was increased to 120 m/min, the highest flank wear was achieved with MQL method. The implementation of cryogenics or hybrid methods reduced the flank wear, temperature and surface roughness as compared to MQL method when the cutting speed was increased to 120 m/min. Therefore, it was concluded that the application of cryogenics or hybrid methods efficiently enhanced the milling performance of Ti6Al4V alloy at higher cutting speeds.
- Hybrid cryogenic method was found to be an effective method considering both machining performance and environmental impact. The implementation of hybrid method as a lubri-cooling method provided a good alternative to MQL technique by ensuring less contaminants, providing sustainable machining and creating an equilibrium in ecological and technical factors. This reduces the number of cutting tools per part which decreases tools used, tool change time and machining cycle time and electricity requirements leading to lower energy consumption.
- When all cutting parameters and conditions were taken into consideration, in general LN₂ or LN₂+MQL lubricating/cooling methods gave promising results with respect to tool wear, temperature, cutting forces and surface roughness.
 - The cryogenics and the hybrid method provided a good alternative to MQL. Lower flank wear, thus longer tool life could be obtained with the cryogenics and the hybrid method ensuring less waste and sustainable machining resulting in an equilibrium in ecological and technological factors.
 - The results can be useful in the industrial applications for selection of lubricating/cooling methods for milling of Ti6Al4V. It can be stated that MQL, the cryogenic and the hybrid method are sustainable techniques that can be used in every machining industries.
 - The potential applications of current work are various manufacturing industries such as turbine engine disks, blisks, impellers etc.
- Hybrid cryogenics are environmentally-benign, hazardless methods producing functionally superior products. Cryogenics reduce cutting temperatures allowing higher material removal rates, lower energy consumption, and higher productivity.

4. HIGH-SPEED MACHINING OF ADDITIVELY MANUFACTURED INCONEL 718 USING HYBRID CRYOGENIC COOLING METHODS

4.1. Experimental Setup

The Inconel 718 powder provided by Oerlikon Metco (Oerlikon Metcoadd In718C) was used to produce the SLM parts, and the Inconel 718 powder provided by Oerlikon Metco (Oerlikon MetcoAdd In718F) was used to produce the DED parts. The morphology of Inconel 718 powders are shown in Fig. 1. The chemical composition and the particle size distribution of Inconel 718 particles are presented in Table 1 and 2, respectively. An EOS M290 SLM machine (EOSINT GmbH-Electro-Optical system, Germany) with a maximum laser power of 370 W was used to build the SLM parts, and a DMG Mori Lasertec 65 3D machine with a maximum laser power of 2500 W was employed to manufacture the DED parts. The working principle of DED process and SLM process are illustrated in Fig. 2. The scanning strategies of 67° and 90° rotate were used to fabricate the SLM and DED test parts, respectively. The SLM and DED parameters used in this study are presented in Table 3.

Table 4-1: Chemical composition

	Weight Percent (nominal)							
	Ni	Cr	Fe	Nb+T a	Mo	Al	Ti	Other
MetcoAdd 718C / 718F	Balanc e	18	18	5	3	0.6	1	< 0.5

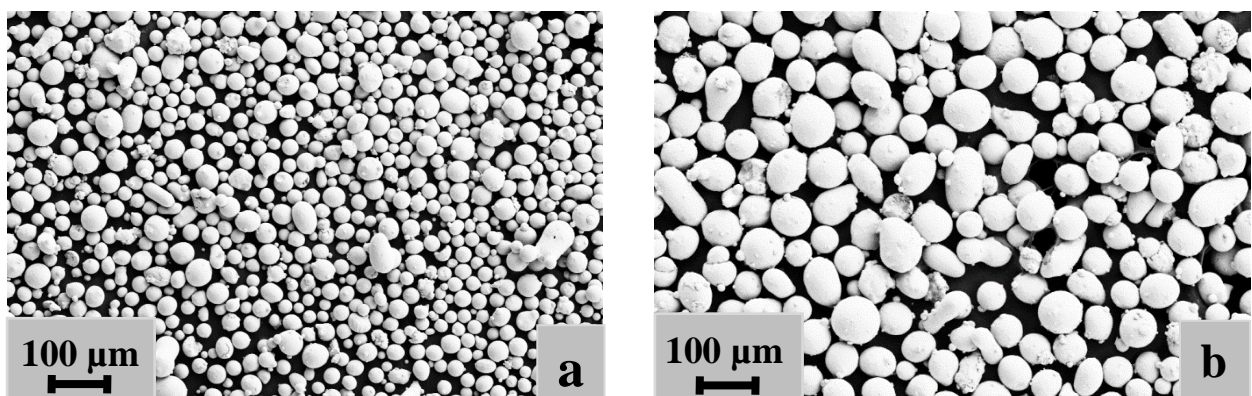


Fig.4-1: The morphology and size of Inconel 718 powders. a) SLM powder b) DED powder

Table 4-2: Particle Size Distribution and Hall Flow

	Nominal Range [μm]	D90 [μm]	D50 [μm]	D10 [μm]	Hall Flow [s/50 g]
MetcoAdd 718C	-45 +15	46	30	18	< 18
MetcoAdd 718F	-106 + 45	-	-	-	-

Table 4-3: SLM and DED parameters used in this study

Process parameters	SLM	DED
Laser power (W)	285	2000
Laser scanning speed(mm/min)	960	1000
Hatch spacing (mm)	0.11	1.5
Layer thickness (mm)	0.04	1.12

According to AMS 5383 and 5662 standards, the steps of additively manufactured SLM and DED parts using three steps heat treatment (homogenization plus solution treatment plus aging) are as follows: homogenization ($1100\text{ }^{\circ}\text{C} \times 1.5\text{ h}$ /water cooling) in addition to solution treatment ($980\text{ }^{\circ}\text{C} \times 1\text{ h}$ /water cooling) and direct aging ($720\text{ }^{\circ}\text{C} \times 8\text{ h}$ /furnace cooling at $50\text{ }^{\circ}\text{C/h}$ to $620\text{ }^{\circ}\text{C} \times 8\text{ h}$ /air cooling). This way, simultaneously, the strengthening is achieved in the material and the distortion of the part would be eliminated during the cutting procedure from the building plate. The specific scenario of the post-heat-treatment is shown in Fig. S1 in Appendix. The goal of the homogenization process is to achieve the elimination of micro-segregation and recrystallization of the deposits where the diffusion of segregation elements and facilitating the precipitation of δ phase are the aim of solution treatment.

The milling tests were carried out on a Mazak Nexus 510C-II milling machine with a motor power of 18.5 kW and a maximum spindle speed of 12000 rpm. Four different additive parts in as-built condition (SLM-manufactured and DED-manufactured) and heat-treated condition (HT-SLM and HT-DED) were selected as workpiece materials in the experiments.

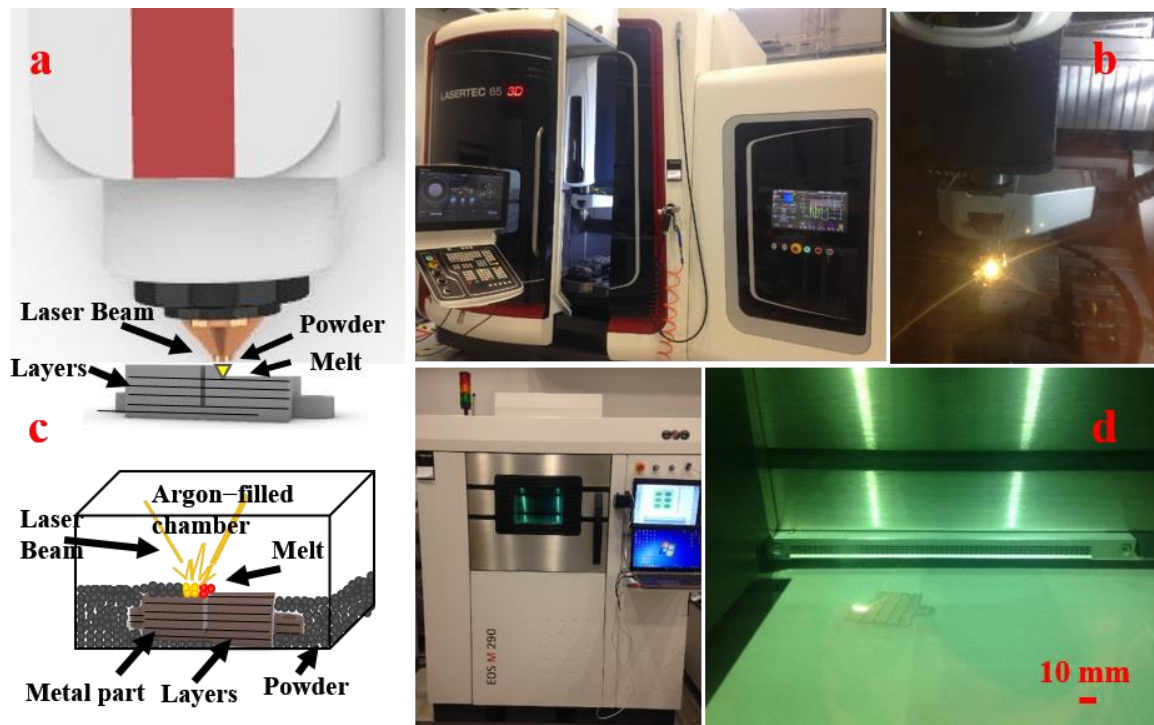


Fig.4-2: a) Working principle of DED process b) hybrid additive/subtractive hybrid machine using DED c) Working principle of SLM process d) SLM machine.

The surfaces of manufactured AM parts analyzed using a NanoFocus Usurf non-contact 3D profilometer are shown Fig. S2 in Appendix. Uncoated carbide inserts (Sandvik R390-11 T3 08M-KM H13A) with a nose radius of 0.8 mm and lead angle of 90° were clamped on the tool holder. The tool holder (Sandvik R390-012A16-11L) had a single cutting edge and a diameter of 12 mm. The cutting parameters were as follows: axial depth of cut, $a_p = 0.5$ mm; radial depth of cut, $a_e = 12$ mm; feed rate = 0.01 mm/ rev; and cutting speed, $v_c = 100$ m/min.

Six different cooling methods namely, wet, MQL, CO_2 , LN_2 , CO_2MQL , and LN_2MQL were applied during milling of the additively manufactured test parts. The cutting fluids were positioned behind the tool with a stand-off distance of 15 mm.

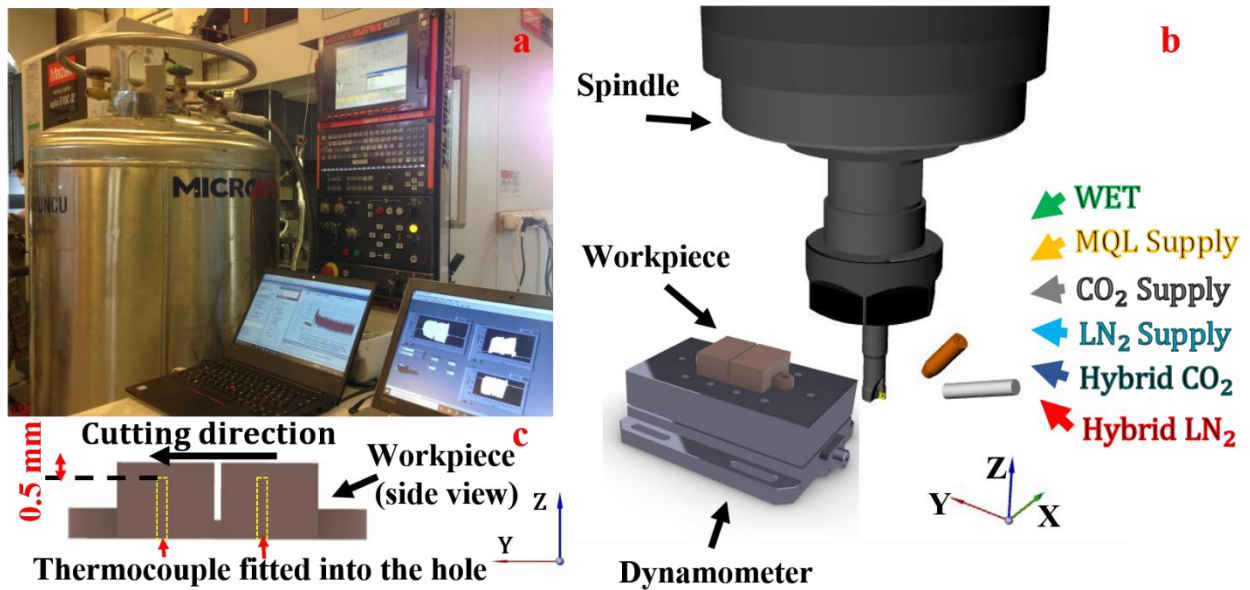


Fig. 4-3: a) Experimental setup of the machining tests b) Schematics of the methods c) position of thermocouples fitted into the workpiece.

In the wet cooling tests, metalworking fluid based on mineral oil (ADRANA D 208 FF) was used. In the MQL system, vegetable oil with boiling point of 200 °C, freezing point of -39 °C and a viscosity of 35 mm²/s was employed. MQL was sprayed to the working zone with pressure of 6 bar, flow rate of 90 ml/h and with the nozzle angle of 45°. In CO₂ spraying tests, carbon dioxide cylinders including both liquid and gaseous CO₂ were used in the tests. The pressure in the CO₂ cylinders was 57 bar at 20 °C. CO₂ was delivered through a nozzle with an inner diameter of 0.5 mm at the flow rate of 10.8 kg/h. When the pressurized liquid CO₂ depressurizes, its temperature drops producing the mixture of CO₂ gas and CO₂ snow. The temperature of the CO₂ snow is theoretically -79.05 °C. In experiments of cryogenic LN₂ supply, LN₂ was delivered at the pressure of 15 bar and mass flow rate of 36 kg/h. LN₂ was sent through a nozzle with a diameter of 4.7 mm at the tool-chip interface. In experiments of hybrid methods (CO₂MQL or LN₂MQL), CO₂ plus MQL or LN₂ plus MQL were sprayed to the working zone using the same conditions in spraying of CO₂, MQL, and LN₂ supply where oil particles came in contact with CO₂ or LN₂ before reaching the working zone converting to frozen oil particles. In each experiment, spraying of CO₂ or LN₂ was activated before starting the cutting process to use stable CO₂ or LN₂ supply during the tests. Each experiment was repeated three times, and the average measurements are reported for tool wear, cutting forces, surface roughness and temperature.

Flank wear was measured on the flank face of the inserts at constant intervals by Dino-Lite digital microscope. The cutting inserts were examined after each predetermined feed length

(60 mm) until they reached the tool wear criteria in accord with ISO 3685 (average flank wear of 300 μm).

The cutting forces were measured using Kistler 9257BA type dynamometer, charge amplifier of Kistler 5233A type, and Lab View Signal Express software. As milling forces are periodic their average values were used.

To measure the temperature during the cutting tests, DED-manufactured parts were drilled with a diameter of 2 mm, and two K-type thermocouples (Omega) with a diameter of 0.25 mm were fitted into the holes. The embedded position of the thermocouples is shown in Fig 3. These holes are additively manufactured in the SLM parts due to the higher precision of the SLM process. A thermally conductive high-temperature cement was produced using magnesium phosphate cement powder (Omegabond 600). To enhance the heat conduction, the space between the workpiece and thermocouple was filled by this cement which had high thermal conductivity. DT9805 data translation device together with QuickDAQ software were used to evaluate temperature data. The temperature values presented in this study were collected from the average of two thermocouple readings. The test was repeated two times.

Measurement of surface roughness in the feed direction was carried out using Mahr PRN10 roughness instrument using sampling number and cut-off length 5 and 0.8 mm, respectively. The surface roughness was measured at three points along the machining path and the average value of these measurements was taken into consideration in the analysis.

To investigate the effectiveness cooling/lubrication strategy, the generated surfaces within the cutting length in the feed direction of $L_f = 6\text{--}18$ mm, were characterized under the scanning electron microscope (SEM). Also, the phase characterization of the machined specimens was performed by X-ray diffraction (XRD, D2 PHASER, Bruker) using a $\text{Cu-K}\alpha$ ($\lambda = 1.54056 \text{ \AA}$) radiation.

4.2. Results and Discussion

4.2.1. Tool life

Fig. 4 and 5 present the tool wear of inserts for all lubricating/cooling methods during machining of SLM and DED fabricated parts, respectively. The results indicate that the heat treatment of SLM-manufactured and DED-manufactured Inconel 718 increased the rate of tool wear as compared to as-built SLM and DED samples. During machining of as-built SLM parts, the flank wear increased at a lower rate under MQL environment. However, the flank

wear increased rapidly under other environments, especially with LN₂. The excessive cooling capability of cryogenics (LN₂ or CO₂) negatively affected the tool wear where the lowest tool life was measured under LN₂. With the application of hybrid methods, a reduction in the tool wear was observed. The addition of MQL to cryogenic coolants balanced the cooling effect of LN₂ and CO₂ (Bagherzadeh et al., 2021a; Bagherzadeh and Budak, 2018b). Therefore, CO₂MQL increased the tool life by 14% as compared to CO₂. LN₂MQL cooling improved the tool life by 50% as compared to LN₂. Wet, MQL, CO₂, CO₂MQL, and LN₂MQL increased the tool life by 43%, 198%, 34%, 54%, and 50% respectively in comparison to LN₂. Therefore, the results show that lubricating effect is more important than the cooling in the machining of SLM-manufactured Inconel 718 parts.

Despite the fact that the lowest tool wear was obtained under MQL in machining of SLM parts, the flank wear increased at a very high rate in machining of HT-SLM parts under MQL. The cooling plays more significant role on the tool life than lubrication in high-speed machining of heat-treated parts. Thus, the flank wear under MQL supply yielding lower cooling effect increases at a very high rate in machining of HT-SLM parts. In general, the highest tool life was achieved with CO₂ and CO₂MQL environments in the machining of HT-SLM parts. However, the lowest tool life was measured during LN₂ machining. The tool life improvements of the Wet and MQL method reduced and CO₂, CO₂MQL, LN₂MQL showed a better result in the machining of HT-SLM parts than machining of as-built SLM. In machining of HT-SLM, the tool life improved by 31%, 60%, 147%, 134%, and 122% under Wet, MQL, CO₂, CO₂MQL, and LN₂MQL environments respectively in comparison to LN₂.

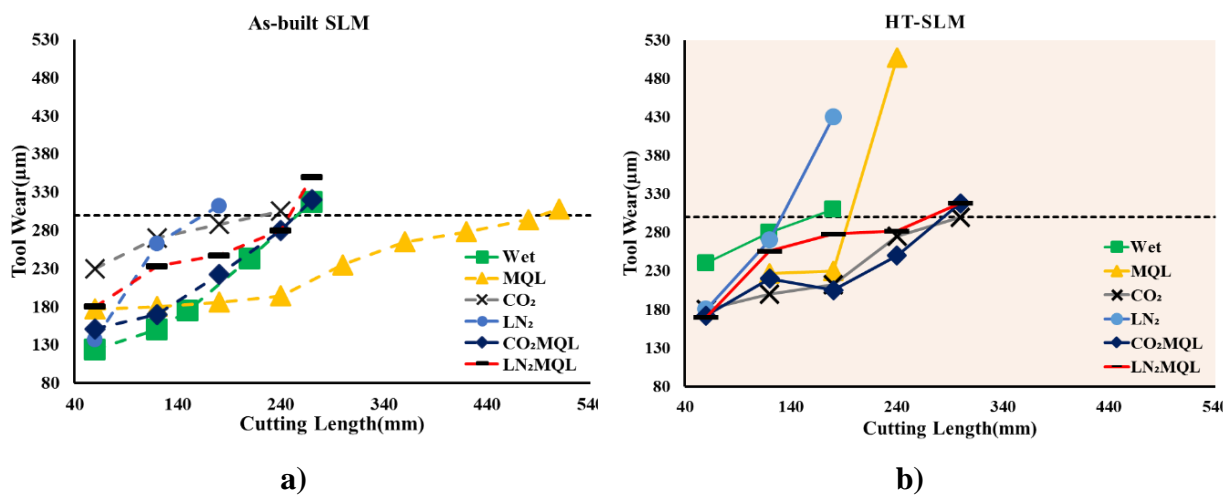


Fig.4-4: Flank wear under all lubricating/cooling methods for a) As-built SLM, b) Heat-treated SLM.

The trend in tool wear growth during milling of DED-manufactured parts was not similar to that of the SLM-manufactured parts due to the dissimilar material properties of DED and SLM-manufactured Inconel 718 resulting in different machinability. The high-speed machining of DED parts using LN₂, Wet, or MQL methods was neither efficient nor possible. The new cutting tool transitioned to a worn tool at the beginning of machining under LN₂, Wet, and MQL environments during machining of both as-built and HT-DED parts. The CO₂ method reduced the tool wear during the machining of as-built DED parts. However, it was not as efficient in the machining of HT-DED parts. The hybrid methods made the high-speed machining of DED parts possible. Among the hybrid methods, LN₂MQL showed a better performance than CO₂MQL by 43% and 49% during machining of as-built and HT-DED parts, respectively.

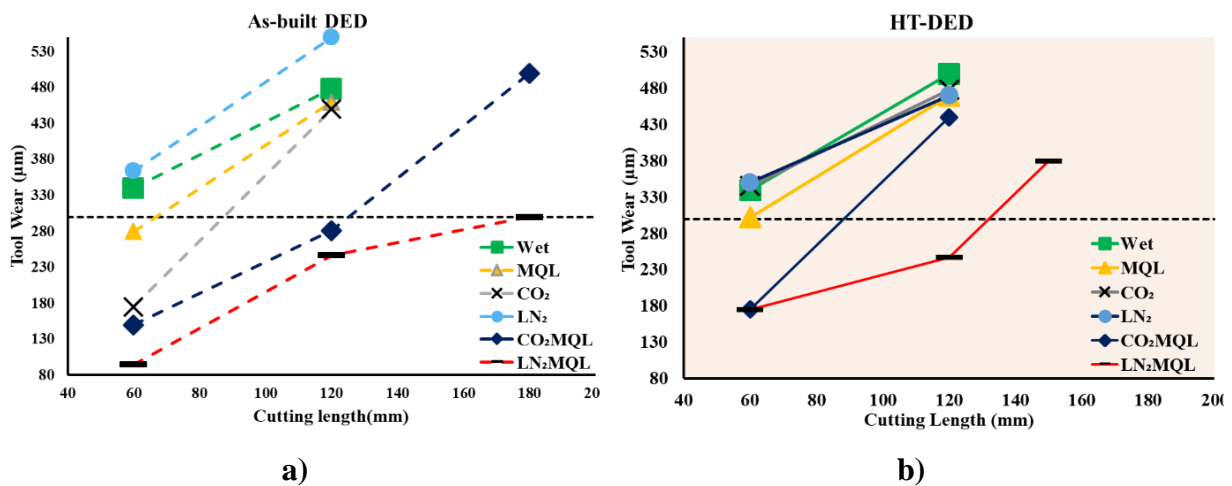


Fig. 4-5: Flank wear under all lubricating/cooling methods for a) DED, b) Heat-treated DED

When the progress of tool wear in the machining of SLM and DED-manufactured parts are compared, it can be deduced that the AM processes influence the machinability of Inconel 718 significantly where the DED-manufactured parts show lower machinability than that of SLM-manufactured parts. Based on this information, it can be concluded that the suitable cooling/lubrication methods should be selected for high-speed machining of AM parts manufactured by different methods. Each additive manufacturing method affects the material characteristics such as hardness, micro-structure and thermal conductivity resulting in the changing of the machinability of Inconel 718. To better understanding, hardness of as-built and heat-treated AM parts were measured. As shown in Fig. S3, the hardness of as-built SLM

samples was higher than that of as-built DED samples. During the DED procedure, the built-layer thickness, the amount of molten material and laser power are much higher. That makes the required time for solidification and cooling down for DED much longer than that of the SLM procedure. Besides, most of the cooling is realized by conduction over previously deposited material that is subjected to heating several times. This procedure causes DED to have lower hardness value compared to SLM process. The similar phenomenon was also previously reported before by Bedmar et al. (Bedmar et al., 2021). Besides, the heat treatment increased the hardness of materials where the hardness of HT-SLM parts were measured higher than that of HT-DED samples. The machining of samples with higher hardness values generates higher heat during the machining. Here, it may be expected the lower machinability under SLM-manufactured parts, but the results indicate the lower machinability for the DED-parts. In addition to the material hardness, thermal conductivity plays a crucial role in machinability, where the thermal conductivity depends on the presence of voids, interfacial resistance, segregation, precipitates and inclusions in the sample matrix. The assessments of machinability using cutting forces, cutting temperature and surface integrity contribute to better understanding of the cooling/lubrication mechanism in machining of additively manufactured parts as is presented in the next chapters.

4.2.2. Cutting Forces

All cutting force components were measured during the milling of AM parts under six cooling strategies. F_x and F_y forces are illustrated as a function of the cutting length in Fig. 6 and Fig. 7 for as-built SLM and HT-SLM and as-built DED and HT-DED parts, respectively. Since F_z values are very low as compared to F_x and F_y forces, they are not considered. The lowest F_x and F_y were obtained with MQL method for as-built SLM and HT-SLM parts while almost all the lowest F_x and F_y values were measured in hybrid conditions for as-built DED and HT-DED parts. The highest F_x and F_y for the machining of SLM-manufactured parts were recorded in spraying CO_2 , whereas the highest F_x and F_y for the machining of DED-fabricated parts were measured in wet and LN_2 environments.

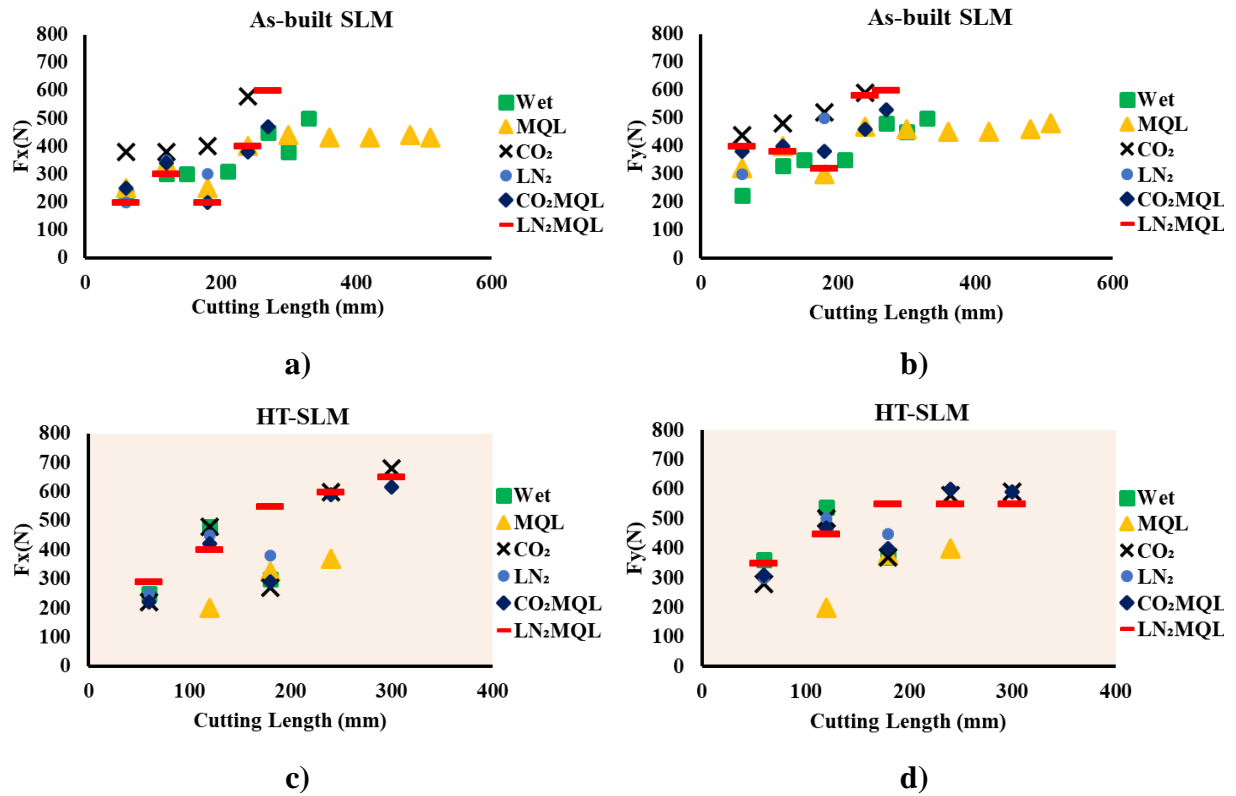


Fig. 4-6: a) F_x during machining of as-built SLM, b) F_y during machining of as-built SLM, c) F_x during machining of heat-treated SLM, and d) F_y during machining of heat-treated SLM under all lubricating/cooling methods.

In general, the cutting forces of machining under low-temperature coolants were measured to be higher than those in wet, MQL, and hybrid conditions. The reason was the hardening of workpiece material become prominent under extreme cooling. Previously, Dai et al. also experienced hardening of the workpiece when low temperature coolant was used for machining of Inconel 718 (Dai et al. 2020). Moreover, similar phenomenon is observed during the cryogenic machining of other materials such as Ti and Co alloys (Yang et al. 2015; Rotella et al. 2014). The low temperature cooling prevents softening, annihilation of the dislocations and grain growth after dynamic recrystallization (Rotella et al. 2012). In the absence of low-temperature coolant use during machining, excessive heat increases the temperature thereby inducing softening and the annihilation of dislocations. Therefore, it is considered that the work hardening cannot be observed in the case of low temperature coolant use. As a consequence, higher milling forces were required to machine the material using low-temperature coolants. In the hybrid application of low-temperature coolants and MQL, cutting force components are reduced as compared to only using CO₂ or LN₂ supply. This is due to the reduction of friction under improved lubrication effect of hybrid methods owing to

MQL which provides superior lubrication. In hybrid methods, the low-temperature coolant improves the efficiency of the oil reducing its temperature, and thus preventing its evaporation or burning directly when it reaches the working zone. Furthermore, the high pressure of coolants helps the oil particles enter the working zone more effectively.

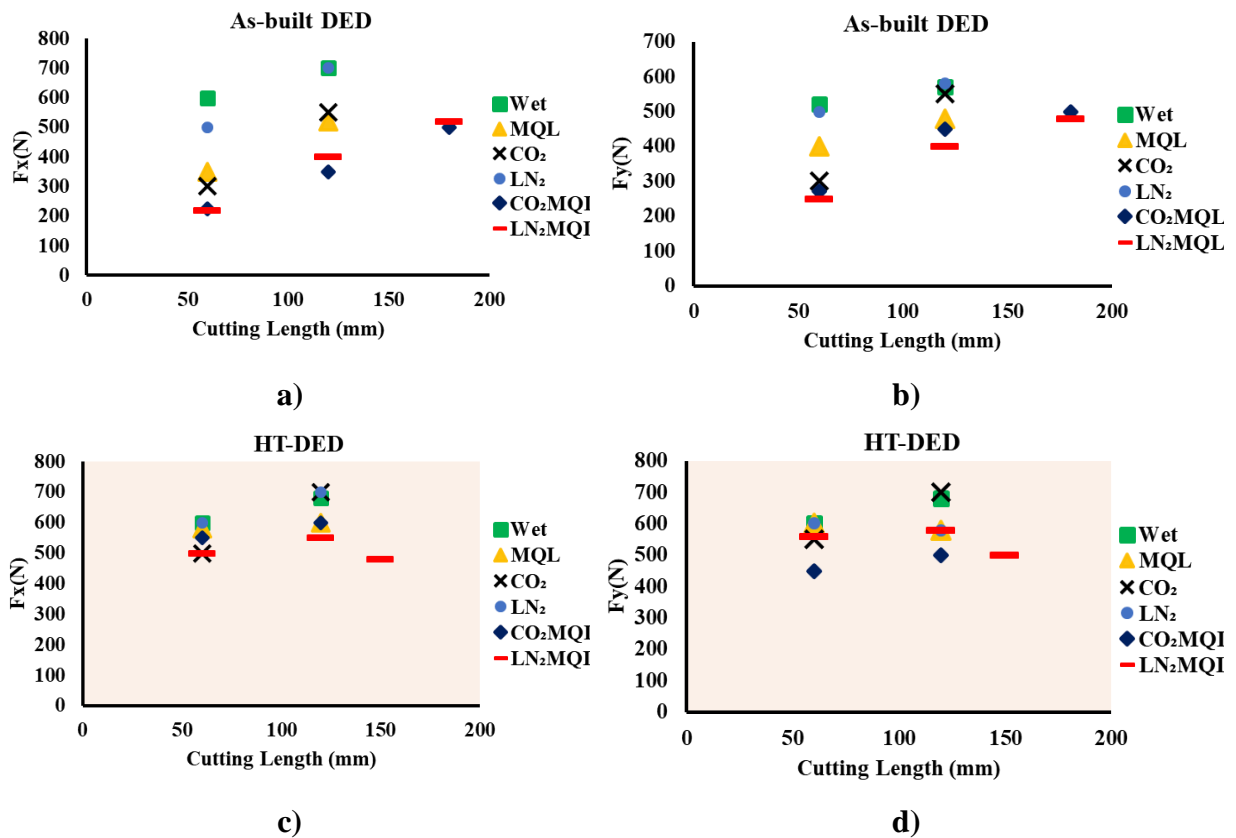


Fig. 4-7: a) F_x during machining of as-built DED, b) F_y during machining of as-built DED, c) F_x during machining of heat-treated DED, and d) F_y during machining of heat-treated DED under all lubricating/cooling methods.

4.2.3. Temperature

The workpiece temperature was measured during machining of AM parts under various lubricating/cooling methods. The temperature of the workpiece before cutting was measured as reported in Table 4. The temperature of the workpiece before cutting was measured as reported in Table 4. As shown in Fig. 8, more heat removal with the use of LN₂ and also hybrid methods were found in comparison to the other cooling strategies employed in this study. In addition to the properties of LN₂, temperature, pressure, and flow of the supply played a significant role in heat removal and penetration of coolant/lubricant into the cutting zone. Better penetration of LN₂ reduces the contact friction at the chip-tool interface resulting in higher heat removal. The maximum workpiece temperature was measured in the MQL

machining of AM parts. Similar results were found in the machining of hybrid CO₂MQL and LN₂MQL machining where the measured temperature under the CO₂MQL was lower than that with the CO₂ supply whereas the measured temperature in LN₂MQL was higher compared to LN₂ cooling. It can be concluded that oil can penetrate the working zone in hybrid methods more effectively than only using MQL. Thus, the application of CO₂MQL outperformed the MQL, and the CO₂ method in terms of workpiece temperature due to the efficient cooling and lubrication effects. In general, the temperatures in the machining of DED parts were higher than those the machining of SLM parts showing the evidence for lower machinability of DED-manufactured parts compared to SLM- ones. The generated temperature of DED parts owing to the lower machinability was enhanced by the application of the hybrid cooling/lubricating methods. The results showed that the efficiency of hybrid strategies was based on the generated temperature where better machinability was obtained at higher cutting temperatures compared to other environments.

Table 4-4: Measured workpiece temperature before milling under different lubricating/cooling methods.

Lubricating/cooling methods	Workpiece temperature before cutting (°C)			
	SLM	HT-SLM	DED	HT-DED
Wet	20	20	20	20
MQL	20	20	20	20
CO ₂	17	17	17	17
LN ₂	-30	-28	-17	4
CO ₂ MQL	15	15	15	15
LN ₂ MQL	-26	-10	-14	8

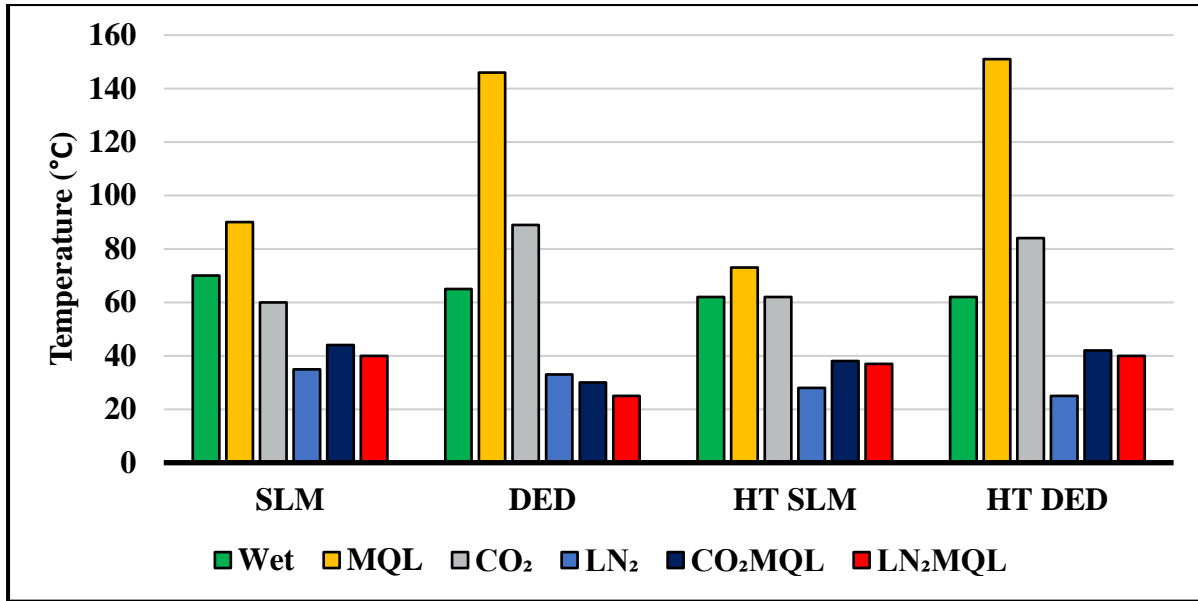


Fig. 4-8: Measured temperatures during milling under different lubricating/cooling methods.

4.2.4. Surface finish

The performance and service life of any machined parts are substantially affected their surface finish. Fig. 9 and Fig. 10 illustrates the average and the mean roughness, i.e. (Ra) and (Rz), variations as a function of cutting length for various machining methods in milling SLM and DED parts respectively. When Ra value of two different surfaces are equal, Rz value determines the surface quality. In this study, since Ra values of the machined surfaces using different methods are equal in some cases, the Rz values were reported for the better understanding and precise comparison of the surface roughness. In general, the post-heat-treatment affected the roughness of the machined surface. When the AM parts were heat-treated, their improved material properties yielded less variations on the surface roughness after machining. Different effects of each method in terms of temperature reduction and cooling/lubricating are the main reasons for the different surface roughness observed. The lowest Ra and Rz values were almost always obtained with MQL and LN₂MQL whereas the highest Ra and Rz values were almost always measured with the application of only the low-temperature coolants in milling of SLM-manufactured parts. The reason can be attributed to the excessive cooling capability of LN₂ (with the low boiling point of $-196\text{ }^{\circ}\text{C}$) which increases the hardness and strength of workpiece material. LN₂MQL showed the lowest Ra and Rz values in milling of as-built DED parts. But in some cases, the lower Ra and Rz were not achieved with LN₂MQL during the machining of HT-DED parts. Since the oil sprayed

periodically, the temperature of LN₂ increases periodically as well. Therefore, the excessive cooling of LN₂, results in higher surface roughness in some cutting lengths.

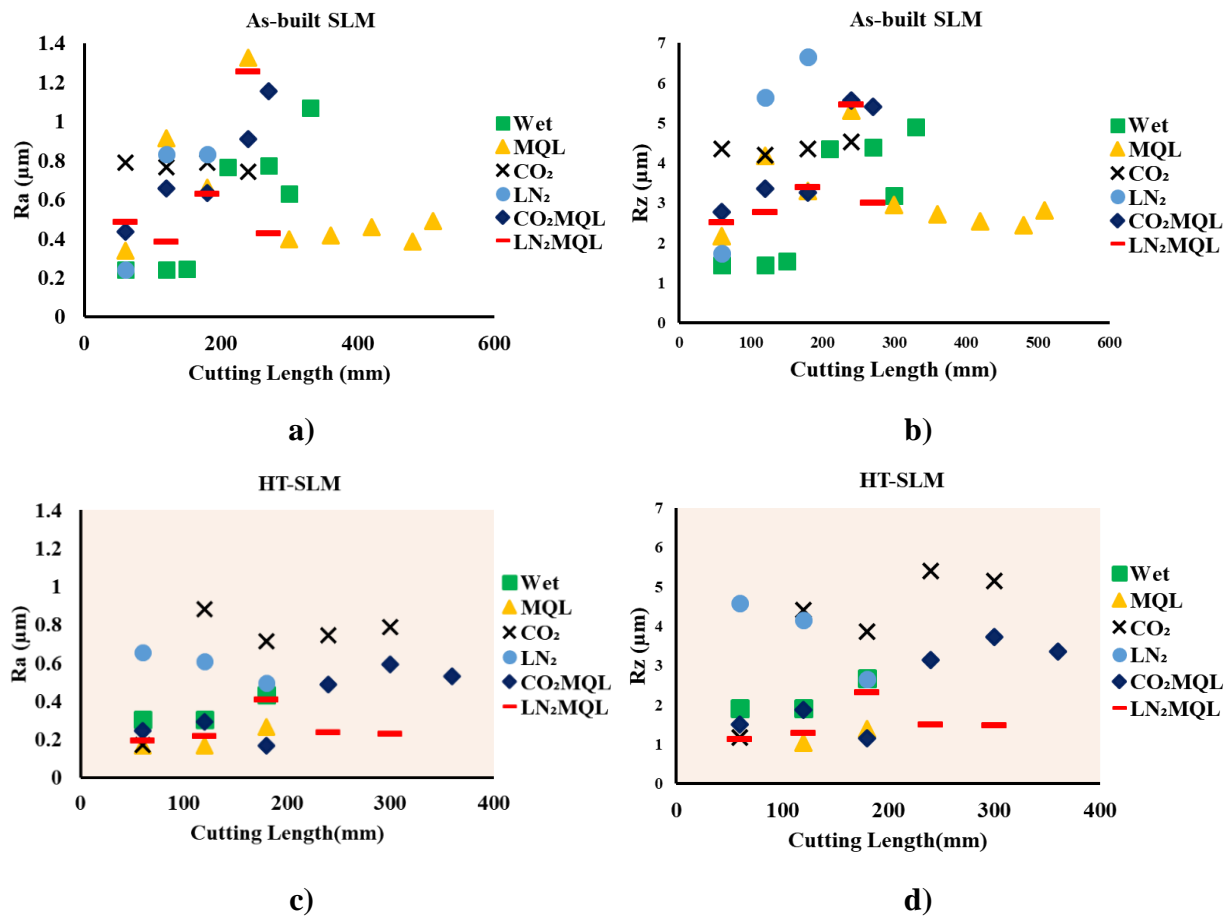
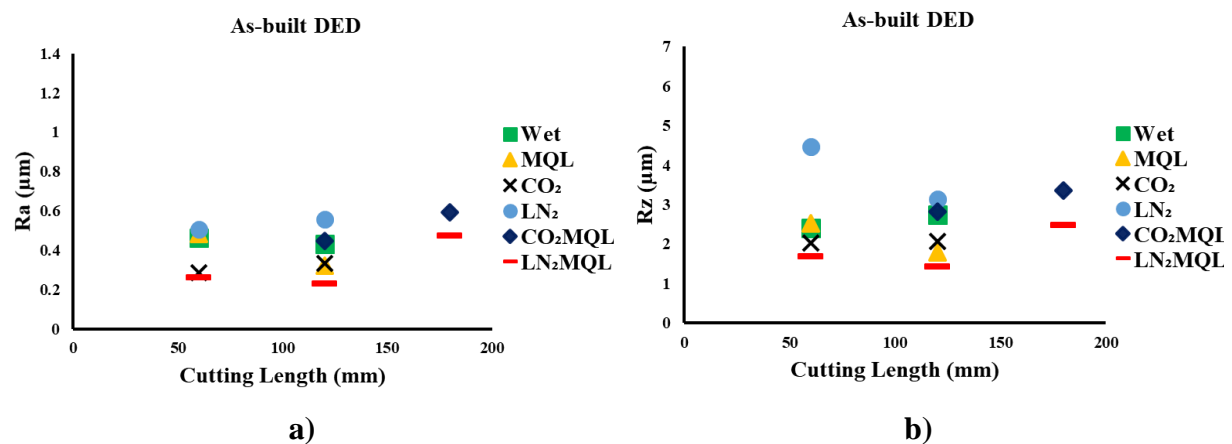


Fig. 4-9: a) Ra during machining of as-built SLM samples, b) Rz during machining of as-built SLM samples, c) Ra during machining of heat-treated SLM samples, and d) Rz during machining of heat-treated SLM samples under all lubricating/cooling methods.



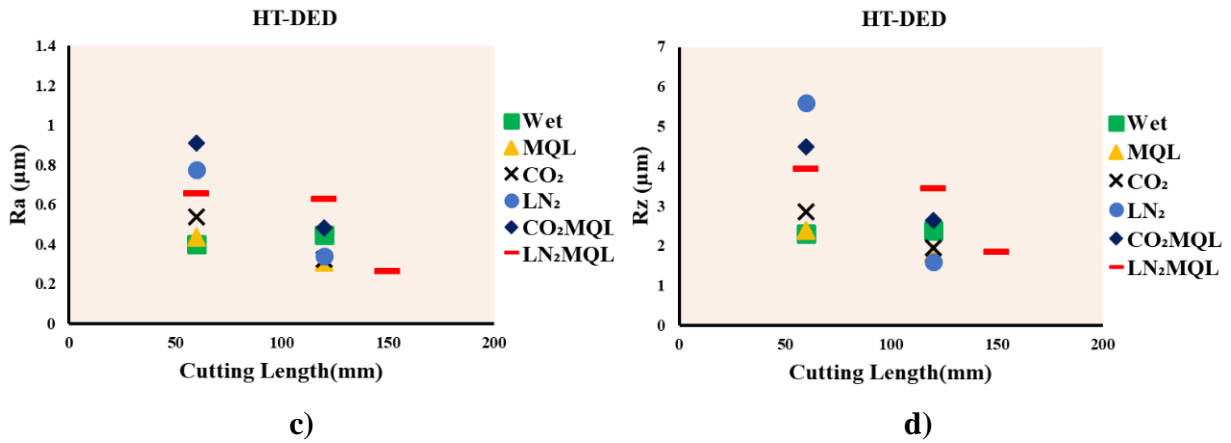


Fig. 4-10: a) Ra during machining of as-built DED samples, b) Rz during machining of as-built DED samples, c) Ra during machining of heat-treated DED samples, and d) Rz during machining of heat-treated DED samples under all lubricating/cooling methods.

Fig.11 shows the SEM images of the surface after machining of as-built SLM parts under different cooling/lubricating conditions. In Appendix, Figs. S4 to S7 show the more detailed SEM images of the surface after machining of as-built SLM, HT-SLM, as-built DED, and HT-DED, respectively. The analyses of the machined surfaces reveal a correlation between the machining method and machined surface quality. The deformed feed lines can be attributed to the consequences of the wet and MQL methods. Besides, CO₂ machined surface shows resettlement, re-deposited, and micro-porosity left from working material, while LN₂ machined samples display debris left from working material. Consequently, it can be deduced that the low-temperature coolants do not provide adequate lubrication needed in high-speed milling of AM-manufactured parts. The simultaneous thermal softening and work hardening affect the material removal. The addition of MQL to CO₂ or LN₂, on the one hand, offered better lubrication to the cutting process and resisted excessive thermal hardening in a balanced manner. Consequently, hybrid methods showed a better surface quality with less deformation in comparison to the other strategies in the machining of AM parts.

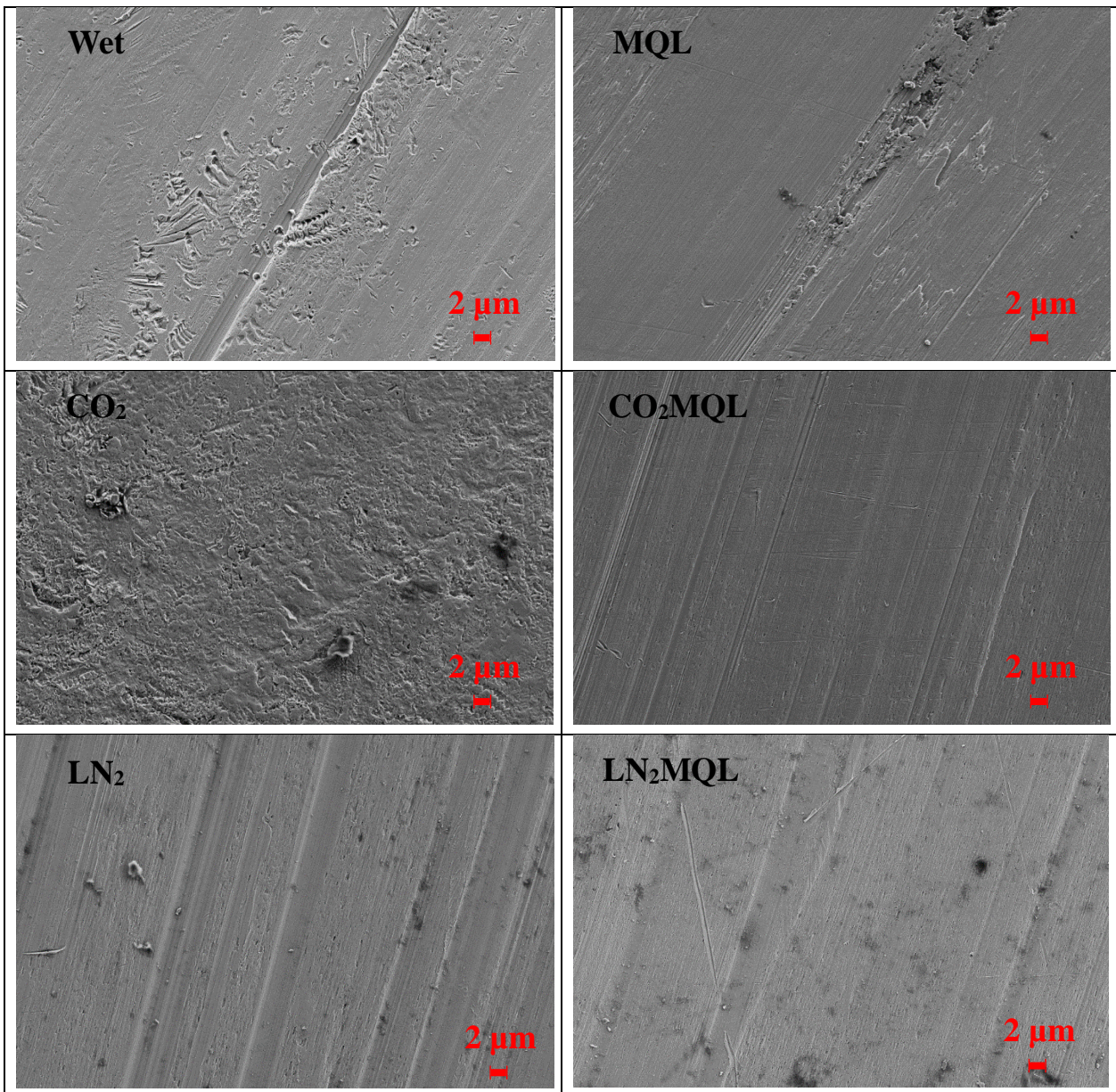


Fig. 4-11: SEM image of the generated surface in the machining of as-built SLM under different machining strategies.

4.2.5. Phase analyses

The identification of the phase constituents and texture changes in the machined samples simultaneously helps to determine the surface mechanical properties, and to better understand the hybrid additive and subtractive manufacturing when the additive process continues again on the machined surface. However, in addition to the phases, the residual coolant or lubricant presence on the surface affects the additive process. Since the cryogenics disperse into the air after application, the residual effects will be reduced, and therefore the requirements for post-machining cleaning will be eliminated.

The remarkable properties of the Inconel 718 alloys could be attributed to their microstructure where main strengthening phases are known to be L12 ordered face-centered cubic (FCC) γ' -Ni₃ (Al,Ti) phase and γ'' -Ni₃Nb with body-centered tetragonal (BCT) structure, and a great deal of orthorhombic D0a structural δ phase (Goel et al., 2019; Komarasamy et al., 2019b; Shao et al., 2019). The high strength and resistance to high temperatures of Inconel 718 arise from γ' and γ'' phases that are acting as impediment for the dislocation movement, and surpassed via two mechanisms either a) by cutting of dislocations or b) by-passing by the bowing of dislocations. With employment of tailoring on the microstructure of the Inconel 718, i.e. controlling the size and distribution of the precipitates, further improvement of mechanical properties such as tensile strength, fatigue and creep properties known to be achieved. In contrast, δ phase is a brittle phases triggering micro-cracks at grain boundaries and therefore avoided to have in microstructure for which it can cause cracks during machining process as well. (Xu et al., 2018)

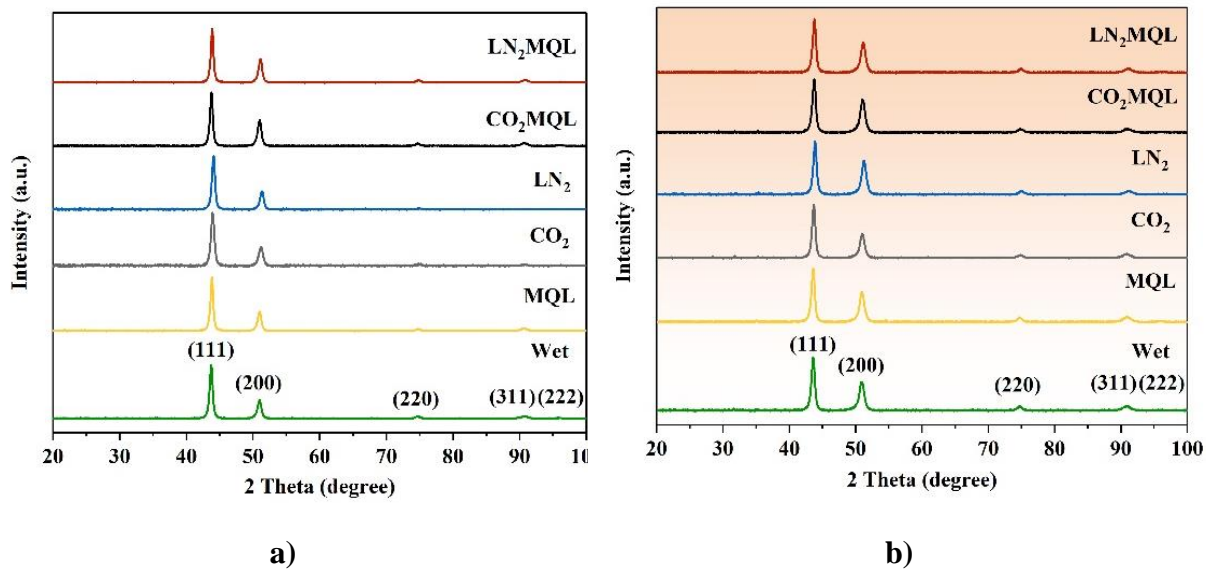
Knowing this information, XRD analyses conducted on the machined Inconel 718 surfaces. Fig. 12 shows the XRD patterns of as-fabricated and heat-treated AM parts after different machining strategies. It can be observed from the XRD patterns that the machining of heat-treated samples manifests the strong (200) texture. Because (200) and (220) diffraction peaks of γ'' -bct (Ni₃Nb) precipitates overlap with the same for the γ -FCC matrix, an enhancement in the peak intensity ratio of I₂₀₀/I₁₁₁ was observed (Komarasamy et al., 2019a). Besides, the strong diffraction intensity of (200) atomic planes is due to the preferred growth along the crystallographic direction of $\langle 100 \rangle$ during crystallization of Inconel 718 (Strondl et al., 2008). Similar peaks belonging to overlapped (111) γ/γ' , (200) $\gamma/\gamma'/\gamma''$ and (220) $\gamma/\gamma'/\gamma''$ are also reported to be observed for the additively manufactured Inconel 718 in the literature (Cao et al., 2018; Luo et al., 2019) which also verifies what was observed in the current study. In contrast, none of the peaks corresponded to the (211) δ phase was not obtained on the basis of observed XRD spectra in Fig. 12.

As observed in machined samples of DED-manufactured parts, a different peak was identified under the CO₂ machining strategy. The rapid experience of high cutting temperature in addition to the cooling affects the material phase composition. Consequently, the high-speed CO₂ milling method resulted in a different peak at 43.21° when compared to other machined conditions. Previously, it was shown that Ni₄Ti₃ is generated through strong thermal cycles during the WAAM processing of Inconel 718 alloy (Zeng et al. 2020). In the current study, the diffraction peak observed at 43.21° can bring the idea that it can be

attributed to the (122) atomic plane of the Ni₄Ti₃ (Khalil-Allafi, Dlouhy, and Eggeler 2002) with a hexagonal crystal structure according to the JCPDS card No. 39-1113. However, since more solid evidence was not found for Ni₄Ti₃ phase's formation, it is commented that this phase more possibly belongs to γ'' phase as was shown before by (Raghavan et al. 2017).

The results of temperature analyses support the claim that using CO₂ as coolant in machining causes formation of γ'' phase peak with a recognizable peak intensity at almost 43°. This phenomenon was not observed when additively manufactured Inconel 718 alloy was machined using other coolants. In the machining of Inconel 718 alloy using coolants other than CO₂, γ'' phase peak at 43° is observed. This outcome is attributed to the fact that even though the temperature increase during the machining using CO₂ is not so significant, it is still enough for increasing the volume fraction of the γ'' phase.

Moreover, when the peak relative intensity of hybrid cooling methods was compared to CO₂ or LN₂ conditions, the stronger texture was observed for (200), (220), (311), and (222).



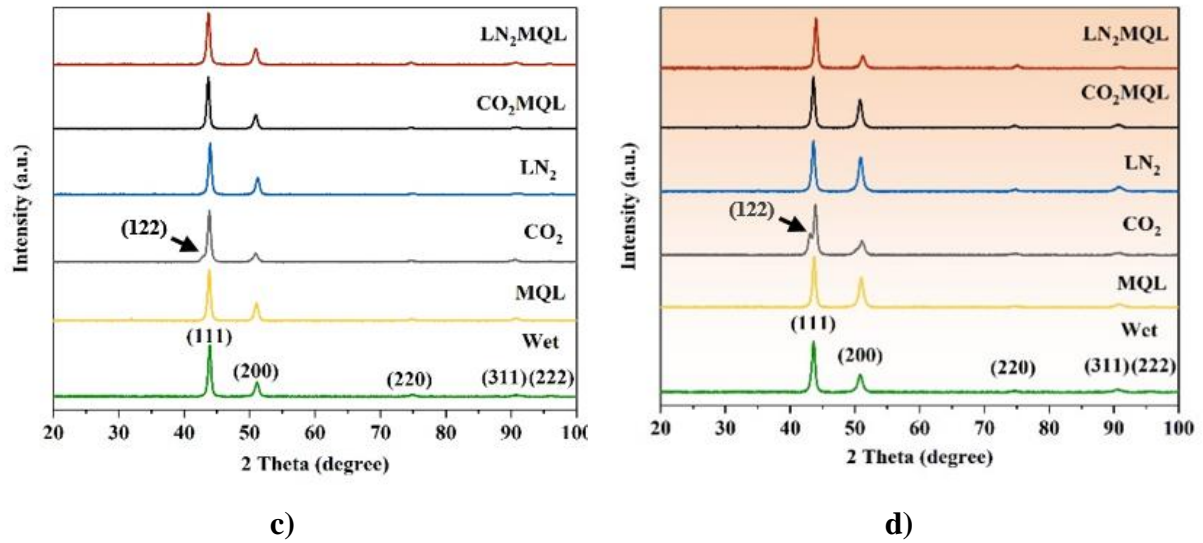


Fig. 4-12: The normalized XRD patterns of (a) machined as-built SLM, (b) machined HT-SLM, (c) machined as-built DED, and (d) machined HT-DED under different cooling/lubrication conditions.

To sum up, the properties of the materials including thermal history, thermal conductivity, and hardness have a significant effect on the machinability of the AM parts. In general, the generated heat in machining process and subsequent the heat removal are the key factors in the selection of cooling or lubrication methods. Meanwhile, in addition to the cooling/lubrication supply, the cutting tool and workpiece also participate in the heat removal from the working zone, and the material properties of both the cutting tool and workpiece are important for the selection of an effective cooling/lubrication method. For example, during the machining of the materials with higher thermal conductivity and/or using the cutting tools with higher thermal conductivity, the hybrid method will show a negative effect on machinability in comparison to the application of hybrid methods using material and/or tools with lower conductivity because of the excessive cooling effect. Thus, the hybrid supply should be optimized in such cases. The hybrid methods are introduced as the best alternative in high-speed machining of the hard to cut materials because of the capability of efficient cooling and lubrication. Nevertheless, the suitable flow should be applied depending on the process parameters (such as cutting speed, feed rate, depth of cut), additively manufactured (using SLM, DED, and etc.) material properties, and the cutting tool type (coated, uncoated, carbide tool, and etc.).

4.2.6. Energy Efficiency and Cost of Additive-Subtractive Production

The additively manufactured materials recently gained enormous interest, however, majority of the already conducted research are focused on parameter studies and studies relating to the energy efficiency and cost estimation of additively manufactured parts are scant. In some of these studies, energy consumption to actually build a functional part was made and efficiency of the procedure was evaluated on the basis of emerging waste material. To build a bracket, buy-to-fly ratio is reported to increase when the conventional machining manner was chosen instead of additive manufacturing (Huang et al., 2016; Liu et al., 2018); it is 8:1 and 1.5:1 (this value is almost the same for all additive manufacturing techniques) for conventional machining and additive manufacturing, respectively. The initial ingot used for the machining was reported to be around 8.7 kg to fabricate a bracket around 1.1 kg while only 0.57 kg powder was utilized during the manufacturing process of additively manufactured bracket with a final weight of 0.38 recommending only 0.3-fold of the initial powder is wasted. Additive manufacturing did not only achieve in the material save part, but also has a significant influence in the energy consumption aspects. The energy consumed during conventional machining of the brackets were reported to be found 226.945 MJ whereas the best result arising pertained to the L-PBF fabricated bracket at around 76.93 MJ suggesting a significant change in the energy save by simply selecting L-PBF type additive manufacturing over conventional machining. To calculate what was required to fabricate components using the DED manner has also recently been one of the most interesting subjects. To reconstruct 5% volume of a turbine blade, 1610.6 MJ energy is reported to be required and knowing this information almost, therefore, almost a 32212 MJ energy is estimated to be enough to complete a whole turbine blade. The mass of a turbine blade is almost 15.6 kg meaning a 2064.87 MJ energy per kg of the product (including ingot, and powder production steps); this almost suggests that the energy consumed during DED fabrication per kg of the part is almost ten folds of L-PBF production. But still DED method is much efficient to give rise less waste material when compared to the conventional machining procedure and also L-PBF. The cost of energy for DED is higher. Similarly, the cost of DED powder is greater, and approximately two times of L-PBF powder per kg. Nevertheless, DED process is still attracts great deal of attention due to its advantages other than just economy such as being faster, producing much larger parts with higher density, being used in repairmen process and for ability to build of multi-materials.

The energy consumed during conventional production such as casting was also reported. Wilson et al. reported the energy for producing a metal in a bar stock form to fabricate a turbine blade was found to be 4586.7 MJ (Wilson et al., 2014). Almost 286.7 MJ of energy was reported to be consumed for remelting during the investment casting process (Morrow et al., 2007). Subsequently, 133.2 MJ (calculated by (Wilson et al., 2014)) and 16.5 MJ (Margolis et al., 1999) energy values was reported to be used for heat treatment and cleaning-finishing process of the nickel-based alloy made turbine blade, respectively. All of these steps foresee almost a 5023.1 MJ energy consumption for production of a turbine blade by means of using casting. The energy consumed during casting fabrication is almost 322 MJ per kg of a part meaning 1.5 times greater energy consumption than L-PBF fabrication but 6.4 times less than DED process.

Cleaning/Finishing operation of the additively manufactured turbine blades reported to be around 0.8 MJ for 5% volume suggesting an approximate value of 16 MJ for a complete turbine blade. This was reported to be around 16.5 MJ by (Margolis et al., 1999) for a complete bracket manufactured using casting method. The energy need for finishing operation of a 0.78 kg part for 5-axis CNC processing was also reported to be around the same value by Wilson et al. (Margolis et al., 1999; Wilson et al., 2014) and that is around 0.8 MJ. Based on this information, it is hypothesized that some of the energy differences may arise through the cleaning process of the parts fabricated using different manufacturing techniques such as between DED compared to the casting or to the L-PBF fabrication. During the high-speed machining, regular cooling cannot be applied due to rapid consumption of the cutting tool, especially in the case of machining of additively manufactured parts. This knowledge is confirmed by tool life graphs of L-PBF and DED graphs in our current work, as shown in Figs. 4 and 5. In addition, owing to the emerging material property variations, such as microstructure and hardness properties, stemming from using different additive manufacturing techniques such as DED and SLM of the Inconel 718 powder, tool life consumption of the DED becomes almost three and two folds of L-PBF fabricated parts for the as-built and heat treated conditions, respectively; this was compared considering the conditions with the best results arising. Moreover, judging from the tool life graphs, the two times and 1.5 times faster consumption of the cutting tool with the introduction of a heat treatment when compared to the as-built condition becomes obvious for the case of L-PBF and DED, respectively. Consequently, the cost of the process will be affected by the choice of

additive manufacturing techniques and the introduction of a post processing such as heat treatment.

4.3. Conclusions

This work investigated the synergistic additive and subtractive mechanism of Inconel 718 using hybrid cryogenic cooling strategies. The machining tests were carried out on four different types of additively manufactured parts including as-built SLM, as-built DED, heat-treated SLM and heat-treated DED parts. Six different cooling/lubricating techniques were used for milling of additive parts, namely wet, MQL, CO₂, LN₂, CO₂MQL, and LN₂MQL. The influence of each strategy on machinability, surface finish, tool life, cutting temperature, cutting forces, and Inconel 718 phases were studied. The important conclusions of this study can be summarized as follows.

- The method of additive manufacturing affects the machinability of Inconel 718 part where DED fabricated samples show lower machinability and higher temperatures during machining compared to the energy efficient SLM manufactured samples whereas DED samples have more consistent surface roughness and surface quality.
- The longest tool life;
 - i) For the SLM, it was obtained with MQL (also the most efficient one for SLM samples) and hybrid cooling methods/CO₂ in as built and heat-treated parts, respectively.
 - ii) For the DED, it was obtained using hybrid method of LN₂MQL.
- The milling forces with MQL were found to be lowest for both as-built SLM and HT-SLM, while hybrid conditions showed the lowest cutting forces in milling of as-built and HT-DED parts. This is because of different thermal history, thermal conductivity and hardness of these AM parts.
- The lowest and highest workpiece temperatures were measured under LN₂ and MQL methods, respectively. However, it was found that the hybrid methods balanced the heat removal and provided balanced cooling and lubrication.
- The hybrid methods enhanced the surface finish and final product quality due to the improvement of lubrication at the same time providing a balance in heat removal and thermal softening.

High speed machining of AM manufactured Inconel 718 using hybrid cooling/lubrication methods can result in reduction of costs associated with the material, energy, and cutting tool and hence brings additional sustainability benefits to the additive manufacturing industry. Producing the parts using SLM with heat treatment and machining them utilizing frozen oil particles as lubricant would be recommended to the industry and other scholars for which it is the most energy efficient fabrication way providing the lower cutting tool consumption and therefore lower cost with higher quality.

5. MACHINING BEHAVIOR OF INCONEL 718 IN HYBRID ADDITIVE AND SUBTRACTIVE MANUFACTURING

5.1. Investigation of additively manufactured metal cutting behavior through thermomechanical approach

The orthogonal cutting resembles a shaping process in which the material is cut by a cutting-edge perpendicular to the direction of cutting velocity.

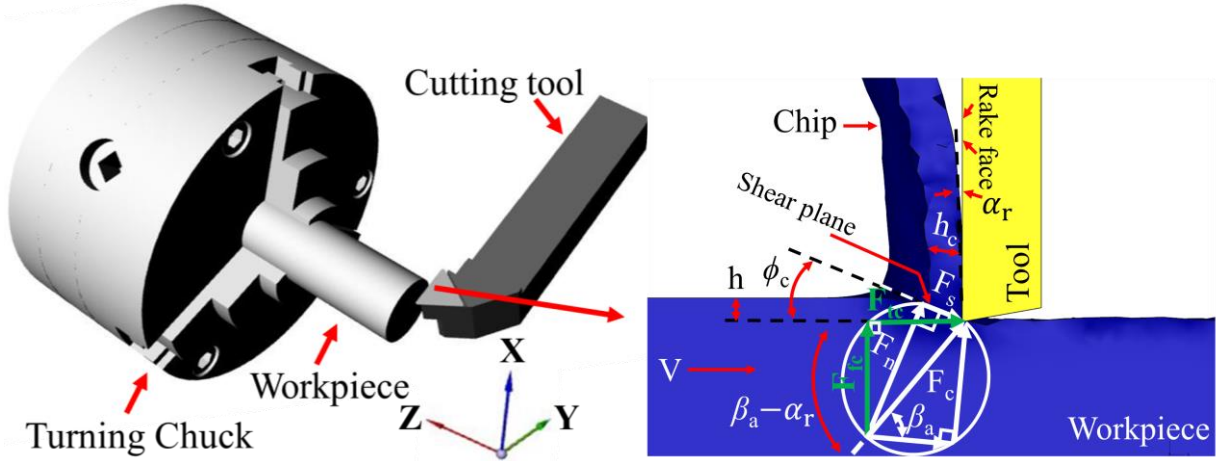


Fig. 5-1: Schematic of orthogonal cutting and the cutting force diagram

The orthogonal cutting is assumed to be a two-dimensional plane strain deformation where it is uniform along the cutting edge without side spreading of the material. Therefore, the cutting forces are exerted in two directions. The direction of velocity is called tangential force (F_t) and the direction of chip thickness is called feed force (F_f). Schematic representation of orthogonal cutting and the cutting force diagram are shown in Fig. 1. Here, a sharp cutting edge without a chamfer and also an infinity thin primary shear deformation zone is assumed for simplification. The detailed formulation for the cutting mechanics can be found in (Altintas, 2012). The shear angle can be found from the geometry as follows:

$$\phi_c = \tan^{-1} \frac{r_c \cos \alpha_r}{1 - r_c \sin \alpha_r}$$

where α_r is the rake angle and r_c is the chip compression ratio. The ratio of the uncut chip thickness (h) over the deformed one (measured chip thickness, h_c) is equal to the chip compression ratio ($r_c = \frac{h}{h_c}$). It is assumed that the chip slides over the rake face of the tool with an average and constant friction coefficient of μ_a and it can be calculated as:

$\mu_a = \tan \beta_a$ where the β_a is the friction angle, can be calculated from the tangential and feed forces as below:

$$\beta_a = \alpha_r + \tan^{-1} \frac{F_{fc}}{F_{tc}}$$

For cutting processes, a thermomechanical dual zone model is provided in our previous study (Budak and Ozlu, 2008a). It is suggested to apply a non-linear regression fitting approach with the experimental data set employing shear stress at shear plane to choose the appropriate parameter set. The flow stress is expressed according to the JC model where strain, strain rate, and temperature effects are taken into consideration as follows:

$$\tau = \frac{1}{\sqrt{3}} \left[A + B \left(\frac{\gamma}{\sqrt{3}} \right)^n \right] \left[1 + \ln \left(\frac{\dot{\gamma}}{\dot{\gamma}_0} \right)^c \right] \left[1 - \left(\frac{T - T_r}{T_m - T_r} \right)^m \right]$$

where A is the yield stress at the reference temperature and strain rate, B is the coefficient of strain hardening, n exponent of strain hardening, C is the coefficient of strain rate hardening, m is the thermal softening exponent, γ is the shear strain, $\dot{\gamma}$ is the shear strain rate, $\dot{\gamma}_0$ is the reference shear strain rate, T is the absolute temperature and T_m and T_r are the melting and the reference temperatures, respectively. A shear stress of τ_0 is applied to the material when it enters the primary shear zone. The shear stress has changed to the value τ_1 when it exits the primary shear zone, which is different from τ_0 when inertia effects are significant. Iterative calculations of τ_0 are possible if the shear zone thickness is assumed to be constant and the pressure distribution is uniform. The shear stress at the exit of the shear plane is estimated using the equations of motion for a continuous type of chip and steady state solution as follows:

$$\tau_1 = \rho(V \sin \phi_c)^2 \gamma_1 + \tau_0$$

where V is the cutting speed, γ_1 is the strain because of plastic deformation at the shear plane. The non-linear regression analysis is used to determine the JC parameters. Since non-linear regression analysis is highly influenced by the initially defined parameters, not all the parameters are calculated simultaneously. The thermo-mechanical properties of nickel alloy 718 and the initial material constant used for calibration and modeling are presented in Table 1 and 2, respectively. The AM process and AM condition have significant effect on the mechanical properties. The Inconel 718 powder was totally melted using the high laser power resulting in the best mechanical strength performance and prevented the development of

fusion defects. High energy density may also result in decreased mechanical strength since so much energy is being applied to the structure of the material. Furthermore, the mechanical strength continues to be influenced by the spot size where the small spot size enhanced the elastic modulus and hardness (Kladovasilakis et al., 2022). Using these initial values, the non-linear regression analysis is applied which minimizes the difference between the predicted and measured shear stresses. To obtain proper values of the parameters, first parameter A is calculated with the given initial values. Then, C, and m values were calculated followed by the coefficients B and exponent n. Finally, the exponent m was calculated. The calibrated material parameters are illustrated in chapter 4.4.

Table 1: Thermo-mechanical properties of Inconel 718

Material	Heat capacity (J/kg*K)	Density (kg/m³)	Thermal conductivity (W/m*K)
SLM-manufactured	435	8190	11.4 (Promoppatum et al., 2018) 8.9 (Romano et al., 2016)
DED-manufactured	435 (Yuan et al., 2019) 440 (England, 2011)	8240 (Yuan et al., 2019) 8150-8190 (England, 2011)	10.22 ± 0.04–15.07 ± 0.03 (Onuikie et al., 2018)
Wrought	515 (Parida and Maity, 2017) 432 (Parida and Maity, 2018)	8200 (Parida and Maity, 2018) 8080 (Parida and Maity, 2017)	11.4 (Parida and Maity, 2018) 8.5 (England, 2011) 10.5 (Parida and Maity, 2017)

Table 2: The initial material constant used for calibration.

Material	A(MPa)	B(MPa)	n	C	m
SLM-manufactured*	963	937	0.333	0.0211	1.3
DED-manufactured (Yuan et al., 2021)	710	1653	0.24	0.02	1.2
Wrought(Mitrofanov et al., 2005)	1241	622	0.652	0.0134	1.3

*Measured and calculated for SLM sample using the tensile test

The model of the viscoplastic flow within the primary shear zone was employed. The rake contact of the cutting tool was represented by the dual-zone model. Sticking friction was used to model the first area of the rake contact, and sliding friction was used to model the subsequent area. The detailed formulation for the dual-zone and stress distributions on the

rake face can be found in (Budak and Ozlu, 2008a; Ozlu et al., 2009). The apparent and sliding friction coefficients were used to determine the rake contact. The apparent friction coefficient is defined as the ratio between the total frictional and normal forces applied on the rake face. Therefore, the following was achieved:

$$\mu = \frac{\tau_1}{P_0} \left[1 + \xi \left(1 - \left(\frac{\tau_1}{P_0 \mu_s} \right)^{\frac{1}{\xi}} \right) \right]$$

where τ_1 is the shear stress at the exit of the shear zone and P_0 is related to the normal force acting on the rake face in the normal direction by considering the pressure distribution throughout the contact length. Finally, the orthogonal tube cutting experiments were used to obtain the sliding friction coefficient as a function of chip velocity v_c .

5.2. Materials and methods

5.2.1. Sample preparation

In this research, wrought, DED, and SLM fabricated tubes with inner and outer diameters of 27 and 31 mm, respectively were selected as samples. The DED components were manufactured utilizing Oerlikon Metco's Inconel 718 powder (Oerlikon MetcoAdd In718F), while the SLM components were fabricated using Inconel 718 powder from the same supplier (Oerlikon MetcoAdd In718C). The morphology of the Inconel 718 powders is depicted in Figure 2. The particle size distribution and chemical composition of the Inconel 718 particles can be found in Table 3 and Table 4, respectively. To produce the DED parts, a DMG Mori Lasertec 65 3D machine with a maximum laser power of 2500 W was employed, while an EOS M290 SLM machine (EOSINT GmbH-Electro-Optical system, Germany) with a maximum laser power of 370 W was used to manufacture the SLM parts. The operational principles of the DED process and SLM process are illustrated in Figure 3. The scanning strategies employed for manufacturing the DED and SLM test parts were 90° and 67° rotation, respectively. The specific DED and SLM parameters utilized in this study are listed in Table 5. In addition, the top surface of AM manufactured samples are illustrated in Fig. 3.

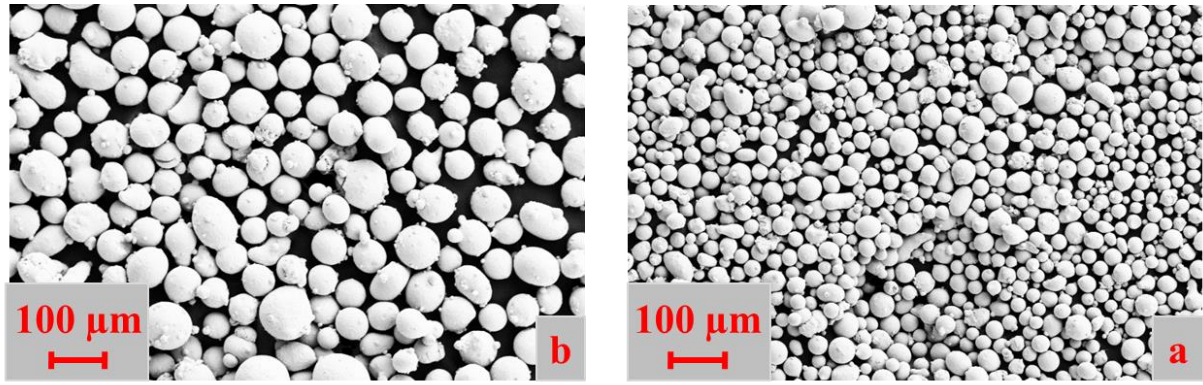


Fig. 5-2: The morphology and size of Inconel 718 powders. a) SLM powder b) DED powder

Table 3: Particle Size Distribution and Hall Flow

	Nominal Range [μm]	D90 [μm]	D50 [μm]	D10 [μm]	Hall Flo [s/50 g]
MetcoAdd 718C	-45 +15	46	30	18	< 18
MetcoAdd 718F	-106 + 45	-	-	-	-

Table 4: Chemical composition of AM powder

	Weight Percent (nominal)							
	Ni	Cr	Fe	Nb+Ta	Mo	Al	Ti	Other
MetcoAdd 718C / 718F	Balance	18	18	5	3	0.6	1	< 0.5

Table 5: SLM and DED parameters used in this study.

Process parameters	SLM	DED
Laser power (W)	285	2000
Laser scanning speed (mm/min)	960	1000
Hatch spacing (mm)	0.11	1.5
Layer thickness (mm)	0.04	1.12

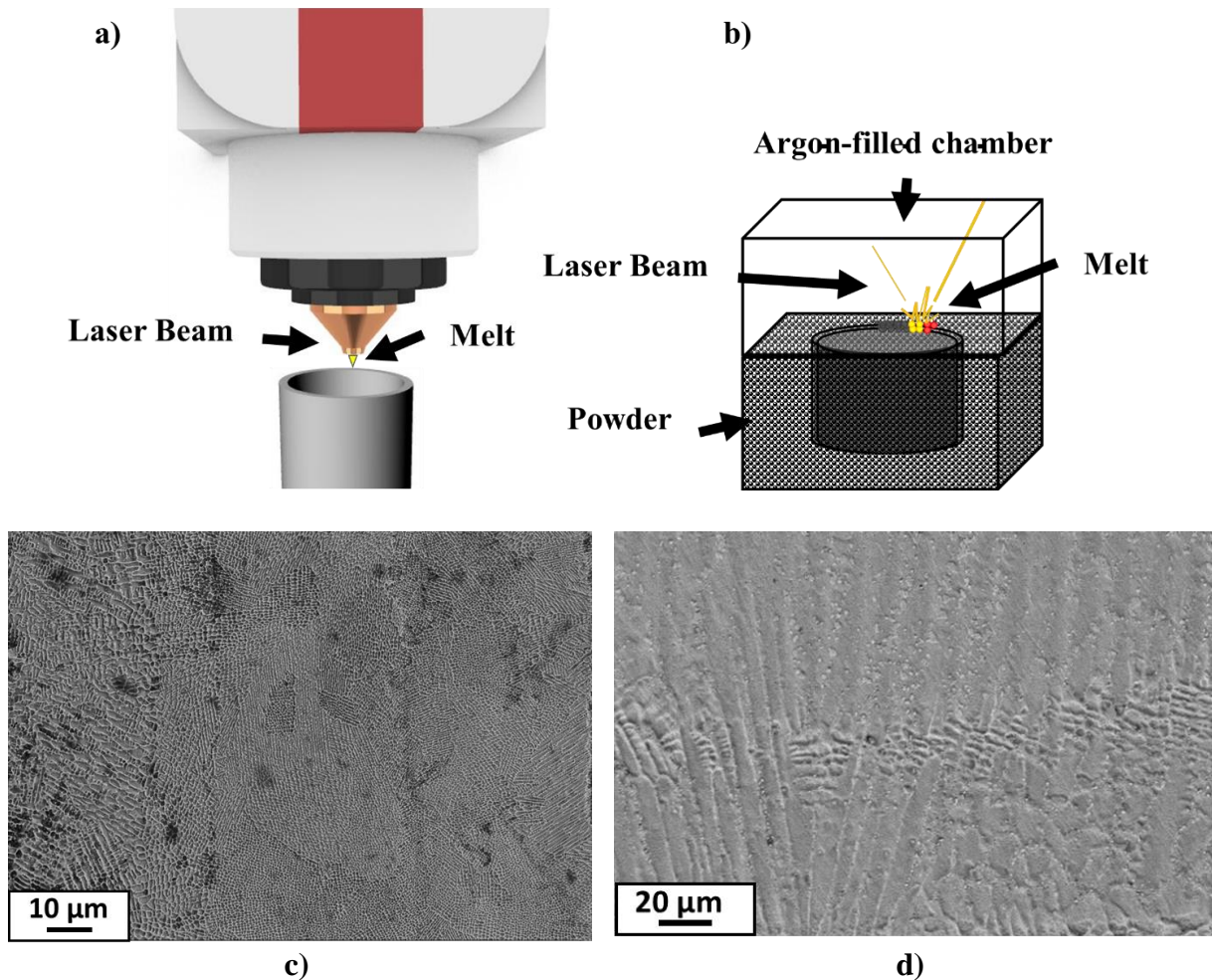


Figure 5-3: a) Working principles of DED process, b) Working principles of SLM process, c) The illustration of SLM manufactured Inconel microstructure, d) The illustration of DED manufactured Inconel microstructure.

5.2.2. Machining tests

The orthogonal cutting tests were carried out on Mori Seiki NL 1500 CNC Turning Machine. Uncoated carbide inserts with the designation of TPGN160308 were mounted on a tool holder to provide a rake angle of 5 and a lead angle of 0. The hone radius of the inserts measured as 3μm. The tool holder was held by a Kistler 9129AA-type dynamometer to measure forces and Lab View Signal Express software was used for the Data logging. Each experiment was repeated three times and the average of the measurements was used. By carrying out trials at variety of feeds and cutting speeds, the impact of uncut chip thickness and cutting speed is also taken into consideration. The details of machining parameters are presented in Table 6.

Table 6: Cutting data.

Experiment Number	Materials	Cutting speed (m/min)	Feed rate (mm/rev)	Depth of cut (mm)
1		30	0.02	
2		30	0.04	
3		30	0.06	
4		30	0.08	
5	SLM-manufactured	60	0.02	
6	(Wet and Dry	60	0.04	
7	condition), DED-	60	0.06	2
8	manufactured	60	0.08	
9	and wrought Inconel	90	0.02	
10	718	90	0.04	
11		90	0.06	
12		90	0.08	

5.3. Results and discussion

5.3.1. Evaluation of edge forces and friction coefficient

Hard-to-cut materials such as Ti6Al4V and Inconel 718 exhibit poor thermal conductivity, high resistance to temperature, and high hardness at elevated temperatures (Bagherzadeh and Budak, 2018c). As a result, these materials have low machinability, and it is recommended to use cooling/lubrication when machining them. In this study, the edge forces of dry and wet cutting conditions for SLM-manufactured parts were identified and compared using the cutting conditions provided in Table 6. By extrapolating the recorded forces to zero chip thickness, the edge forces were determined (Altintas, 2012). The edge forces in the feed direction are normally higher than those in tangential direction. However, as shown in Table 7, under dry conditions, the edge forces in the feed direction are equal to or greater than the edge forces in the tangential direction. This is due to the high tool wear on the cutting edge during the cutting of Inconel 718. Similar behavior was observed for the edge forces using wet cooling as wet cooling did not significantly control the tool wear. Notably, there are significant differences in edge forces between wet and dry cutting at different speeds, as cooling greatly affects the cutting mechanism in cutting Inconel 718. Therefore, in this study, dry cutting was chosen to conduct the fundamental analyses of AM Inconel 718 machining, where no cooling effect is present. In addition, the commonly used wet cutting condition was compared to dry cutting of SLM parts to identify the possible fundamental effect of wet condition during hybrid manufacturing. The edge forces of wrought, SLM, and DED cutting are reported in Table 8, where the edge forces decrease almost similarly with increasing cutting speed. The edge effect is less noticeable at high cutting speeds compared to other

additional effects. However, in DED cutting, the edge forces notably decrease at a cutting speed of 60 m/min. The edge radius also plays a significant role in the edge effect, as an increased edge radius reduces the edge effect with increasing cutting speed (Sela et al., 2019).

Table 7: The edge forces in cutting of SLM-manufactured samples in wet and dry condition.

Cutting Speed (m/min)	SLM-manufactured in Dry condition		SLM-manufactured in Wet condition	
	F_{te} (N)	F_{fe} (N)	F_{te} (N)	F_{fe} (N)
30	120	115	190	220
60	133	170	81	106
90	73	73	90	117.5

Table 8: The edge forces in dry machining of SLM, DED and wrought samples

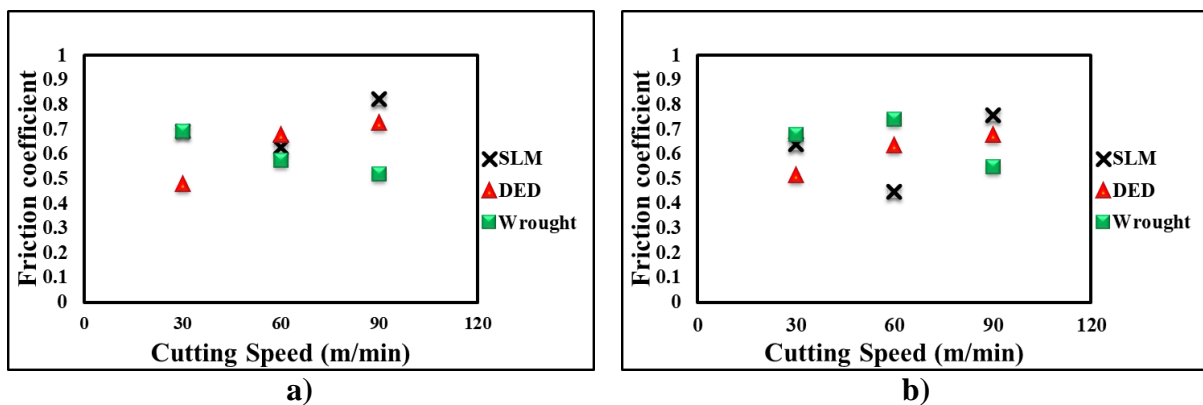
Cutting Speed (m/min)	SLM-manufactured		DED-manufactured		Wrought	
	F_{te} (N)	F_{fe} (N)	F_{te} (N)	F_{fe} (N)	F_{te} (N)	F_{fe} (N)
30	120	115	135	137.5	145	140
60	133	170	87.5	87.5	130	117.5
90	73	73	77.5	82.5	70	96

The standard material parameters derived from tensile and friction testing pose a challenge when attempting to predict stress in the shear plane, shear angle, and average friction coefficient on the rake face of the cutting tool. Such fundamental characteristics are determined using orthogonal cutting experiments, which evaluate the feed and tangential cutting forces by utilizing the deformed chip thickness. Fig. 4 presents the friction coefficient for wrought, SLM, and DED materials at feed rates of 0.02, 0.04, 0.06, and 0.08 mm/rev. As depicted in the figure, in the cutting of wrought parts, the friction coefficient decreases with increasing cutting speed. The reason can be attributed to the higher temperatures reached at the contacting surfaces due to the elevated speed. However, the behavior of the friction coefficient in the cutting of SLM and DED parts differs from that of wrought parts.

In high-speed machining, most of the heat generated is carried away by the chip's fast movement, resulting in a reduced heat transfer into the workpiece. Additionally, the cutting tool's limited thermal conductivity and specific heat contribute to lower heat transfer, causing higher temperatures at the tool-chip contact area. This localized temperature rise increases the

local plastic flow of the chip material and reduces friction at the chip-tool interface. During low cutting speeds, the chip velocity is low, resulting in more rubbing action between the chip and the tool. This causes the grain to lengthen, leading to higher strain rates compared to high-speed cutting. As the cutting speed increases, the grain orientation angle decreases. This is due to a drop in the thermal gradient, an increase in the velocity gradient across the body of the chip, and a decrease in frictional conditions at the tool-chip interface with increasing cutting speed (Sela et al., 2019). In additively manufactured Inconel 718 parts, the columnar grains that are aligned in the same direction as the build will conduct heat more effectively than grains oriented in other directions. As a result, areas of the material with a high thermal gradient parallel to the build direction will experience a smaller temperature increase compared to regions with a high thermal gradient perpendicular to the build direction. However, the thermal conductivity of AM Inconel 718 parts may vary due to different process parameters and the orientation of the part during the build. For example, parts constructed using higher laser power and scan speeds may exhibit a more substantial thermal gradient between the build direction and transverse direction due to the greater thermal gradient during solidification.

It is unrealistic to assume that all work materials with a comparable microstructure reflect the same friction model. In addition, tool wear affects friction and various components, such as adhesion or ploughing components, in diverse ways that might become the primary friction mechanisms (Grzesik and Rech, 2019). Furthermore, the antifriction characteristics are particularly impacted by the size of the nanoscale γ' and γ'' phases in the γ phase matrix (Zhao et al., 2018). As shown in Fig. 5, the addition of flood supply to the cutting process reduces the range of friction coefficient, which changes between 0.3 and 0.7 depending on the cutting conditions. In contrast, in dry conditions, the friction coefficient changes over a larger range, from about 0.4 to 1, in different cutting conditions.



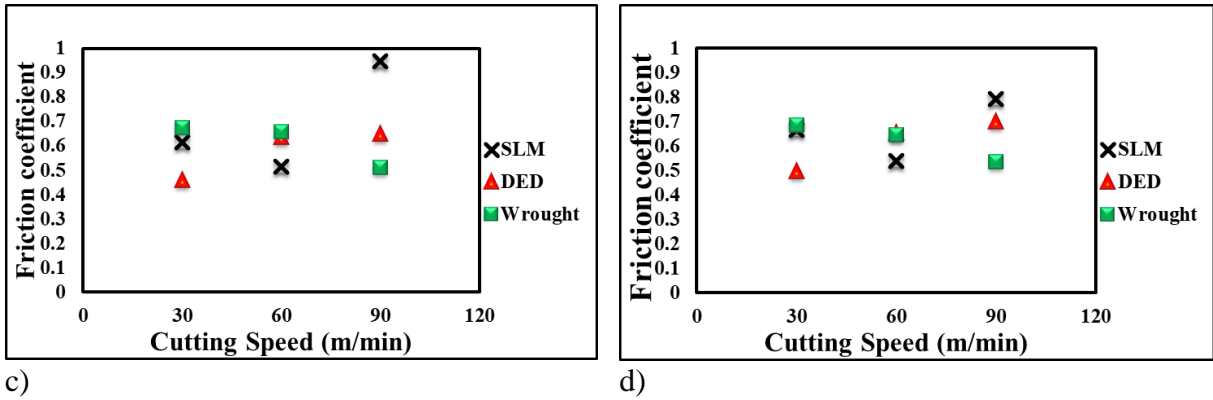


Figure 5-4: Friction coefficient of nickel alloy 718 in hybrid manufacturing compared to machining of the wrought samples. a) at the feed rate of 0.02, b) at the feed rate of 0.04, c) at the feed rate of 0.06, d) at the feed rate of 0.08 (mm/rev).

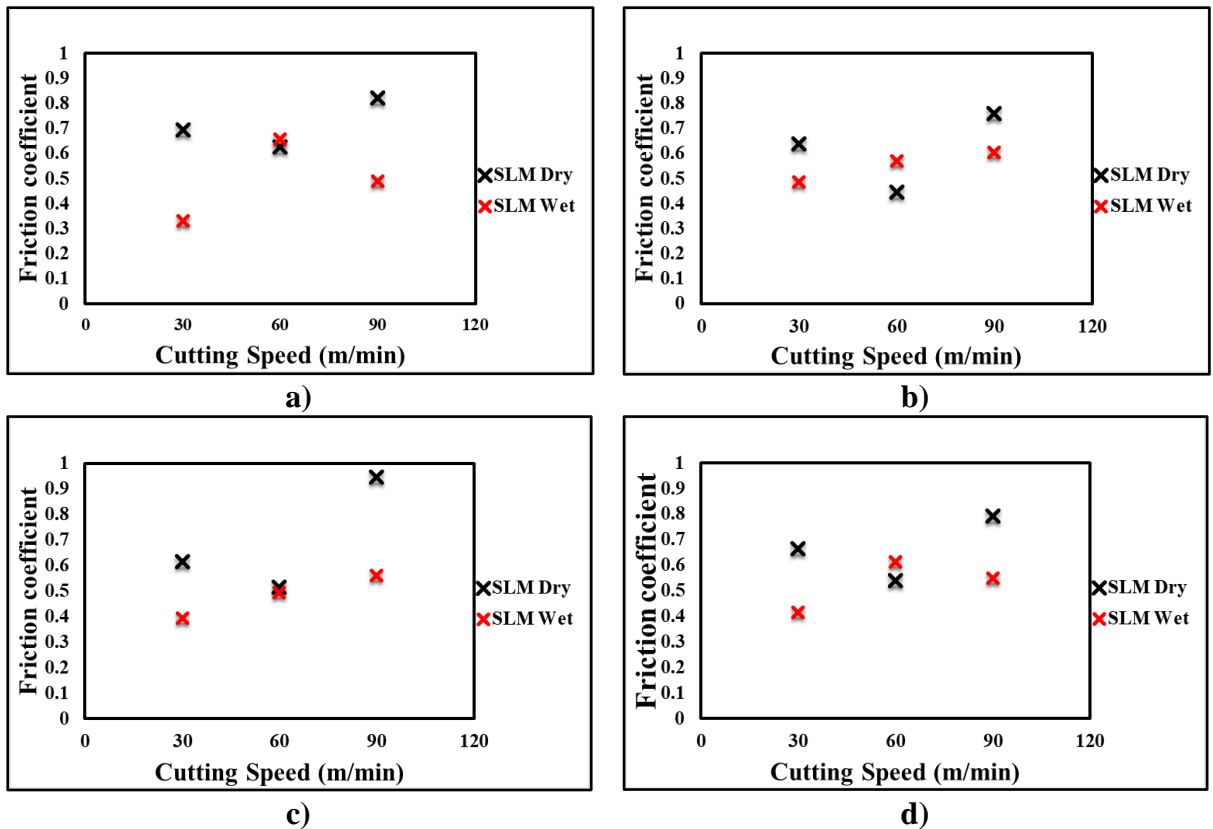


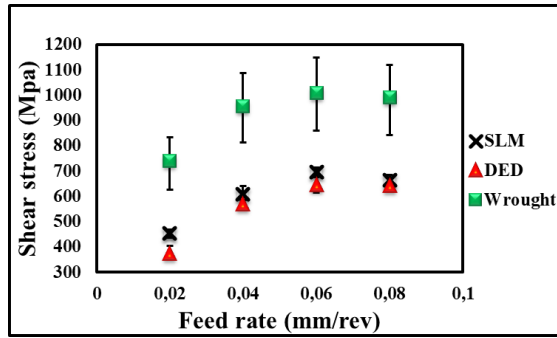
Figure 5-5: Comparison of the friction coefficient between dry and wet orthogonal cutting of SLM Inconel 718. a) at the feed rate of 0.02, b) at the feed rate of 0.04, c) at the feed rate of 0.06, d) at the feed rate of 0.08 (mm/rev).

5.3.2. Evaluation of shear stress

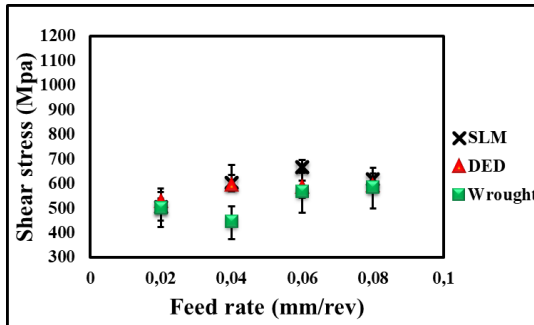
Fig. 6 shows the shear stress of Inconel 718 in hybrid manufacturing compared to orthogonal cutting of the wrought samples for different cutting speeds. In general, during the orthogonal cutting of Inconel 718, shear stresses were found in the order of high to low as Wrought>SLM>DED. The increase of the feed rate resulted in the increase of shear stress.

The grain geometries such as grain shape and size significantly affect the properties of crystalline materials (Droste et al., 2021; Woods et al., 2020). The wrought Inconel 718 material has fine equiaxed crystals due to the sub-grain coarsening and recrystallization during the forging process. The SLM-manufactured Inconel 718 materials have large columnar dendrite grains in the build direction due to the intricate cyclic process involving heating, melting, and solidification during SLM manufacturing. In the SLM-manufactured material, the grain has a similar shape and size because of no recrystallization during the AM process. Nevertheless, the DED-manufactured material has a large columnar grain with a zigzag shape in the scanning direction, where the small equiaxed grains are presented between the layers. The grain boundary acts as an obstacle to the movement of dislocations, impeding their flow. When the material is subjected to stress, dislocations move within the textured grain zone, which has higher resolved shear stress (Pérez-Ruiz et al., 2021b). When a dislocation encounters a grain boundary, local stress is developed. The resistance offered by the grain boundaries has a significant role in the resistance to the shear angle. The model of Zerilli–Armstrong and the theory of Hall–Petch (Zerilli and Armstrong, 2008, 1987) can explain how a decrease in grain size leads to an increase in yield and flow stresses. Thus, both cutting forces (Ducroux et al., 2021) and stresses are proportional to the grain boundary density.

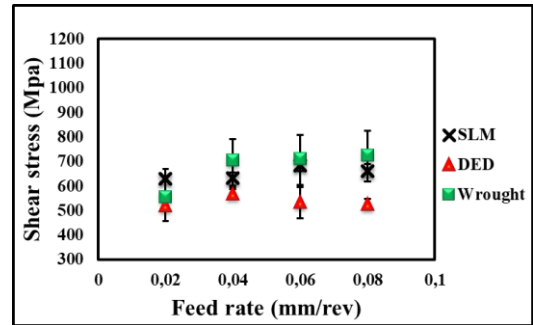
Fig. 7 shows the shear stresses between dry and wet orthogonal cutting of SLM Inconel 718 for different cutting speeds. A reduction in workpiece temperature increases the shear stress of SLM material increasing the cutting force. In the lower cutting speeds, the shear stresses in wet and dry cutting of SLM samples are almost equal. Nevertheless, there are obvious differences in stresses between dry and wet conditions in higher cutting speeds of 60 and 90 m/min since the high-speed machining generates higher temperature than the normal speeds resulting in higher temperature reduction. Higher speeds also cause higher strain rates and thus strain hardening effect. The effect of cutting speed is on the temperature and strain rates. The dominant effect determines the change in the shear stress. In some speeds ranges thermal softening is more dominant resulting in decreasing shear stress. In some other speeds ranges strain hardening effect is more dominant causing higher shear stresses. The assessment of shear stress and shear angle using different cutting parameters have been described in the next chapter to give better visible to the characteristics of AM and wrought Inconel 718 machining.



a)

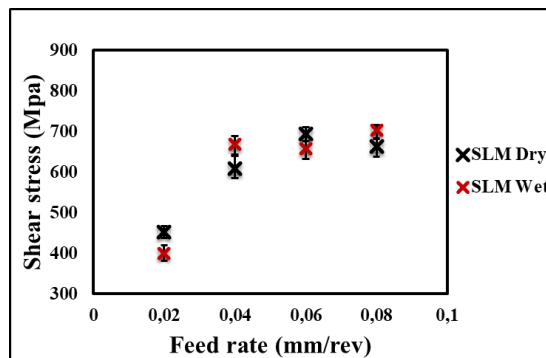


b)

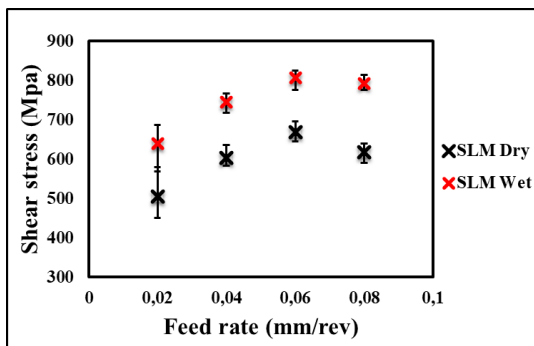


c)

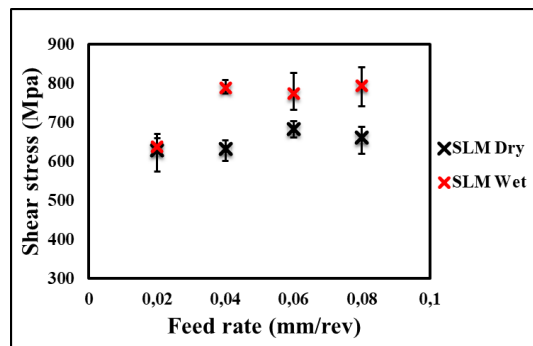
Figure 5-6: Shear stress of nickel alloy 718 in hybrid manufacturing compared to orthogonal cutting of the wrought samples for cutting speeds of a) 30 m/min b) 60 m/min c) 90m/min.



a)



b)



c)

Figure 5-7: Comparison of the shear stresses between dry and wet orthogonal cutting of SLM Inconel 718 for cutting speeds of a) 30 m/min b) 60 m/min c) 90m/min.

5.3.3. Evaluation of shear angle

In general, an equilibrium shear angle corresponding to the constant chip thickness would be reached in the cutting process depending on the material properties and the cutting parameters. The change in the material properties of the workpiece including the mechanical and microstructural properties alters the chip thickness resulting in the shear angle change.

The softening of the material in the secondary zone would lead to a rise in ϕ_e . Thus, the size of the shear angle alters between a larger shear angle due to the material with microstructural softening and a lower shear angle due to the material with a work hardening state (Droste et al., 2021; Pu et al., 2016). As is shown in Fig. 8, the shear angle of wrought material was higher than that of SLM-manufactured samples in the cutting process. The predominant factor impacting the machining processes of wrought Inconel 718 is the response of thermal-induced recrystallization. It has been noted that the presence of a fine equiaxed crystal microstructure in the wrought samples results in higher cutting forces and elevated heat in the cutting zone when compared to the cutting of SLM-manufactured samples with dendrite grain microstructure. Another significant factor is the grain refinement behavior induced by severe plastic deformation during the cutting of AM Inconel 718 (Ji et al., 2021). This is also the reason for the higher shear angle of SLM samples compared to DED samples. Moreover, the higher temperature was measured in the near-dry machining of DED-manufactured Inconel 718 material than those the machining of SLM-manufactured parts (Bagherzadeh et al., 2022). The grain structure of the DED part in its original state consists of elongated grains that exhibit zigzag patterns within each layer, as well as fine equiaxed grains that are present between the layers. In the case of as-built DED components, the prevalent grain structure consists of both fine equiaxed grains and inclined elongated grains. The formation of elongated grains occurs in the direction with the highest temperature gradient, whereas the presence of fine equiaxed grains depends on the ratio between the temperature gradient and the rate of solidification. When the temperature gradient decreases and the solidification rate increases, nucleation becomes more favorable than growth (Parimi et al., 2014). Nevertheless, the as-built SLM component has a very tiny dislocation-cell substructure and a cubic texture with columnar grains aligned in the building direction. The solidification direction for the FCC crystal structure is 001 (Sun et al., 2018), and the cells resemble long, thin tubes in appearance. The majority of the dislocations are found in the center of the cells. During the SLM construction of an Inconel 718 component, this type of substructure is frequently discovered (Mostafa et al., 2017; Tucho et al., 2017). The rapid cooling and

repeated heating of the region with each additional layer during the SLM process are linked to the high percentage of dislocations within the cell (Tucho et al., 2017). The dislocation movement is hampered by the low stacking-fault energy of the nickel superalloys. As a result, a significant portion of dislocations still exists in the dislocation cells (Godec et al., 2021b).

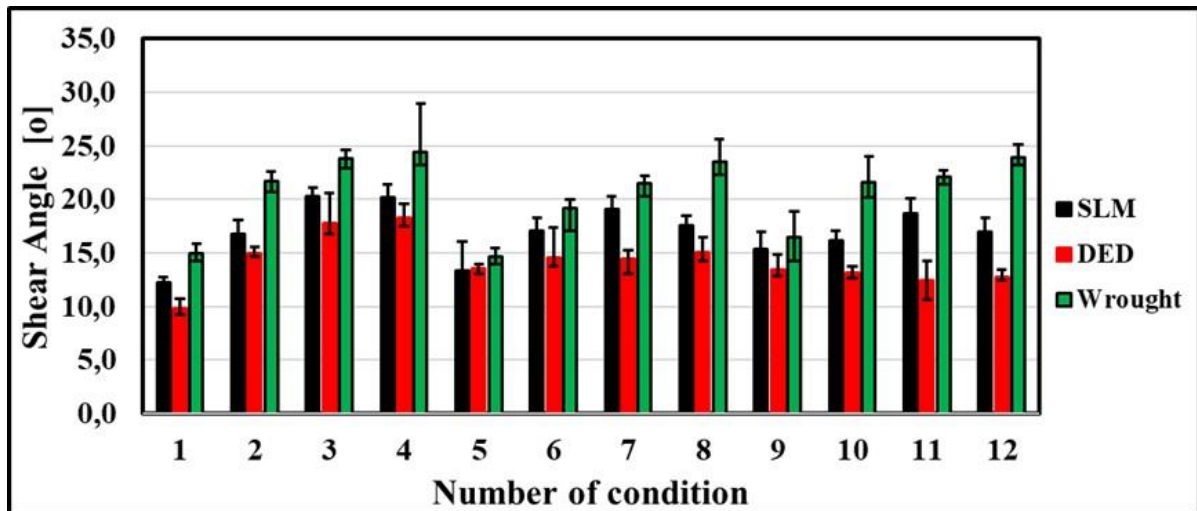


Fig.5.9: Comparison of the shear angle between dry and wet orthogonal cutting of SLM Inconel 718

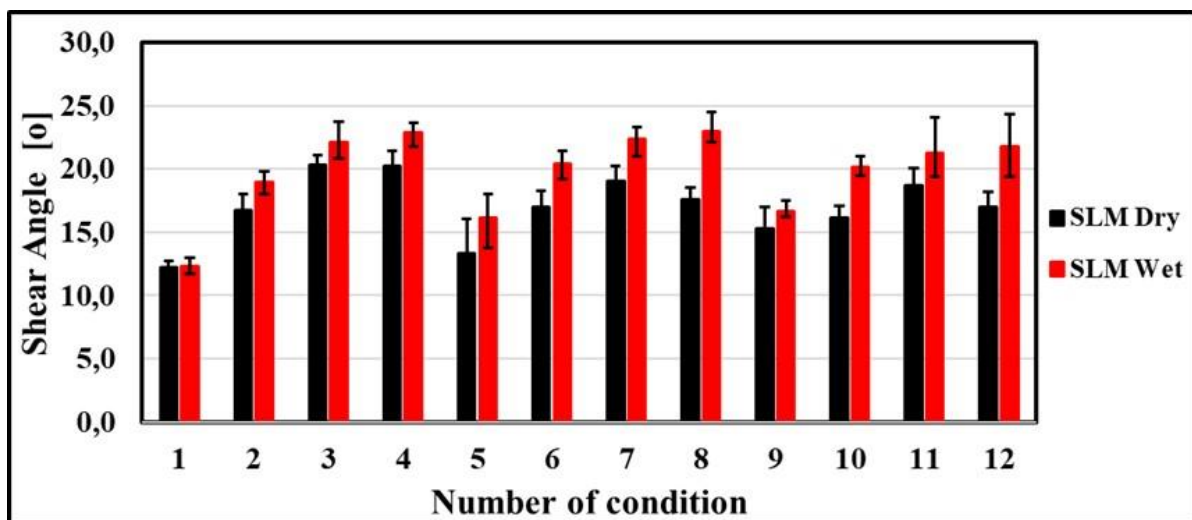


Fig.5.8: Shear angle of nickel alloy 718 in hybrid manufacturing compared to machining of wrought samples.

Fig. 8 illustrates that the shear angle of a wrought component is greater than that of an AM part. With an increase in shear angle, cutting forces and power consumption decrease (Altintas, 2012). As a result, cutting AM components requires more force and power than cutting wrought parts. In addition, the cutting force decreases as the shear angle increases. The reduction in the cutting force results in a decrease in the cutting temperature and contribute to the tool wear reduction. It is recommended that the friction coefficient between

the tool and the chip must be reduced by using lubricants or materials with a lower friction coefficient, and the rake angle of the cutting tool must be increased as much as possible, provided the weak cutting edge is able to withstand the pressure and friction load applied by the chip at the rake face contact zone (Altintas, 2012). Although cooling/lubrication plays a significant role in machining of hard-to-cut materials, it is much more crucial in machining of AM hard-to-cut materials than that of wrought materials. To forecast the force in cutting, it is crucial to know the shear angle, which measures plastic deformation in cutting. Fig. 9 illustrates the effect of flood supply on the shear angle in SLM part machining. The shear angle is increased by adding the flood supply to the cutting process. The wet condition shows the increase in the shear angle of SLM material. This is because the thinner chip reduces the area of the shear plane, increasing the shear angle.

5.3.4. Evaluation of cutting constants and the identification of a sliding friction coefficient model

The machining operations would be significantly altered by the material flow stress and yield strength. The material flow stress strongly depends on the microstructure characteristics of the material. The main differences in microstructure parameters between the wrought, SLM, and DED materials that have major impacts on material flow stress include grain size, phase composition, misorientation (KAM), texture, precipitates, and dislocation density. The majority of recent research has been worked on the JC flow stress model which has been updated to take into account a probable microstructure changes in the shear zone (Pan et al., 2017). The conventional JC flow stress model was modified to include a TANH (hyperbolic tangent) factor to account for the observed strain softening effect during the high-speed machining process (Calamaz et al., 2008). Then, A semi-empirical flow stress model was created to represent the change in dislocation density in the primary shear zone (Guo et al., 2005). The JC model's TANH factor is a component that considers the weakening of material strength caused by strain softening. It's a mathematical function that reflects the correlation between material strength and deformation. When the deformation increases, the TANH factor approaches zero, signifying a complete loss of material strength. This characteristic helps the JC model to simulate the strain softening behavior of the material in high-speed machining.

Table 9 shows the calibrated JC parameters and Table 10 shows the Modified JC constitutive equation for AM and wrought Inconel 718 machining where $\varepsilon^* = \dot{\gamma} / \dot{\gamma}_0$ is the dimensionless

strain rate and T^* is the homologous temperature. Different cooling rates in each production method can be used to explain the differences in sensitivity to strain rate between the SLM, DED, and wrought samples. One of the primary factors influencing the strain rate sensitivity behavior of Inconel 718 is grain boundary sliding (Urdanpilleta et al., n.d.). Due to the slower cooling rate in the wrought samples, it is anticipated that the resultant microstructure would be more uniform than in the as-built samples, showing equiaxed grain formation with no preferred growth direction (Vieille et al., 2020; Zhang et al., 2018). However, it has been established that the microstructure of Inconel 718 alloy samples produced through laser metal deposition exhibits an anisotropic nature, primarily composed of columnar dendrites aligned in the building direction. This is attributed to the rapid cooling rates and unidirectional deposition. The presence of dendrite arms significantly affects the mechanical behavior of the laser metal deposited material, particularly under high strain rates. These dendrite arms contribute to a decrease in flow stress and material hardening when subjected to external loads along the building direction. Consequently, the strain rate sensitivity of laser metal deposited samples is reduced, leading to an increased occurrence of sliding between adjacent grains compared to the wrought samples (Mazzucato et al., 2021).

Table 9: Material constants for hybrid manufacturing and wrought Inconel 718

Material	A(MPa)	B(MPa)	n	C	M
SLM-manufactured	837.5	617.9	0.378	0.0211	1.2
DED-manufactured	833	1642	0.244	0.02	1.3
Wrought	1241	232	0.657	0.0134	1.3

Table 10: Modified JC constitutive equation for hybrid manufacturing and machining of wrought Inconel 718

Material	Modified JC constitutive equation
SLM-manufactured	$\sigma = (837.5 + 617.9\varepsilon^{0.378})(1 + 0.0211\ln\dot{\varepsilon}^*)(1 - T^{*1.2})$
DED-manufactured	$\sigma = (833 + 1642\varepsilon^{0.244})(1 + 0.02\ln\dot{\varepsilon}^*)(1 - T^{*1.3})$
Wrought	$\sigma = (1241 + 232\varepsilon^{0.657})(1 + 0.0134\ln\dot{\varepsilon}^*)(1 - T^{*1.3})$

The sliding friction coefficient model for AM and wrought Inconel 718 are presented in Table 11. In this model, y is the sliding friction coefficient where x is friction speed or the chip velocity (m/min). The sliding friction coefficient of AM samples has a decreasing trend with the friction speed. Nonetheless, there is an increasing trend for wrought material. The plastic

deformation, the evolution of crystallographic texture, and work-hardening, all of which can occur throughout the wear process, are factors that affect the friction of nickel alloy 718 materials.

Differences in microstructure and processing can lead to variations in the effect of temperature on the material flow stress of wrought and additively manufactured Inconel 718. Typically, wrought Inconel 718 has a more uniform and refined microstructure due to the rolling or forging process, resulting in a higher material flow stress at room temperature than additively manufactured Inconel 718. However, at elevated temperatures, additively manufactured Inconel 718 can exhibit a higher material flow stress than wrought Inconel 718 due to the presence of residual stresses and defects such as pores and voids, in the material. The thermal history and cooling rates during additive manufacturing can also influence the material flow stress of additively manufactured Inconel 718. Depending on the additive manufacturing technique used, such as laser powder bed fusion or direct energy deposition, cooling rates and microstructure can vary, ultimately affecting the material flow stress response to temperature changes. To fully understand the effect of temperature on the material flow stress behavior of both wrought and additively manufactured Inconel 718, it is essential to characterize their microstructure and mechanical properties at different temperatures. For instance, the hot tensile tests at 450 °C, which were performed to determine the mechanical characteristics at high temperatures, revealed that the UTS of SLM and wrought material were reduced by 220 MPa and 200 MPa respectively. The UTS of the SLM samples, which is measured at 650 °C, falls within the range of the wrought samples. The yield strength of SLM material drops more quickly than that of wrought material. At higher temperatures (>450 °C), the SLM materials tend to lose their ductility to a greater extent than the wrought samples respecting the elongation to failure (Strößner et al., 2015; Trosch et al., 2016). This is due to the distribution of the δ -phase within the microstructure. In wrought material, δ -phase particles are deposited at the grain boundaries, but in the SLM samples the δ -phase is dispersed both within the grains and at the boundaries due to micro segregations of Nb resulting from the rapid cooling of the melted material.

It is demonstrated that the SLM microstructure is ten times finer than the wrought microstructure based on the relative area fraction over average grain diameter (Strößner et al., 2015; Trosch et al., 2016). The UTS and yield strength of the SLM material decrease more quickly with rising temperature than those of wrought material due to the overall considerably smaller grain size. UTS and yield strength of the SLM samples significantly

drop at 650°C because the fine-grained SLM structure's hardening effect is lost at higher temperatures, whereas UTS and yield strength of wrought samples are more linearly dependent upon temperature between room temperature and 650 °C. Thus, the creation of the intragranular δ -phase needs to be reduced to enhance the mechanical characteristics of the SLM samples, especially at high temperatures.

Table 11: The presented formula for the identification of the sliding friction coefficient in hybrid manufacturing compared to Wrought Inconel 718 machining.

Material	The achieved formula for the identification of the sliding friction coefficient
SLM-manufactured	$y = 0.0161x + 0.4976$
DED-manufactured	$y = 0.0213x + 0.3749$
Wrought	$y = -0.0087x + 0.8981$

5.4.Conclusion

In this study, a detailed investigation of parts made by hybrid additive and subtractive manufacturing processes using SLM and DED methods showed significant differences with machining of wrought Inconel 718 in terms of material deformation, friction, and material constant. Therefore, the JC parameters calibrated for hybrid manufacturing and the model of sliding friction was presented. The major observations are briefly stated as follows:

- With the increase in cutting speed, the friction coefficient showed an increase in wrought material nevertheless, a decrease in AM materials since the size of the nanoscale γ' and γ'' phases in the γ phase matrix has a significant influence on the antifriction properties.
- The flood supply reduced the friction coefficient up to 52% and 40% in comparison to dry SLM cutting in cutting speeds of 30 m/min and 90 m/min, respectively.
- The characteristics of crystalline materials are impacted by the grain geometries, resulting in shear stresses in the order of high to low as Wrought>SLM>DED. Wrought Inconel 718 material has fine equiaxed crystals. Nevertheless, the SLM and the DED-manufactured material have large columnar dendrite grains in the build direction and large columnar grain with a zigzag shape in the scanning direction, respectively.
- The hybrid manufacturing of nickel alloy 718 decreased the shear angle up to 29% and 46% in comparison to dry machining of wrought material due to thermal-induced

recrystallized behavior of wrought Inconel 718 and the severe plastic deformation-induced grain refinement behavior of AM Inconel 718 in machining process.

- The specific material properties of AM materials such as noticeable changes in the mechanical characteristics between the horizontal and vertical specimens as well as the considerable differences in material characteristics at high temperatures highlight the significance of this calibration method for modeling of hybrid manufacturing where only a few cutting trials are required for calibration.
- The formulas for identifying coefficients of sliding friction are presented, showing that the wrought alloy 718 exhibits an increasing trend with friction speed, while the trend is decreasing for AM samples. This model can be used for further studies such as modeling of hybrid manufacturing processes.

The findings of this study on the effect of hybrid additive/subtractive manufacturing on Inconel 718 can have a positive impact on environmentally friendly and clean production. The insights gained from investigating material deformation, friction, and material constants can help optimize manufacturing processes to reduce waste, energy consumption, and environmental impact. Moreover, the observations on the impact of cooling and lubrication on reducing friction coefficient, and thus the total energy used in the process, can contribute to the development of more sustainable machining operations. Overall, the findings of this study have the clear potential to enhance the sustainability of manufacturing through reduced material waste and energy, and thus decreased production foot-print, by providing information and insight for better and efficient machining conditions of especially hard-to-machine materials. The proposed approach in this study is believed to provide inspiration and guidance for future research and development in the field.

6. FUTURE WORK

Further investigation of alternative green machining solutions:

While this thesis focused on cryogenics and hybrid cooling methods using vegetable-based cutting fluids, there are other eco-friendly approaches that warrant further exploration. Future research should delve into the performance and feasibility of these alternative lubricating/cooling methods in various machining, grinding, and polishing processes and materials.

Modeling and optimization of machining under cooling/lubrication environment:

The proposed model and optimization technique can be enhanced by incorporating an adjustable system to regulate the cooling and lubrication supply based on the cutting speed. This adjustment can lead to higher machinability and improved surface quality.

Optimization of hybrid manufacturing processes:

The findings from the study on hybrid additive and subtractive manufacturing can be further refined and optimized. Future work should focus on developing more accurate material models, exploring different additive manufacturing and cutting parameters, and investigating the influence of process variables on surface quality and dimensional accuracy of hybrid-manufactured parts. Development of material and friction models for the excessive cooling and hybrid methods environment should be pursued.

Integration of surface improvement techniques:

As the thesis highlighted the need for post-processing to improve the surface quality of additively manufactured parts, future research should explore the integration of surface improvement techniques such as abrasive machining, micromachining, and polishing to achieve higher-quality finishes and functional surfaces.

Sustainability and cost analysis:

To provide valuable insights for decision-making in industry and guide the adoption of more sustainable and economically viable manufacturing practices, future work should involve conducting a comprehensive sustainability analysis. This analysis should evaluate the environmental impact and cost-effectiveness of different machining and additive manufacturing processes.

References

- Al-Rubaie, K.S., Melotti, S., Rabelo, A., Paiva, J.M., Elbestawi, M.A., Veldhuis, S.C., 2020. Machinability of SLM-produced Ti6Al4V titanium alloy parts. *J Manuf Process* 57, 768–786. <https://doi.org/10.1016/j.jmapro.2020.07.035>
- Altintas, Y., 2012. *Manufacturing automation : metal cutting mechanics, machine tool vibrations, and CNC design*. Cambridge University Press.
- Aramcharoen, A., 2016. Influence of Cryogenic Cooling on Tool Wear and Chip Formation in Turning of Titanium Alloy, in: *Procedia CIRP*. <https://doi.org/10.1016/j.procir.2016.03.184>
- Aramcharoen, A., Chuan, S.K., 2014. An experimental investigation on cryogenic milling of inconel 718 and its sustainability assessment, in: *Procedia CIRP*. <https://doi.org/10.1016/j.procir.2014.03.076>
- Augspurger, T., Koch, M., Klocke, F., Döbbeler, B., 2019. Investigation of transient temperature fields in the milling cutter under CO₂ cooling by means of an embedded thermocouple, in: *Procedia CIRP*. <https://doi.org/10.1016/j.procir.2019.02.007>
- Avila, J.D., Isik, M., Bandyopadhyay, A., 2020. Titanium–Silicon on CoCr Alloy for Load-Bearing Implants Using Directed Energy Deposition-Based Additive Manufacturing. *ACS Appl Mater Interfaces* 12, 51263–51272. <https://doi.org/10.1021/acsami.0c15279>
- Bagherzadeh, A., 2018a. EXPERIMENTAL INVESTIGATION OF ALTERNATIVE COOLING METHODS IN MACHINING OPERATIONS.
- Bagherzadeh, A., 2018b. Experimental Investigation of Alternative Cooling Methods in Machining Operations [WWW Document]. URL <http://risc01.sabanciuniv.edu/record=b1918106> (Table of Contents)
- Bagherzadeh, A., Budak, E., 2018a. Investigation of machinability in turning of difficult-to-cut materials using a new cryogenic cooling approach. *Tribol Int* 119, 510–520. <https://doi.org/10.1016/j.triboint.2017.11.033>
- Bagherzadeh, A., Budak, E., 2018b. Investigation of machinability in turning of difficult-to-cut materials using a new cryogenic cooling approach. *Tribol Int* 119, 510–520. <https://doi.org/10.1016/j.triboint.2017.11.033>
- Bagherzadeh, A., Budak, E., 2018c. Investigation of machinability in turning of difficult-to-cut materials using a new cryogenic cooling approach. *Tribol Int*. <https://doi.org/10.1016/j.triboint.2017.11.033>
- Bagherzadeh, A., Koc, B., Budak, E., Isik, M., 2022. High-speed machining of additively manufactured Inconel 718 using hybrid cryogenic cooling methods. *Virtual Phys Prototyp* 17, 419–436. <https://doi.org/10.1080/17452759.2022.2034081>
- Bagherzadeh, A., Kuram, E., Budak, E., 2021a. Experimental evaluation of eco-friendly hybrid cooling methods in slot milling of titanium alloy. *J Clean Prod* 289, 125817. <https://doi.org/10.1016/j.jclepro.2021.125817>

- Bagherzadeh, A., Kuram, E., Budak, E., 2021b. Experimental evaluation of eco-friendly hybrid cooling methods in slot milling of titanium alloy. *J Clean Prod* 289, 125817. <https://doi.org/10.1016/j.jclepro.2021.125817>
- Bandyopadhyay, A., Shivaram, A., Isik, M., Avila, J.D., Dernell, W.S., 2019a. Additively manufactured calcium phosphate reinforced CoCrMo alloy : Bio-tribological and biocompatibility evaluation for load-bearing implants. *Addit Manuf* 28, 312–324. <https://doi.org/10.1016/j.addma.2019.04.020>
- Bandyopadhyay, A., Shivaram, A., Isik, M., Avila, J.D., Dernell, W.S., Bose, S., 2019b. Additively manufactured calcium phosphate reinforced CoCrMo alloy: Bio-tribological and biocompatibility evaluation for load-bearing implants. *Addit Manuf* 28, 312–324. <https://doi.org/10.1016/j.addma.2019.04.020>
- Bedmar, J., Riquelme, A., Rodrigo, P., Torres, B., Rams, J., 2021. Comparison of different additive manufacturing methods for 316l stainless steel. *Materials* 14. <https://doi.org/10.3390/ma14216504>
- Bergs, T., Pusavec, F., Koch, M., Grguras, D., Dobbeler, B., Klocke, F., 2019. Investigation of the solubility of liquid CO₂ and liquid oil to realize an internal single channel supply in milling of Ti6Al4V, in: *Procedia Manufacturing*. <https://doi.org/10.1016/j.promfg.2019.04.024>
- Bordin, A., Sartori, S., Bruschi, S., Ghiotti, A., 2017. Experimental investigation on the feasibility of dry and cryogenic machining as sustainable strategies when turning Ti6Al4V produced by Additive Manufacturing. *J Clean Prod* 142. <https://doi.org/10.1016/j.jclepro.2016.09.209>
- Brown, D., Li, C., Liu, Z.Y., Fang, X.Y., Guo, Y.B., 2018a. Surface integrity of Inconel 718 by hybrid selective laser melting and milling. *Virtual Phys Prototyp* 13, 26–31. <https://doi.org/10.1080/17452759.2017.1392681>
- Brown, D., Li, C., Liu, Z.Y., Fang, X.Y., Guo, Y.B., 2018b. Surface integrity of Inconel 718 by hybrid selective laser melting and milling. *Virtual Phys Prototyp* 13, 26–31. <https://doi.org/10.1080/17452759.2017.1392681>
- Budak, E., Altintas, Y., Armarego, E.J.A., 1996. Prediction of Milling Force Coefficients From Orthogonal Cutting Data. *J Manuf Sci Eng* 118, 216–224. <https://doi.org/10.1115/1.2831014>
- Budak, E., Ozlu, E., 2008a. Development of a thermomechanical cutting process model for machining process simulations. *CIRP Ann Manuf Technol* 57, 97–100. <https://doi.org/10.1016/j.cirp.2008.03.008>
- Budak, E., Ozlu, E., 2008b. Development of a thermomechanical cutting process model for machining process simulations. *CIRP Ann Manuf Technol* 57, 97–100. <https://doi.org/10.1016/j.cirp.2008.03.008>
- Calamaz, M., Coupard, D., Girot, F., 2008. A new material model for 2D numerical simulation of serrated chip formation when machining titanium alloy Ti-6Al-4V. *Int J Mach Tools Manuf* 48, 275–288. <https://doi.org/10.1016/j.ijmachtools.2007.10.014>

- Cao, G.H., Sun, T.Y., Wang, C.H., Li, X., Liu, M., Zhang, Z.X., Hu, P.F., Russell, A.M., Schneider, R., Gerthsen, D., Zhou, Z.J., Li, C.P., Chen, G.F., 2018. Investigations of γ' , γ'' and δ precipitates in heat-treated Inconel 718 alloy fabricated by selective laser melting. *Mater Charact* 136, 398–406. <https://doi.org/10.1016/j.matchar.2018.01.006>
- Ceretti, E., Taupin, E., Altan, T., 1997. Simulation of Metal Flow and Fracture Applications in Orthogonal Cutting, Blanking, and Cold Extrusion. *CIRP Annals* 46, 187–190. [https://doi.org/10.1016/S0007-8506\(07\)60805-1](https://doi.org/10.1016/S0007-8506(07)60805-1)
- Chen, Z., Han, C., Gao, M., Kandukuri, S.Y., Zhou, K., 2022. A review on qualification and certification for metal additive manufacturing. <https://doi.org/10.1080/17452759.2021.2018938>
- Cheng, B., Shrestha, S., Chou, K., 2016. Stress and deformation evaluations of scanning strategy effect in selective laser melting. *Addit Manuf* 12, 240–251. <https://doi.org/10.1016/j.addma.2016.05.007>
- Chetan, Ghosh, S., Rao, P. V., 2016. Environment Friendly Machining of Ni-Cr-Co Based Super Alloy using Different Sustainable Techniques. *Materials and Manufacturing Processes* 31. <https://doi.org/10.1080/10426914.2015.1037913>
- Dinesh, S., Senthilkumar, V., Asokan, P., 2017. Experimental studies on the cryogenic machining of biodegradable ZK60 Mg alloy using micro-textured tools. *Materials and Manufacturing Processes* 32. <https://doi.org/10.1080/10426914.2016.1221096>
- Dinesh, S., Senthilkumar, V., Asokan, P., Arulkirubakaran, D., 2015. Effect of cryogenic cooling on machinability and surface quality of bio-degradable ZK60 Mg alloy. *Mater Des* 87. <https://doi.org/10.1016/j.matdes.2015.08.099>
- Do, D.K., Li, P., 2016. The effect of laser energy input on the microstructure, physical and mechanical properties of Ti-6Al-4V alloys by selective laser melting. *Virtual Phys Prototyp* 11, 41–47. <https://doi.org/10.1080/17452759.2016.1142215>
- Droste, M., Järvenpää, A., Jaskari, M., Motylenko, M., Weidner, A., Karjalainen, P., Biermann, H., 2021. The role of grain size in static and cyclic deformation behaviour of a laser reversion annealed metastable austenitic steel. *Fatigue Fract Eng Mater Struct* 44, 43–62. <https://doi.org/10.1111/ffe.13326>
- Ducroux, E., Fromentin, G., Viprey, F., Prat, D., D'Acunto, A., 2021. New mechanistic cutting force model for milling additive manufactured Inconel 718 considering effects of tool wear evolution and actual tool geometry. *J Manuf Process* 64, 67–80. <https://doi.org/10.1016/j.jmapro.2020.12.042>
- Dureja, J.S., Singh, R., Singh, T., Singh, P., Dogra, M., Bhatti, M.S., 2015. Performance evaluation of coated carbide tool in machining of stainless steel (AISI 202) under minimum quantity lubrication (MQL). *International Journal of Precision Engineering and Manufacturing - Green Technology* 2. <https://doi.org/10.1007/s40684-015-0016-9>
- England, C., 2011. © Woodhead Publishing Limited, 2011.
- Faga, M.G., Priarone, P.C., Robiglio, M., Settineri, L., Tebaldo, V., 2017. Technological and sustainability implications of dry, near-dry, and wet turning of Ti-6Al-4V alloy.

International Journal of Precision Engineering and Manufacturing - Green Technology 4.
<https://doi.org/10.1007/s40684-017-0016-z>

Fayed, E.M., Saadati, M., Shahriari, D., Brailovski, V., Jahazi, M., Medraj, M., 2021. Effect of homogenization and solution treatments time on the elevated-temperature mechanical behavior of Inconel 718 fabricated by laser powder bed fusion. *Sci Rep* 11, 1–17.
<https://doi.org/10.1038/s41598-021-81618-5>

Flynn, Joseph M, Shokrani, A., Newman, S.T., Dhokia, V., 2016. International Journal of Machine Tools & Manufacture Hybrid additive and subtractive machine tools – Research and industrial developments. *Int J Mach Tools Manuf* 101, 79–101.
<https://doi.org/10.1016/j.ijmachtools.2015.11.007>

Flynn, Joseph M., Shokrani, A., Newman, S.T., Dhokia, V., 2016. Hybrid additive and subtractive machine tools - Research and industrial developments. *Int J Mach Tools Manuf* 101, 79–101. <https://doi.org/10.1016/j.ijmachtools.2015.11.007>

Ford, S., Despeisse, M., 2016. Additive manufacturing and sustainability: an exploratory study of the advantages and challenges. *J Clean Prod* 137, 1573–1587.
<https://doi.org/10.1016/j.jclepro.2016.04.150>

Gajrani, K.K., Suvin, P.S., Kailas, S.V., Sankar, M.R., 2019. Hard machining performance of indigenously developed green cutting fluid using flood cooling and minimum quantity cutting fluid. *J Clean Prod* 206. <https://doi.org/10.1016/j.jclepro.2018.09.178>

Godec, M., Malej, S., Feizpour, D., Donik, Balažic, M., Klobčar, D., Pambaguian, L., Conradi, M., Kocijan, A., 2021a. Hybrid additive manufacturing of Inconel 718 for future space applications. *Mater Charact* 172.
<https://doi.org/10.1016/j.matchar.2020.110842>

Godec, M., Malej, S., Feizpour, D., Donik, Balažic, M., Klobčar, D., Pambaguian, L., Conradi, M., Kocijan, A., 2021b. Hybrid additive manufacturing of Inconel 718 for future space applications. *Mater Charact* 172.
<https://doi.org/10.1016/j.matchar.2020.110842>

Goel, S., Sittiho, A., Charit, I., Klement, U., Joshi, S., 2019. Effect of post-treatments under hot isostatic pressure on microstructural characteristics of EBM-built Alloy 718. *Addit Manuf* 28, 727–737. <https://doi.org/10.1016/j.addma.2019.06.002>

Gross, D., Appis, M., Hanenkamp, N., 2019. Investigation on the productivity of milling ti6al4v with cryogenic minimum quantity lubrication. *MM Science Journal* 2019.
https://doi.org/10.17973/MMSJ.2019_11_2019098

Grzesik, W., Rech, J., 2019. Influence of machining conditions on friction in metal cutting process – A review. *Mechanik* 92, 242–248.
<https://doi.org/10.17814/mechanik.2019.4.33>

Guo, Y.B., Wen, Q., Horstemeyer, M.F., 2005. An internal state variable plasticity-based approach to determine dynamic loading history effects on material property in manufacturing processes. *Int J Mech Sci* 47, 1423–1441.
<https://doi.org/10.1016/j.ijmecsci.2005.04.015>

- Hanenkamp, N., Amon, S., Gross, D., 2018. Hybrid supply system for conventional and CO₂/MQL-based cryogenic cooling, in: *Procedia CIRP*.
<https://doi.org/10.1016/j.procir.2018.08.293>
- Huang, R., Riddle, M., Graziano, D., Warren, J., Das, S., Nimbalkar, S., Cresko, J., Masanet, E., 2016. Energy and emissions saving potential of additive manufacturing: the case of lightweight aircraft components. *J Clean Prod* 135, 1559–1570.
<https://doi.org/10.1016/j.jclepro.2015.04.109>
- Isik, M., Avila, J.D., Bandyopadhyay, A., 2020a. Alumina and tricalcium phosphate added CoCr alloy for load-bearing implants. *Addit Manuf* 36, 101553.
<https://doi.org/10.1016/j.addma.2020.101553>
- Isik, M., Avila, J.D., Bandyopadhyay, A., 2020b. Alumina and tricalcium phosphate added CoCr alloy for load-bearing implants. *Addit Manuf* 36, 101553.
<https://doi.org/10.1016/j.addma.2020.101553>
- Isik, M., Kisa, E., Koc, B., Yildiz, M., Pehlivanogullari, B., Orhangul, A., Poyraz, O., Akbulut, G., 2019. Topology optimization and finite elemental analysis for an inconel 718 engine mounting bracket manufactured via electron beam melting.
- Iturbe, A., Hormaetxe, E., Garay, A., Arrazola, P.J., 2016. Surface Integrity Analysis when Machining Inconel 718 with Conventional and Cryogenic Cooling, in: *Procedia CIRP*.
<https://doi.org/10.1016/j.procir.2016.02.095>
- Jamil, M., Khan, A.M., Gupta, M.K., Mia, M., He, N., Li, L., Sivalingam, V.K., 2020. Influence of CO₂-snow and subzero MQL on thermal aspects in the machining of Ti-6Al-4V. *Appl Therm Eng* 177. <https://doi.org/10.1016/j.applthermaleng.2020.115480>
- Jawahir, I.S., Attia, H., Biermann, D., Duflou, J., Klocke, F., Meyer, D., Newman, S.T., Pusavec, F., Putz, M., Rech, J., Schulze, V., Umbrello, D., 2016. Cryogenic manufacturing processes. *CIRP Ann Manuf Technol* 65.
<https://doi.org/10.1016/j.cirp.2016.06.007>
- Ji, H., Gupta, M.K., Song, Q., Cai, W., Zheng, T., Zhao, Y., Liu, Z., Pimenov, D.Y., 2021. Microstructure and machinability evaluation in micro milling of selective laser melted Inconel 718 alloy. *Journal of Materials Research and Technology* 14, 348–362.
<https://doi.org/10.1016/j.jmrt.2021.06.081>
- Ke, W.C., Oliveira, J.P., Cong, B.Q., Ao, S.S., Qi, Z.W., Peng, B., Zeng, Z., 2022. Multi-layer deposition mechanism in ultra high-frequency pulsed wire arc additive manufacturing (WAAM) of NiTi shape memory alloys. *Addit Manuf* 50, 102513.
<https://doi.org/10.1016/j.addma.2021.102513>
- Kladovasilakis, N., Charalampous, P., Tsongas, K., Kostavelis, I., Tzovaras, D., Tzetzis, D., 2022. Influence of Selective Laser Melting Additive Manufacturing Parameters in Inconel 718 Superalloy 1–19.
- Komarasamy, M., Shukla, S., Williams, S., Kandasamy, K., Kelly, S., Mishra, R.S., 2019a. Microstructure, fatigue, and impact toughness properties of additively manufactured nickel alloy 718. *Addit Manuf* 28, 661–675.
<https://doi.org/10.1016/j.addma.2019.06.009>

- Komarasamy, M., Shukla, S., Williams, S., Kandasamy, K., Kelly, S., Mishra, R.S., 2019b. Microstructure, fatigue, and impact toughness properties of additively manufactured nickel alloy 718. *Addit Manuf* 28, 661–675. <https://doi.org/10.1016/j.addma.2019.06.009>
- Lam, L.P., Zhang, D.Q., Liu, Z.H., Chua, C.K., 2015. Phase analysis and microstructure characterisation of AlSi10Mg parts produced by Selective Laser Melting. *Virtual Phys Prototyp* 10, 207–215. <https://doi.org/10.1080/17452759.2015.1110868>
- Le, V.T., Paris, H., Mandil, G., 2017. Environmental impact assessment of an innovative strategy based on an additive and subtractive manufacturing combination. *J Clean Prod* 164, 508–523. <https://doi.org/10.1016/j.jclepro.2017.06.204>
- Lee, I., Bajpai, V., Moon, S., Byun, J., Lee, Y., Park, H.W., 2015. Tool life improvement in cryogenic cooled milling of the preheated Ti–6Al–4V. *International Journal of Advanced Manufacturing Technology* 79. <https://doi.org/10.1007/s00170-015-6849-0>
- Liu, W., Deng, K., Wei, H., Zhao, P., Li, J., Zhang, Y., 2021. A decision-making model for comparing the energy demand of additive-subtractive hybrid manufacturing and conventional subtractive manufacturing based on life cycle method. *J Clean Prod* 311, 127795. <https://doi.org/10.1016/j.jclepro.2021.127795>
- Liu, Z.Y., Li, C., Fang, X.Y., Guo, Y.B., 2018. Energy Consumption in Additive Manufacturing of Metal Parts 26, 834–845. <https://doi.org/10.1016/j.promfg.2018.07.104>
- Loh, L.E., Liu, Z.H., Zhang, D.Q., Mapar, M., Sing, S.L., Chua, C.K., Yeong, W.Y., 2014. Selective Laser Melting of aluminium alloy using a uniform beam profile: The paper analyzes the results of laser scanning in Selective Laser Melting using a uniform laser beam. *Virtual Phys Prototyp* 9, 11–16. <https://doi.org/10.1080/17452759.2013.869608>
- Lopes, J.G., Machado, C.M., Duarte, V.R., Rodrigues, T.A., Santos, T.G., Oliveira, J.P., 2020. Effect of milling parameters on HSLA steel parts produced by Wire and Arc Additive Manufacturing (WAAM). *J Manuf Process* 59, 739–749. <https://doi.org/10.1016/j.jmapro.2020.10.007>
- Luo, S., Huang, W., Yang, H., Yang, J., Wang, Z., Zeng, X., 2019. Microstructural evolution and corrosion behaviors of Inconel 718 alloy produced by selective laser melting following different heat treatments. *Addit Manuf* 30, 100875. <https://doi.org/10.1016/j.addma.2019.100875>
- Margolis, N., Jamison, K., Dove, L., 1999. Energy and Environmental Profile of the U.S. Metal Casting Industry. Office of Industrial Technologies, Washington, D.C..
- Mazzucato, F., Forni, D., Valente, A., Cadoni, E., 2021. Laser metal deposition of inconel 718 alloy and as-built mechanical properties compared to casting. *Materials* 14, 1–21. <https://doi.org/10.3390/ma14020437>
- Merchant, M.E., 1945. Mechanics of the Metal Cutting Process. I. Orthogonal Cutting and a Type 2 Chip. *J Appl Phys* 16, 267–275. <https://doi.org/10.1063/1.1707586>

- Mitrofanov, A. V., Babitsky, V.I., Silberschmidt, V. V., 2005. Thermomechanical finite element simulations of ultrasonically assisted turning. *Comput Mater Sci* 32, 463–471. <https://doi.org/10.1016/j.commatsci.2004.09.019>
- Morrow, W.R., Qi, H., Kim, I., Mazumder, J., Skerlos, S.J., 2007. Environmental aspects of laser-based and conventional tool and die manufacturing. *J Clean Prod* 15, 932–943. <https://doi.org/10.1016/j.jclepro.2005.11.030>
- Mostafa, A., Rubio, I.P., Brailovski, V., Jahazi, M., Medraj, M., 2017. Structure, texture and phases in 3D printed IN718 alloy subjected to homogenization and HIP treatments. *Metals (Basel)* 7. <https://doi.org/10.3390/met7060196>
- Nalbant, M., Yildiz, Y., 2011. Effect of cryogenic cooling in milling process of AISI 304 stainless steel. *Transactions of Nonferrous Metals Society of China (English Edition)* 21. [https://doi.org/10.1016/S1003-6326\(11\)60680-8](https://doi.org/10.1016/S1003-6326(11)60680-8)
- Oliveira, J.P., LaLonde, A.D., Ma, J., 2020a. Processing parameters in laser powder bed fusion metal additive manufacturing. *Mater Des* 193, 1–12. <https://doi.org/10.1016/j.matdes.2020.108762>
- Oliveira, J.P., Santos, T.G., Miranda, R.M., 2020b. Revisiting fundamental welding concepts to improve additive manufacturing: From theory to practice. *Prog Mater Sci* 107, 100590. <https://doi.org/10.1016/j.pmatsci.2019.100590>
- Onuiké, B., Heer, B., Bandyopadhyay, A., 2018. Additive manufacturing of Inconel 718—Copper alloy bimetallic structure using laser engineered net shaping (LENS™). *Addit Manuf* 21, 133–140. <https://doi.org/10.1016/j.addma.2018.02.007>
- Oyelola, O., Crawforth, P., M'Saoubi, R., Clare, A.T., 2018. Machining of functionally graded Ti6Al4V/WC produced by directed energy deposition. *Addit Manuf* 24, 20–29. <https://doi.org/10.1016/j.addma.2018.09.007>
- Ozlu, E., Budak, E., Molinari, A., 2009. Analytical and experimental investigation of rake contact and friction behavior in metal cutting. *Int J Mach Tools Manuf* 49, 865–875. <https://doi.org/10.1016/j.ijmachtools.2009.05.005>
- Pan, Z., Feng, Y., Liang, S.Y., 2017. Material microstructure affected machining: A review. *Manuf Rev (Les Ulis)* 4. <https://doi.org/10.1051/mfreview/2017004>
- Papadakis, L., Loizou, A., Risse, J., Bremen, S., Schrage, J., 2014. A computational reduction model for appraising structural effects in selective laser melting manufacturing: A methodical model reduction proposed for time-efficient finite element analysis of larger components in Selective Laser Melting. *Virtual Phys Prototyp* 9, 17–25. <https://doi.org/10.1080/17452759.2013.868005>
- Parida, A.K., Maity, K., 2018. Comparison the machinability of Inconel 718, Inconel 625 and Monel 400 in hot turning operation. *Engineering Science and Technology, an International Journal* 21, 364–370. <https://doi.org/10.1016/j.jestch.2018.03.018>
- Parida, A.K., Maity, K., 2017. Effect of nose radius on forces, and process parameters in hot machining of Inconel 718 using finite element analysis. *Engineering Science and*

- Technology, an International Journal 20, 687–693.
<https://doi.org/10.1016/j.jestch.2016.10.006>
- Parimi, L.L., Ravi, G., Clark, D., Attallah, M.M., 2014. Microstructural and texture development in direct laser fabricated IN718. *Mater Charact* 89, 102–111.
<https://doi.org/10.1016/j.matchar.2013.12.012>
- Park, K.H., Suhaimi, M.A., Yang, G.D., Lee, D.Y., Lee, S.W., Kwon, P., 2017. Milling of titanium alloy with cryogenic cooling and minimum quantity lubrication (MQL). *International Journal of Precision Engineering and Manufacturing* 18.
<https://doi.org/10.1007/s12541-017-0001-z>
- Park, K.H., Yang, G.D., Suhaimi, M.A., Lee, D.Y., Kim, T.G., Kim, D.W., Lee, S.W., 2015. The effect of cryogenic cooling and minimum quantity lubrication on end milling of titanium alloy Ti-6Al-4V. *Journal of Mechanical Science and Technology* 29.
<https://doi.org/10.1007/s12206-015-1110-1>
- Peng, S., Li, T., Zhao, J., Lv, S., Tan, G.Z., Dong, M., Zhang, H., 2019. Towards energy and material efficient laser cladding process: Modeling and optimization using a hybrid TS-GEP algorithm and the NSGA-II. *J Clean Prod* 227, 58–69.
<https://doi.org/10.1016/j.jclepro.2019.04.187>
- Peng, T., Kellens, K., Tang, R., Chen, C., Chen, G., 2018. Sustainability of additive manufacturing: An overview on its energy demand and environmental impact. *Addit Manuf* 21, 694–704. <https://doi.org/10.1016/j.addma.2018.04.022>
- Pereira, O., Rodríguez, A., Barreiro, J., Fernández-Abia, A.I., de Lacalle, L.N.L., 2017. Nozzle design for combined use of MQL and cryogenic gas in machining. *International Journal of Precision Engineering and Manufacturing - Green Technology* 4.
<https://doi.org/10.1007/s40684-017-0012-3>
- Pereira, O., Rodríguez, A., Fernández-Abia, A.I., Barreiro, J., López de Lacalle, L.N., 2016. Cryogenic and minimum quantity lubrication for an eco-efficiency turning of AISI 304. *J Clean Prod* 139. <https://doi.org/10.1016/j.jclepro.2016.08.030>
- Pérez-Ruiz, J.D., de Lacalle, L.N.L., Urbikain, G., Pereira, O., Martínez, S., Bris, J., 2021a. On the relationship between cutting forces and anisotropy features in the milling of LPBF Inconel 718 for near net shape parts. *Int J Mach Tools Manuf* 170.
<https://doi.org/10.1016/j.ijmachtools.2021.103801>
- Pérez-Ruiz, J.D., de Lacalle, L.N.L., Urbikain, G., Pereira, O., Martínez, S., Bris, J., 2021b. On the relationship between cutting forces and anisotropy features in the milling of LPBF Inconel 718 for near net shape parts. *Int J Mach Tools Manuf* 170.
<https://doi.org/10.1016/j.ijmachtools.2021.103801>
- Pérez-Ruiz, J.D., Marin, F., Martínez, S., Lamikiz, A., Urbikain, G., López de Lacalle, L.N., 2022. Stiffening near-net-shape functional parts of Inconel 718 LPBF considering material anisotropy and subsequent machining issues. *Mech Syst Signal Process* 168, 108675. <https://doi.org/10.1016/j.ymsp.2021.108675>
- Promopattam, P., Yao, S.C., Pistorius, P.C., Rollett, A.D., Coutts, P.J., Lia, F., Martukanitz, R., 2018. Numerical modeling and experimental validation of thermal history and

- microstructure for additive manufacturing of an Inconel 718 product. *Progress in Additive Manufacturing* 3, 15–32. <https://doi.org/10.1007/s40964-018-0039-1>
- Pu, C.L., Zhu, G., Yang, S., Yue, E.B., Subramanian, S. V., 2016. Effect of microstructure softening events on the chip morphology of AISI 1045 steel during high speed machining. *International Journal of Advanced Manufacturing Technology* 82, 2149–2155. <https://doi.org/10.1007/s00170-015-7472-9>
- Qian, C., Zhang, Y., Liu, Y., Wang, Z., 2019. A cloud service platform integrating additive and subtractive manufacturing with high resource efficiency. *J Clean Prod* 241, 118379. <https://doi.org/10.1016/j.jclepro.2019.118379>
- Ravi, S., Kumar, M.P., 2012. Experimental investigation of cryogenic cooling in milling of AISI D3 tool steel. *Materials and Manufacturing Processes* 27. <https://doi.org/10.1080/10426914.2011.654157>
- Ravi, S., Pradeep Kumar, M., 2011. Experimental investigations on cryogenic cooling by liquid nitrogen in the end milling of hardened steel. *Cryogenics (Guildf)* 51. <https://doi.org/10.1016/j.cryogenics.2011.06.006>
- Rodrigues, T.A., Escobar, J.D., Shen, J., Duarte, V.R., Ribamar, G.G., Avila, J.A., Maawad, E., Schell, N., Santos, T.G., Oliveira, J.P., 2021. Effect of heat treatments on 316 stainless steel parts fabricated by wire and arc additive manufacturing: Microstructure and synchrotron X-ray diffraction analysis. *Addit Manuf* 48, 102428. <https://doi.org/10.1016/j.addma.2021.102428>
- Romano, J., Ladani, L., Sadowski, M., 2016. Laser Additive Melting and Solidification of Inconel 718: Finite Element Simulation and Experiment. *Jom* 68, 967–977. <https://doi.org/10.1007/s11837-015-1765-1>
- Sela, A., Ortizde-Zarate, G., Arrieta, I., Soriano, D., Aristimuño, P., Medina-Clavijo, B., Arrazola, P.J., 2019. A mechanistic model to predict cutting force on orthogonal machining of Aluminum 7475-T7351 considering the edge radius, in: *Procedia CIRP*. Elsevier B.V., pp. 32–36. <https://doi.org/10.1016/j.procir.2019.04.066>
- Shakil, S.I., Smith, N.R., Yoder, S.P., Ross, B.E., Alvarado, D.J., Hadadzadeh, A., Haghshenas, M., 2022. Post fabrication thermomechanical processing of additive manufactured metals: A review. *J Manuf Process* 73, 757–790. <https://doi.org/10.1016/j.jmapro.2021.11.047>
- Shao, S., Khonsari, M.M., Guo, S., Meng, W.J., Li, N., 2019. Overview: Additive Manufacturing Enabled Accelerated Design of Ni-based Alloys for Improved Fatigue Life. *Addit Manuf* 29, 100779. <https://doi.org/10.1016/j.addma.2019.100779>
- Shokrani, A., Dhokia, V., Newman, S.T., 2016a. Comparative investigation on using cryogenic machining in CNC milling of Ti-6Al-4V titanium alloy. *Machining Science and Technology* 20. <https://doi.org/10.1080/10910344.2016.1191953>
- Shokrani, A., Dhokia, V., Newman, S.T., 2016b. Investigation of the effects of cryogenic machining on surface integrity in CNC end milling of Ti-6Al-4V titanium alloy. *J Manuf Process* 21. <https://doi.org/10.1016/j.jmapro.2015.12.002>

- Shokrani, A., Dhokia, V., Newman, S.T., Imani-Asrai, R., 2012. An initial study of the effect of using liquid nitrogen coolant on the surface roughness of inconel 718 nickel-based alloy in CNC milling, in: *Procedia CIRP*. <https://doi.org/10.1016/j.procir.2012.07.022>
- Sing, S.L., Kuo, C.N., Shih, C.T., Ho, C.C., Chua, C.K., 2021. Perspectives of using machine learning in laser powder bed fusion for metal additive manufacturing. *Virtual Phys Prototyp* 16, 372–386. <https://doi.org/10.1080/17452759.2021.1944229>
- Sing, S.L., Yeong, W.Y., 2020. Laser powder bed fusion for metal additive manufacturing: perspectives on recent developments. *Virtual Phys Prototyp* 15, 359–370. <https://doi.org/10.1080/17452759.2020.1779999>
- Singh, A., Kapil, S., Das, M., 2020. A comprehensive review of the methods and mechanisms for powder feedstock handling in directed energy deposition. *Addit Manuf* 35, 101388. <https://doi.org/10.1016/j.addma.2020.101388>
- Song, H., McGaughy, T., Sadek, A., Zhang, W., 2019. Effect of structural support on microstructure of nickel base superalloy fabricated by laser-powder bed fusion additive manufacturing. *Addit Manuf* 26, 30–40. <https://doi.org/10.1016/j.addma.2018.12.017>
- Strondl, A., Fischer, R., Frommeyer, G., Schneider, A., 2008. Investigations of MX and γ'/γ'' precipitates in the nickel-based superalloy 718 produced by electron beam melting. *Materials Science and Engineering A* 480, 138–147. <https://doi.org/10.1016/j.msea.2007.07.012>
- Strößner, J., Terock, M., Glatzel, U., 2015. Mechanical and Microstructural Investigation of Nickel-Based Superalloy IN718 Manufactured by Selective Laser Melting (SLM). *Adv Eng Mater* 17, 1099–1105. <https://doi.org/10.1002/adem.201500158>
- Sun, Z., Tan, X., Tor, S.B., Chua, C.K., 2018. Simultaneously enhanced strength and ductility for 3D-printed stainless steel 316L by selective laser melting. *NPG Asia Mater* 10, 127–136. <https://doi.org/10.1038/s41427-018-0018-5>
- Tan, J.H., Wong, W.L.E., Dalgarno, K.W., 2017. An overview of powder granulometry on feedstock and part performance in the selective laser melting process. *Addit Manuf* 18, 228–255. <https://doi.org/10.1016/j.addma.2017.10.011>
- Tan, J.H.K., Sing, S.L., Yeong, W.Y., 2020a. Microstructure modelling for metallic additive manufacturing: a review. *Virtual Phys Prototyp* 15, 87–105. <https://doi.org/10.1080/17452759.2019.1677345>
- Tan, J.H.K., Sing, S.L., Yeong, W.Y., 2020b. Microstructure modelling for metallic additive manufacturing: a review. *Virtual Phys Prototyp* 15, 87–105. <https://doi.org/10.1080/17452759.2019.1677345>
- Torres-Carrillo, S., Siller, H.R., Vila, C., López, C., Rodríguez, C.A., 2020. Environmental analysis of selective laser melting in the manufacturing of aeronautical turbine blades. *J Clean Prod* 246. <https://doi.org/10.1016/j.jclepro.2019.119068>
- Trosch, T., Strößner, J., Völkl, R., Glatzel, U., 2016. Microstructure and mechanical properties of selective laser melted Inconel 718 compared to forging and casting. *Mater Lett* 164, 428–431. <https://doi.org/10.1016/j.matlet.2015.10.136>

- Truesdale, S.L., Shin, Y.C., 2009. Microstructural analysis and machinability improvement of Udimet 720 via cryogenic milling. *Machining Science and Technology* 13. <https://doi.org/10.1080/10910340902776010>
- Tucho, W.M., Cuvillier, P., Sjolyst-Kverneland, A., Hansen, V., 2017. Microstructure and hardness studies of Inconel 718 manufactured by selective laser melting before and after solution heat treatment. *Materials Science and Engineering A* 689, 220–232. <https://doi.org/10.1016/j.msea.2017.02.062>
- Tucho, W.M., Hansen, V., 2019. Characterization of SLM-fabricated Inconel 718 after solid solution and precipitation hardening heat treatments. *J Mater Sci* 54, 823–839. <https://doi.org/10.1007/s10853-018-2851-x>
- Tyler, C.T., Schmitz, T.L., 2014. Examining the effects of cooling/lubricating conditions on tool wear in milling Hastelloy X, in: *Transactions of the North American Manufacturing Research Institution of SME*.
- Urdanpilleta, M., Manuel Martínez-Esnaola, J., Sevillano, J.G., n.d. Strain Rate Sensitivity of Superplastic Inconel 718.
- Vieille, B., Keller, C., Mokhtari, M., Briatta, H., Breteau, T., Nguejio, J., Barbe, F., Ben Azzouna, M., Baustert, E., 2020. Investigations on the fracture behavior of Inconel 718 superalloys obtained from cast and additive manufacturing processes. *Materials Science and Engineering A* 790. <https://doi.org/10.1016/j.msea.2020.139666>
- Wang, B., Liu, Z., Cai, Y., Luo, X., Ma, H., Song, Q., Xiong, Z., 2021. Advancements in material removal mechanism and surface integrity of high speed metal cutting: A review. *Int J Mach Tools Manuf.* <https://doi.org/10.1016/j.ijmachtools.2021.103744>
- Weng, J., Saelzer, J., Berger, S., Zhuang, K., Bagherzadeh, A., Budak, E., Biermann, D., 2023. Analytical and experimental investigations of rake face temperature considering temperature-dependent thermal properties. *Journal of Materials Processing Tech.* 314, 117905. <https://doi.org/10.1016/j.jmatprotec.2023.117905>
- Williams, J.A., 1991. Mechanics of machining: an analytical approach to assessing machinability. *Wear* 150, 380–381. [https://doi.org/10.1016/0043-1648\(91\)90332-O](https://doi.org/10.1016/0043-1648(91)90332-O)
- Wilson, J.M., Piya, C., Shin, Y.C., Zhao, F., Ramani, K., 2014. Remanufacturing of turbine blades by laser direct deposition with its energy and environmental impact analysis. *J Clean Prod* 80, 170–178. <https://doi.org/10.1016/j.jclepro.2014.05.084>
- Wippermann, A., Gutowski, T.G., Denkena, B., Dittrich, M.A., Wessarges, Y., 2020. Electrical energy and material efficiency analysis of machining, additive and hybrid manufacturing. *J Clean Prod* 251, 119731. <https://doi.org/10.1016/j.jclepro.2019.119731>
- Wolff, S.J., Gan, Z., Lin, S., Bennett, J.L., Yan, W., Hyatt, G., Ehmann, K.F., Wagner, G.J., Liu, W.K., Cao, J., 2019. Experimentally validated predictions of thermal history and microhardness in laser-deposited Inconel 718 on carbon steel. *Addit Manuf* 27, 540–551. <https://doi.org/10.1016/j.addma.2019.03.019>

- Woods, T.W., Genareau, K., Wallace, K.L., 2020. Influence of grain size and shape on volcanic ash electrical conductivity. *Journal of Volcanology and Geothermal Research* 393. <https://doi.org/10.1016/j.jvolgeores.2020.106788>
- Xie, D., Lv, F., Liang, H., Shen, L., Tian, Z., Zhao, J., 2021. Towards a comprehensive understanding of distortion in additive manufacturing based on assumption of constraining force. <https://doi.org/10.1080/17452759.2021.1881873>
- Xu, Z., Murray, J.W., Hyde, C.J., Clare, A.T., 2018. Effect of post processing on the creep performance of laser powder bed fused Inconel 718. *Addit Manuf* 24, 486–497. <https://doi.org/10.1016/j.addma.2018.10.027>
- Yap, C.Y., Chua, C.K., Dong, Z.L., 2016. An effective analytical model of selective laser melting. *Virtual Phys Prototyp* 11, 21–26. <https://doi.org/10.1080/17452759.2015.1133217>
- Yen, Y.-C., Jain, A., Altan, T., 2004. A finite element analysis of orthogonal machining using different tool edge geometries. *J Mater Process Technol* 146, 72–81. [https://doi.org/10.1016/S0924-0136\(03\)00846-X](https://doi.org/10.1016/S0924-0136(03)00846-X)
- Yi, L., Glatt, M., Thomas Kuo, T.Y., Ji, A., Ravani, B., Aurich, J.C., 2020. A method for energy modeling and simulation implementation of machine tools of selective laser melting. *J Clean Prod* 263. <https://doi.org/10.1016/j.jclepro.2020.121282>
- Yong, H., Sun, Y., Ge, M., Li, J., Su, J., 2011. Milling experimental investigation on titanium alloy Ti6Al4V under different cooling/lubrication conditions, in: *Advanced Materials Research*. <https://doi.org/10.4028/www.scientific.net/AMR.325.406>
- Yu, X., Lin, X., Liu, F., Wang, L., Tang, Y., Li, J., Zhang, S., Huang, W., 2020. Influence of post-heat-treatment on the microstructure and fracture toughness properties of Inconel 718 fabricated with laser directed energy deposition additive manufacturing. *Materials Science and Engineering A* 798, 140092. <https://doi.org/10.1016/j.msea.2020.140092>
- Yuan, K., Guo, W., Li, D., Li, P., Zhang, Y., Wang, P., 2021. Influence of heat treatments on plastic flow of laser deposited Inconel 718: Testing and microstructural based constitutive modeling. *Int J Plast* 136, 102865. <https://doi.org/10.1016/j.ijplas.2020.102865>
- Yuan, K., Guo, W., Li, P., Zhang, Y., Li, X., Lin, X., 2019. Thermomechanical behavior of laser metal deposited Inconel 718 superalloy over a wide range of temperature and strain rate: Testing and constitutive modeling. *Mechanics of Materials* 135, 13–25. <https://doi.org/10.1016/j.mechmat.2019.04.024>
- Zerilli, F.J., Armstrong, R.W., 2008. Constitutive relations for the plastic deformation of metals. AIP Publishing, pp. 989–992. <https://doi.org/10.1063/1.46201>
- Zerilli, F.J., Armstrong, R.W., 1987. Dislocation-mechanics-based constitutive relations for material dynamics calculations. *J Appl Phys* 61, 1816–1825. <https://doi.org/10.1063/1.338024>
- Zhang, D., Feng, Z., Wang, C., Wang, W., Liu, Z., Niu, W., 2018. Comparison of microstructures and mechanical properties of Inconel 718 alloy processed by selective

laser melting and casting. *Materials Science and Engineering A* 724, 357–367.
<https://doi.org/10.1016/j.msea.2018.03.073>

Zhang, X., Mu, H., Huang, X., Fu, Z., Zhu, D., Ding, H., 2015. Cryogenic milling of Aluminium-lithium alloys: Thermo-mechanical modelling towards fine-tuning of part surface residual stress, in: *Procedia CIRP*. <https://doi.org/10.1016/j.procir.2015.03.055>

Zhang, Y., Lee, Y.J., Chang, S., Chen, Y., Bai, Y., Zhang, J., Wang, H., 2022. Microstructural modulation of TiAl alloys for controlling ultra-precision machinability. *Int J Mach Tools Manuf* 174. <https://doi.org/10.1016/j.ijmachtools.2022.103851>

Zhao, Z., Qu, H., Bai, P., Li, J., Wu, L., Huo, P., 2018. Friction and wear behaviour of Inconel 718 alloy fabricated by selective laser melting after heat treatments. *Philos Mag Lett* 98, 547–555. <https://doi.org/10.1080/09500839.2019.1597991>

Zhu, Y., Peng, T., Jia, G., Zhang, H., Xu, S., Yang, H., 2019. Electrical energy consumption and mechanical properties of selective-laser-melting-produced 316L stainless steel samples using various processing parameters. *J Clean Prod* 208, 77–85.
<https://doi.org/10.1016/j.jclepro.2018.10.109>

APPENDIX

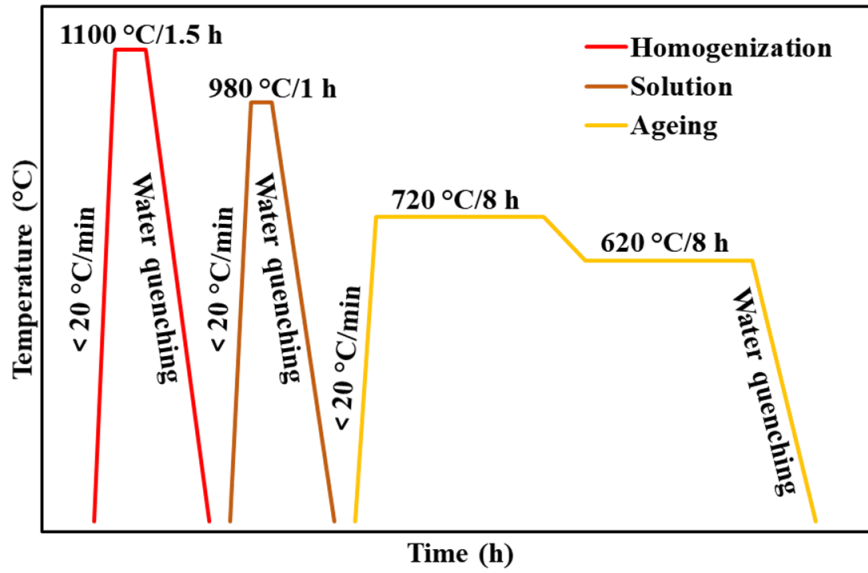


Fig. S0-1: The specific scenarios of heat treatment method

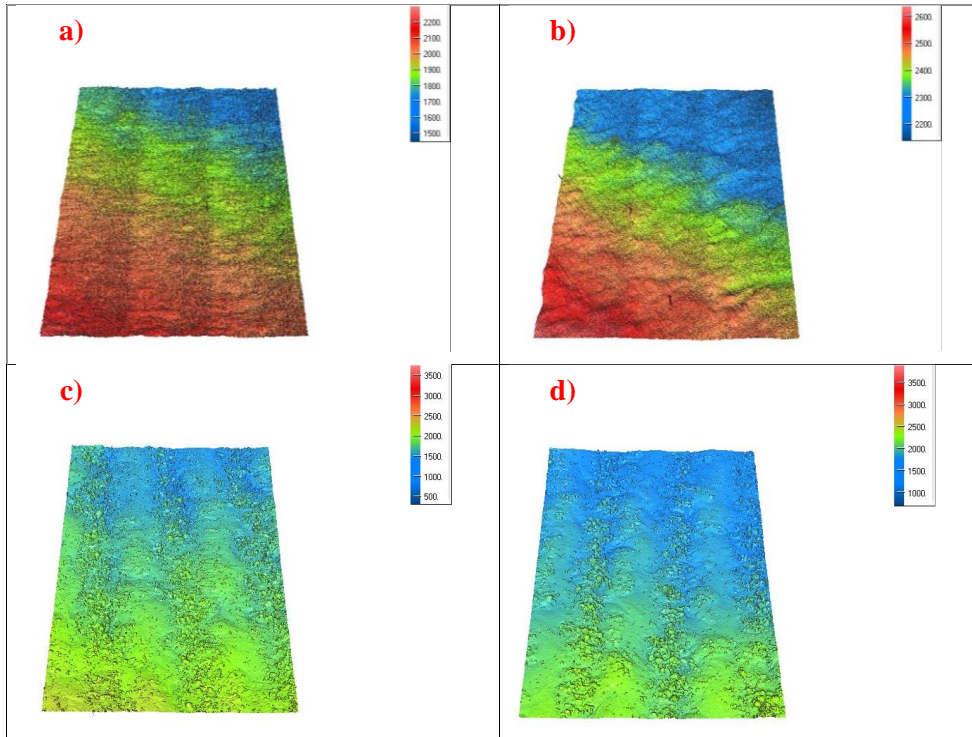


Fig. S0-2: The surface of manufactured AM parts a) as-built SLM, b) HT-SLM, c) as-built DED, d) HT-DED.

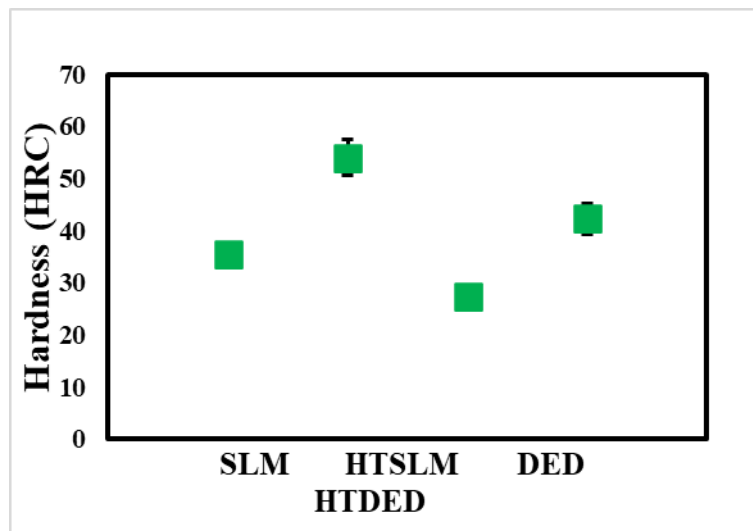


Fig. S0-3. Hardness value of as-built and heat-treated additively manufactured parts.

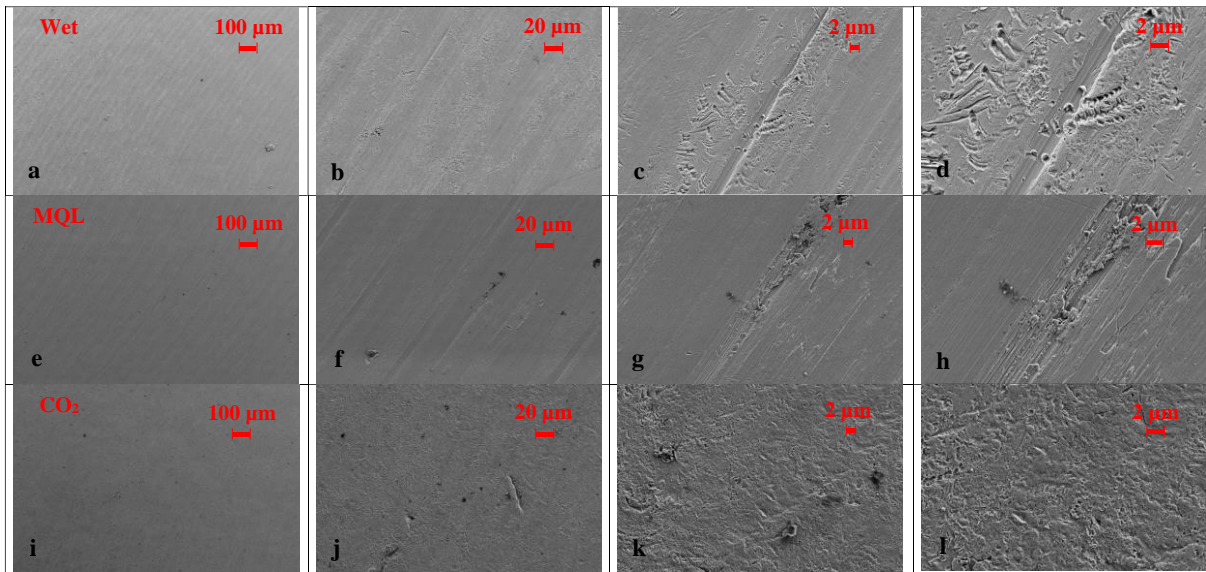


Fig. S0-4: SEM image of the generated surface in the machining of as-built SLM under Wet (a-d), MQL (e-h), CO₂ (i-l), LN₂ (m-p), CO₂MQL (q-t), LN₂MQL (u-x).

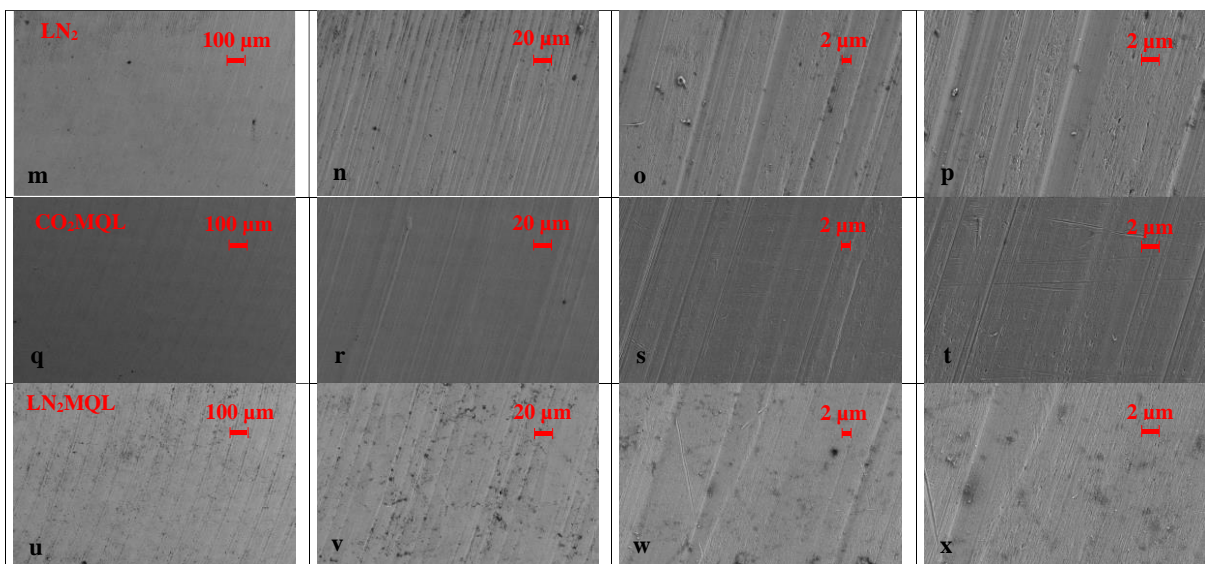


Fig. S4 (continued)

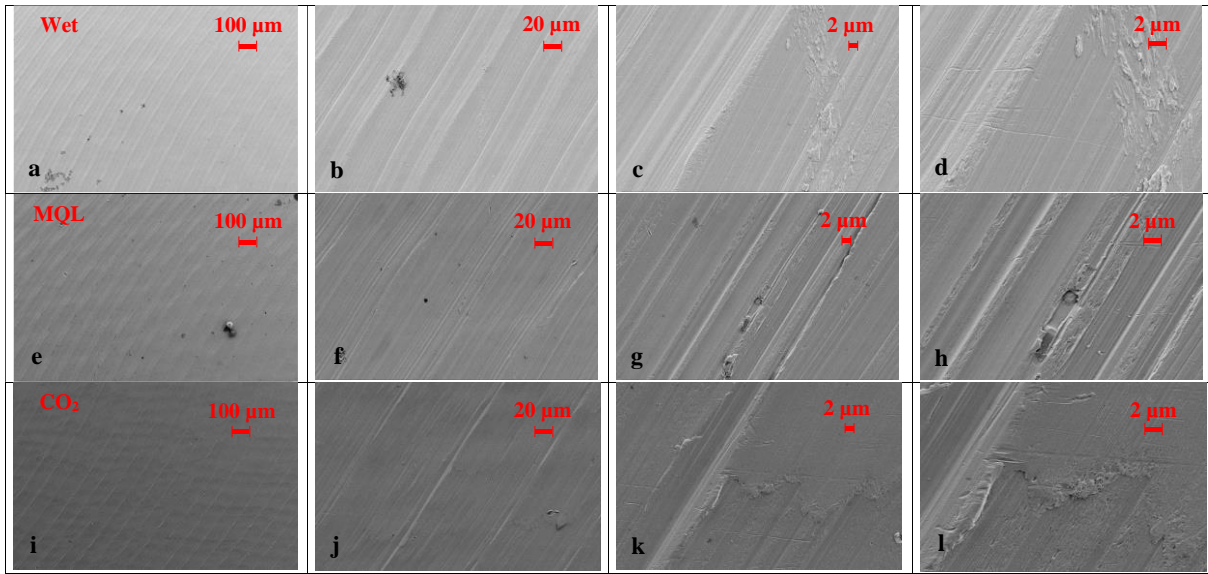


Fig. S0-5: SEM image of the generated surface in the machining of HT-SLM under Wet (a-d), MQL (e-h), CO₂ (i-l), LN₂ (m-p), CO₂MQL (q-t), LN₂MQL (u-x).

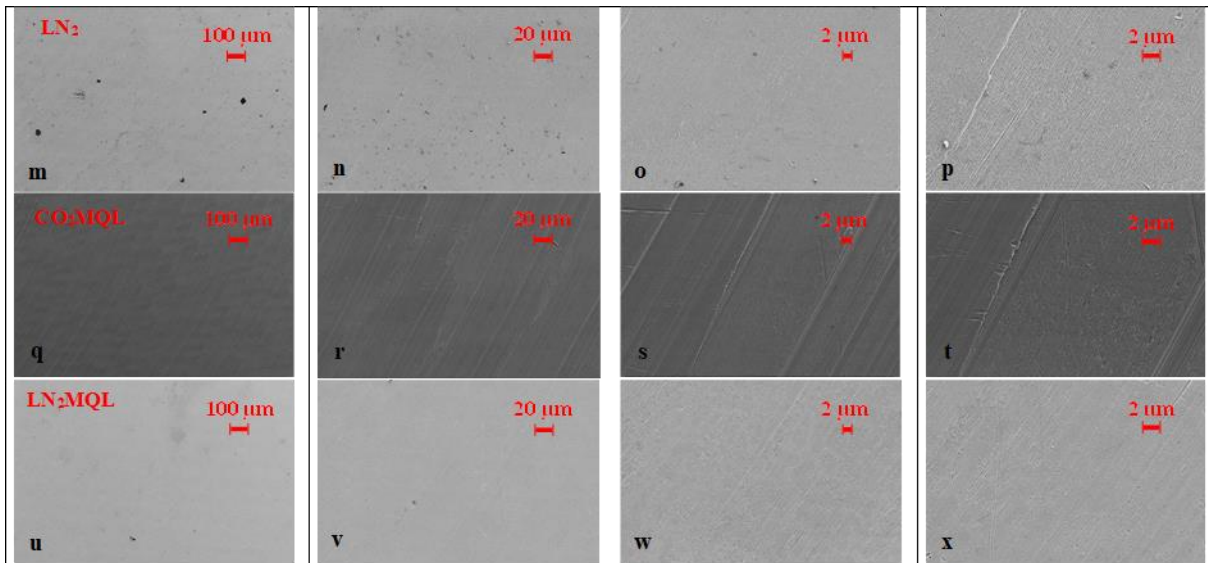


Fig. S5 (continued)

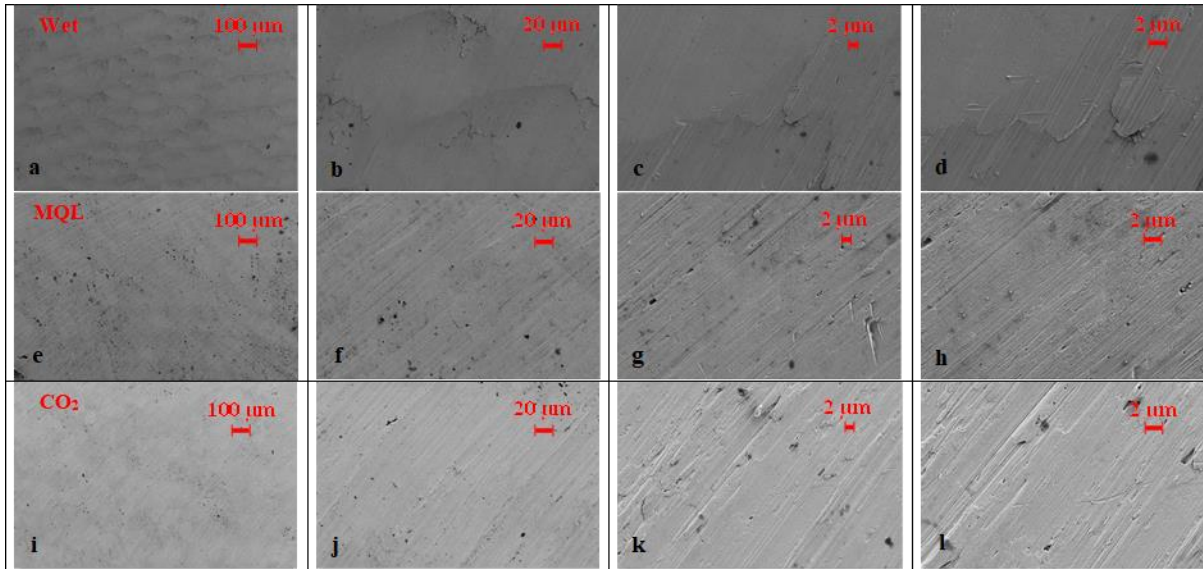


Fig. S0-6: SEM image of the generated surface in the machining of as-built DED under Wet (a-d), MQL (e-h), CO₂ (i-l), LN₂ (m-p), CO₂MQL (q-t), LN₂MQL (u-x).

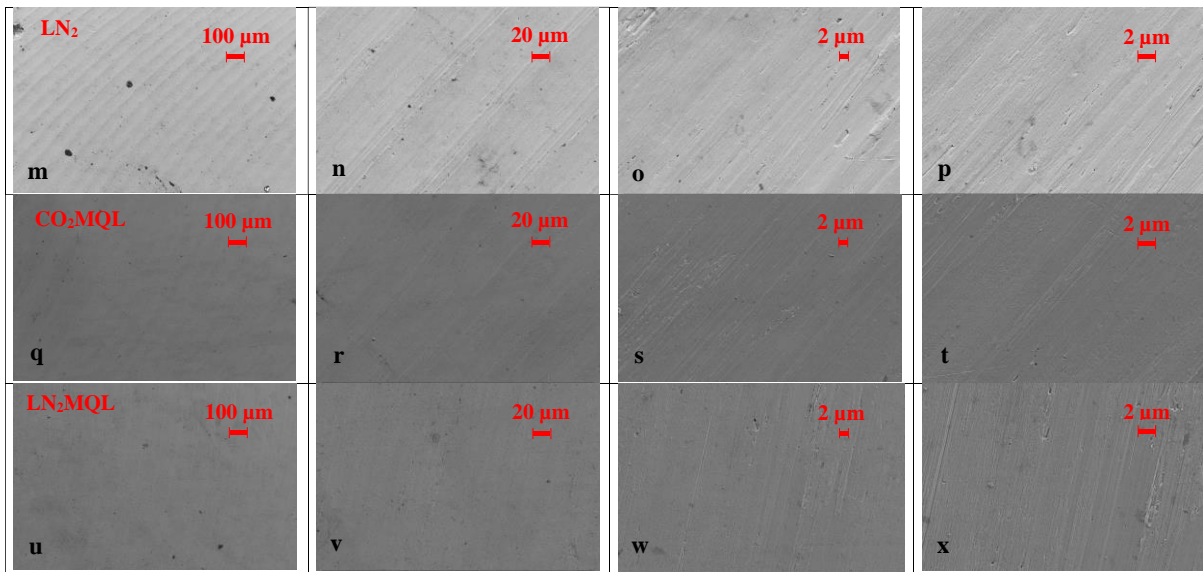


Fig. S6 (continued)

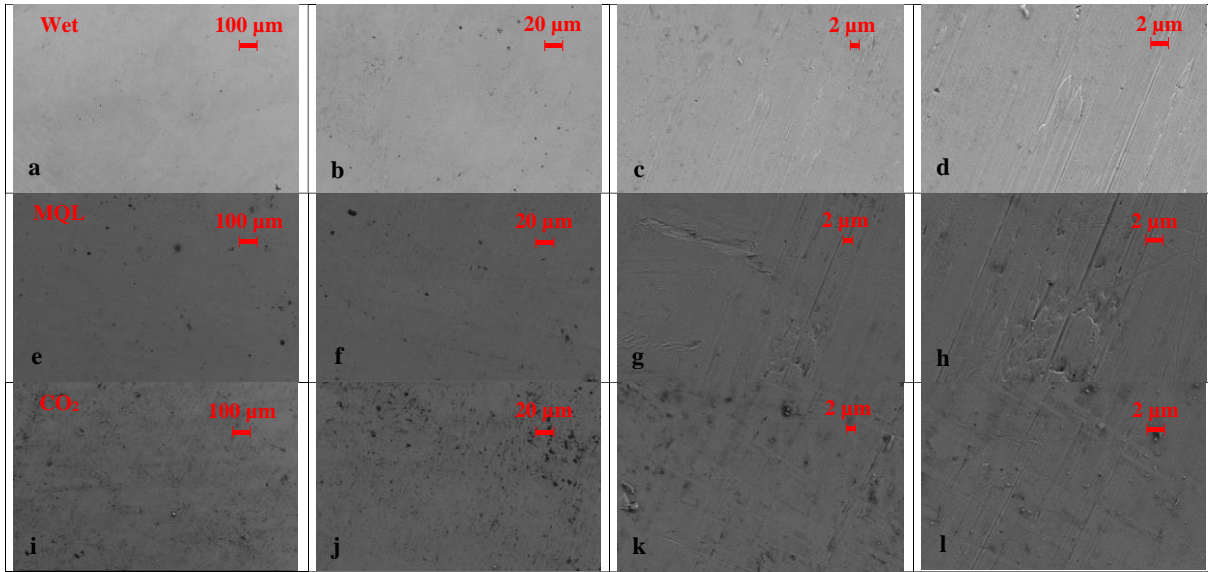


Fig. S0-7: SEM image of the generated surface in the machining of HT-DED under Wet (a-d), MQL (e-h), CO₂ (i-l), LN₂ (m-p), CO₂MQL (q-t), LN₂MQL (u-x).

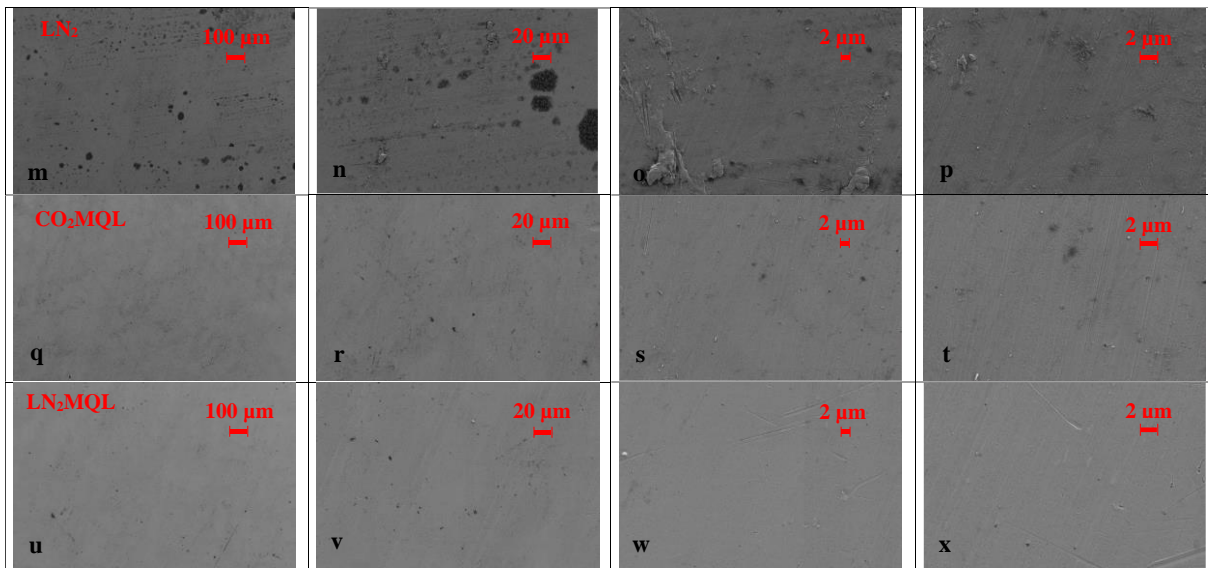


Fig. S7 (continued)